TECHNISCHE UNIVERSITÄT MÜNCHEN

Friedrich-Schiedel Institut für Neurowissenschaften

In vivo functional mapping of single synapses in the vibrissal cortex of the mouse

Zsuzsanna Varga

Vollständiger Abdruck der von der Fakultät für Medizin der Technischen Universität München zur Erlangung des akademischen Grades eines

Doctor of Philosophy (Ph.D.)

genehmigten Dissertation.

Vorsitzender: apl. Prof. Dr. Helmuth K. H. Adelsberger

Prüfer der Dissertation:

1. Univ.-Prof. Dr. Arthur Konnerth

2. Priv.-Doz. Dr. Jana E. Hartmann

3. Jun.-Prof. Dr. Albrecht Stroh, Johannes Gutenberg Universität , Mainz

Die Dissertation wurde am 03.09.2012. bei der Fakultät für Medizin der Technischen Universität München eingereicht und durch die Fakultät für Medizin am 25.10.2012. angenommen.

Abstract

Single neurons, which represent the elementary units of brain function, organize into larger circuits that integrate external and internal brain signals. To understand the operation of these cortical circuits it is essential to identify the functional connections among the neurons. Recently, in vivo two-photon calcium imaging made it possible to identify the location of these connections by imaging dendrites and spines of single neurons. In this study, an improved procedure of two-photon imaging was applied to map the distribution of inputs on the dendrites of neurons in the whisker representation part of the primary somatosensory cortex of the mouse. This cortical region is widely used to study circuit functions because the functional representation of single whiskers is tightly linked to the anatomical structures of defined barrels. Thus, mapping the distribution of sensory stimulation-evoked inputs on the dendrites of the neurons located here allows studying the interaction of functional connections and anatomy. In this study, sensory stimulation-evoked inputs were mapped on the dendrites of neurons residing in the upper half of the vibrissal cortex. These neurons are responsible for the initial steps in the processing of sensory signals in the cortex, thereby determining the structure and timing of the incoming sensory information. Together, this study gives insight in sensory signal processing at the level of single synapses in anatomically organized cortical region.

Abstrakt

Funktionelle Charakterisierung einzelner Synapsen im Barrel-Kortex der Maus *in vivo*

Einzelne Neurone, die grundlegenden Verarbeitungs-Einheiten des Gehirns, sind in Netzwerken organisiert, welche externe und interne Signale im Gehirn integrieren. Um die Arbeitsweise dieser Nervenzell-Netzwerke zu verstehen, ist es wichtig, die funktionellen Verbindungen zwischen den einzelnen Neuronen zu verstehen. Seit kurzem ist es mittels Zwei-Photonen-Mikroskopie möglich, die Lage dieser Verbindungen zu identifizieren und Kalzium-Messungen an Dendriten und sogar dendritischen Dornfortsätzen einzelner Neurone durchzuführen.

In der hier vorliegenden Dissertation wurde eine verbesserte Form der Zwei-Photonen-Bildgebung angewendet, um die räumliche Verteilung der synaptischen Eingänge an Nervenzell-Dendriten in dem Teil der primären somatosensorischen Großhirnrinde der Maus zu untersuchen, welche für die Repräsentation der Barthaare verantwortlich ist (Barrel-Kortex). Der Barrel-Kortex wird häufig für die Untersuchung der Netzwerkfunktion verwendet. Dies ist darauf zurückführen, dass die funktionelle Repräsentation einzelner Barthaare in diesem Kortexareal streng mit der anatomischen Aufteilung in Barrels korrespondiert. Dies erlaubt somit die Untersuchung der Wechselbeziehung zwischen funktionellen und anatomischen Verbindungen. In dieser Arbeit wurden nun durch sensorische Stimulation hervorgerufene synaptische Eingänge an Dendriten von Neuronen, welche sich in der oberen Hälfte des Barrel-Kortex befanden, identifiziert und ihre räumliche Verteilung untersucht. Diese Neuronen sind für die ersten Schritte der Verarbeitung sensorischer Signale im Kortex zuständig und bestimmen also die Struktur und den zeitlichen Verlauf der eingehenden sensorischen Information. Zusammenfassend gibt diese Studie Einblick in die sensorische Signalverarbeitung auf der Ebene einzelner Synapsen in einer anatomisch strikt organisierten Hirnregion.

Table of Contents

In vivo functional mapping of single synapses in the vibrissal cortex of the mouse

1. Introduction

To understand the operation of cortical circuits it is essential to study the functional connections among the individual elements, the neurons. Although previously it was possible to identify synaptic connections among neurons (for example with the help of electron microscopy), these anatomical studies in vitro could give little insight to the dynamic functional properties of the connections in vivo. Recently, this problem could be addressed with the help of two-photon microscopy. Sensory stimulation evoked input sites were mapped on the dendrites of individual neurons in the visual (Jia et el., 2010) and in the auditory cortex (Chen et al., 2011) with the help of in vivo two-photon calcium imaging. Thus, the location of active synaptic sites in response to sensory stimulation could be identified in the living brain.

Here two-photon calcium imaging was used to study the distribution of active synaptic sites on the dendrites of layer 2 (L2) neurons in the whisker region of the primary somatosensory cortex (wS1) in the mouse. In the mouse, in contrast to the visual and the auditory cortex, wS1 follows a strict columnar organization. Cortical columns are assumed to be the basic units of cortical computation. Thus, the effect of anatomical organization on the functional representation of sensory stimulus could be directly addressed. Moreover, the technique was extended to map the input sites on the dendrites of L4 neuron. L4 neurons are located approximately 200 - 250 µm deeper than the superficial L2/3 neurons where the previous studies were performed. L4 neurons receive the information reaching the cortex, and in wS1 they are organized to the special structures of barrels (see under 1.1.3.1). Thus, the present study describes the spatial distribution of sensory stimulation evoked inputs on the

dendrites of single neurons residing in cortical columns for the first time. Moreover, this is the first time demonstration of input distribution in the dendrites of L4 neurons.

Although in the present study L2 neurons were located in cortical columns, the distribution of input sites was similar to those in cortical regions without columns (Jia et al., 2010; Chen et al., 2011). Input sites were found throughout the whole dendritic tree without any spatial preference. Whisker stimulation also triggered the activation of input sites on the dendrites of neurons which were residing in columns other than the column corresponding to that whisker. However, the amount of activation depended on the distance. Spines activated by multiple whiskers were also observed.

In contrast to L2 neurons, a specific morphological subgroup of L4 neurons (spiny stellates) showed location preference in the distribution of input sites. These neurons had the highest input density around their somata. However, another subgroup of L4 neurons (star pyramids) showed no preference in the distribution of input sites. Additionally, in L4 neurons the inputs were highly dominated by the whisker corresponding to barrel in which the neuron was residing.

Altogether, this study is the first time description of the input distribution on the dendrites of neurons in two cortical layers which are consecutive in the processing of sensory signals. Before describing the results in detail, a short introduction will be given on points used in the later parts of the study. An extensive review on numerous aspects of the rodent wS1 can be found in Fox (2008).

1.1. The anatomy of the mouse whisker system

1.1.1. Peripheral sensory organs: vibrissae

For detailed reviews on this topic please refer to Bosman et al. (2011), Diamond et al. (2008) and Sarko et al. (2011). In the following only a short description will be given.

Whiskers or vibrissae are located in mystacial pads on both sides of the snout of mice. Each whisker pad contains approximately 30-40 macrovibrissae and 70-100 microvibrissae (Brecht et al., 1997). Macrovibrissae are long whiskers organized into 5 rows (A-E). The upper 2 rows (A-B) contain 4-5 whiskers in each, while each lower row (C-E) has 7-9 whiskers. At the caudal end of the rows, 4 straddler whiskers (α-δ) grow slightly displaced from the rows. Macrovibrissae are associated with object localization. Microvibrissae are shorter, more densely packed and are not strictly organized. They participate mostly in object identification (Brecht et al., 1997). Macrovibrissae participate in rhythmic forth and back movements called whisking. The frequency of large amplitude exploratory whisking is around 10 Hz in rats, which is replaced by the smaller amplitude higher frequency (around 15-25 Hz) foveal whisking when the animals focus on object identification (Berg and Kleinfeld, 2003, see also Carvell and Simons, 1995 and Berg et al., 2001). Recently it was shown that while the protraction of whiskers is directly controlled by the primary motor cortex, the retraction is mediated by S1 (Matyas et al., 2010).

The follicle of vibrissae is surrounded by a capsule of thick connective tissue (Rice et al., 1986), which contains two blood sinuses. The blood sinuses are responsible for the modulation of dynamic range of mechanoreceptors by changing their blood pressure. Each follicle is innervated by several smaller superficial vibrissal nerves, one deep vibrissal nerve (containing 100-200 fibers)(Rice et al., 1986) and some unmyelinated C fibers at the bottom of the follicle (Ebara et al., 2002). The superficial and deep vibrissal nerves innervate Merkel cells and lanceolate endings. Merkel cells are thought to transmit information on ongoing movements, while lanceolate endings transmit information on change in movement.

1.1.2. Sensory pathways connecting vibrissae to S1

The sensory nerve fibers innervating the whisker follicles, with nerve fibers innervating other parts of the face, make up the trigeminal nerve. The cell bodies of the nerve fibers are located in the trigeminal ganglion. The neurons in the trigeminal ganglion fire only during whisker movement (in the rat: Jones et al., 2004; Leiser and Moxon, 2007). They are organized in somatotopic fashion (Leiser and Moxon, 2006) and receive input only from single vibrissa (Gibson and Welker, 1983). However, large movements can activate neighboring pathways.

From the trigeminal ganglion, neurons project to the sensory trigeminal nucleus which is a complex of the principal trigeminal nucleus, and the oral, the interpolar and the caudal spinal trigeminal nuclei. The principal trigeminal nucleus and the caudal part of the spinal trigeminal nuclei contain barrellettes (Belford and Killackey, 1979; Ma 1991; for review see Erzurumlu et al., 2010). Barrelettes represent somatotopically organized groups of neurons receiving information from the same whisker. The neurons located in between the barrelettes typically receive information from multiple whiskers (Veinante and Deschenes, 1999).

The neurons of the trigeminal nucleus send their projections to the ventral posterior medial (VPM) and the medial posterior (POm) nuclei of the thalamus. The VPM contains barreloids (Van der Loos, 1976; Haidarliu and Ahissar, 2001), which topographically connects to the barrelettes in the trigeminal nucleus (Veinante and Deschenes, 1999). Comparing the sensory responses of VPM and POm neurons show that VPM neurons had shorter latencies and could respond either to single whisker or to multiple whiskers. In contrast, POm neurons had responses to multiple whiskers with longer latency (Diamond et al., 1992).

The neurons of the VPM and POm of the thalamus project to the wS1. Based on the course of projections two main pathways can be distinguished. The lemniscal pathway connects the barrelettes in trigeminal nucleus with the barreloids of the VPM (Veinante and Deschenes, 1999; Williams et al., 1994) and terminates in L4 of wS1 (Land et al., 1995; Wimmer et al., 2010). As a result, this pathway is considered to convey predominantly information from single whiskers, although neurons responsive to multiple whiskers have been found in VPM (Brecht and Sakmann, 2002a). The paralemniscal pathway connects the multi-whisker neurons of the trigeminal nucleus with the POm and terminates in L5A-L1 (in L4 in the septum regions). As a

result, this pathway is considered to convey multi-whisker information. The axons of VPM and POm neurons remain separated throughout most of the cortical depth (Wimmer et al., 2010). Moreover, the barrel-related and septum-related projections were found to be part of distinct functional units in the rat (Shepherd and Svoboda, 2005). In the mouse, the information coming from lemniscal and paralemniscal pathways was found to be segregated also along the cortex (Bureau et al., 2006). Recently, the modulatory function of the paralemniscal pathway was suggested (Viaene et al., 2011).

1.1.3. The mouse wS1

The mouse wS1 is a neocortical region located from 0.38 mm anterior to bregma to 1.94 mm posterior to bregma, and 2.5-4 mm lateral from the midline (as estimated from the mouse brain atlas Paxinos, 2001). As a sensory area, it has a distinct L4 (granular cortex). In a very simplistic view, the excitatory circuitry within the neocortex goes as the following. Afferent fibres from the thalamus terminate in L4 of sensory cortices from L4, the information is spread to supragranular layers (L2/3), and then leaves the cortical area through L5. For more details on neocortical circuitry, please refer to reviews Thomson and Bannister, 2003 and Thomson and Lamy, 2007.

1.1.3.1. Barrels

The term “barrel” was introduced by Thomas Woolsey and Hendrik van der Loos (Woolsey and Van der Loos, 1970). With the help of Nissl staining, they identified multicellular structures of 100-400 µm in diameter. They named these structures “barrels” because of their 3 dimensonal appearance. Each barrel consists of a side region rich in neuronal somata and a center barrel hollow region, which contains less neurons. The regions in between the barrels are also sparse in neurons and are called septa. Woolsey and Van der Loos identified 170-210 barrels/barrel field in one hemisphere. Within the barrel field, they distinguished the posteromedial barrel subfield (PMBSF), which contained (34-40) large barrels, and the spatial arrangement of these barrels resembled the vibrissa arrangement on the snout. Based on this

similarity of spatial arrangements and the electrophysiological study in the rat by Welker (Welker, 1971), Woolsey and Van der Loos concluded that one barrel in the PMBSF represents one large vibrissa on the contralateral side. Later several other studies confirmed this conclusion (e.g. Armstrong-James and Fox, 1987; Simons, 1978; Welker, 1976), however functionally the receptive field of L4 neurons can vary (see section 1.2.1). The whisker that is represented by a barrel is called the principal whisker (PW) of that barrel. The other whiskers are called the surround whisker (SW) of that barrel.

The barrel structure is the result of the spatial organization of thalamic afferents in wS1. The thalamic afferents in L4 terminate in clusters and form the barrel hollows. However, the barrel organization is not necessary for somatotopy. Although mice with the barrelless mutation lack the structural organization of barrels, the topology of whisker representation is preserved (Gheorghita et al., 2006; Welker et al., 1996). Yet while wild-type mice showed latency differences in spiking response between PW and SW stimulation, the barrelless mice showed no significant difference (Welker et al., 1996).

As a result of the barrel organization, neurons in the barrel wall have asymmetric dendritic tree sending their projections toward the barrel hollow (in rat: Feldemeyer et al., 1999; Lübke et al., 2000; Oberlaender et al., 2011; Simons and Woolsey, 1984). The dendrites of most neurons are confined to the barrel (Simons and Woolsey, 1984; Lübke et al., 2000), however some of them also project to neighboring barrels (in mouse: Woolsey et al., 1975; in rat: Lübke et al., 2000). There are approximately 1000-2600 neurons in a single barrel of the mouse (Lee and Woolsey 1975).

1.1.3.2. Connections of mouse wS1

In the mouse, the whole size of the barrel field is around 1100 x 2800 µm (Woolsey and Van der Loos, 1970). However, wS1 makes intensive connections to other cortical and subcortical regions. For review on the connectivity of the mouse wS1, please refer to Aronoff et al. (2010).

One of the cortical regions connected to wS1 is the whisker part of the secondary somatosensory cortex (wS2) (Welker et al., 1988; White and DeAmicis, 1977). Projections to

wS2 originate from both barrel and septa of the extragranular regions (in rat: Chakrabarti and Alloway, 2006). Specifically, the connection is established between L3 and L5 of wS1 and L3, L5 and L6 of wS2 (Hooks et al., 2011), and retains somatotopy (Carvell and Simons, 1986; in rat: Koralek et al., 1990), however the receptive field of wS2 neurons is larger than that of wS1 neurons (in rat: Kwegyir-Afful and Keller, 2004).

Similarly, a strong connection exists between wS1 and the primary motor cortex (M1) (Welker et al., 1988; White and DeAmicis, 1977). The neurons participating in this connection are mostly residing in septal regions (in rat: Alloway et al., 2004) and outside layer 4 (in rat: Chakrabarti and Alloway, 2006). They send their projections preferentially to L2/3 and L5A (Mao et al., 2011). A recent study suggests that neurons in the wS1 that project to M1 have larger receptive fields than those projecting to wS2 (Sato and Svoboda, 2010). The sensory map in the whisker part of M1 suggests somatotopy, although whisker representing regions are compressed closer to each other (Ferezou et al., 2007; in rat: Hoffer et al., 2003; Izraeli and Porter; 1995).

The area wS1 also connects to several subcortical regions. One of the subcortical targets is the thalamus itself (Hoogland et al., 1987). The VPM, POm, and the GABAergic neurons of the thalamic reticular nucleus receive projections from the infragranular layers of wS1 in an ipsilateral fashion (in rat: Bourassa et al., 1995; Veinante et al., 2000). The projection to VPM is topographic, although barrels partially overlap (Bourassa et al., 1995; Land et al., 1995; Wright et al., 2000). The projection to POm originates from the L5 below septal regions of wS1 (Wright et al., 2000).

In addition to the above mentioned main projections, several other connections exist. For example, other cortical targets include the contralateral wS1 (Ferezou et al., 2007; Larsen et al., 2007; Petreanu et al., 2007). Examples for other subcortical targets are the striatum part of the basal ganglia (Mercier et al., 1990), pontine nuclei and superior colliculus (Veinante et al., 2000).

1.1.3.3. Microcircuitry of mouse S1

A single barrel column contains approximately 6500 neurons, out of which ~ 5700 are excitatory and the rest are inhibitory neurons (Lefort et al., 2009). In the following the focus will be on the connection pattern of excitatory neurons. For details on this topic, please refer to reviews Lübke and Feldmeyer (2007) and Petersen (2007).

The thalamocortical projections, carrying the sensory information from the peripheries, terminate in L4 (see section 1.1.2.). However, recently thalamocortical projections were found to innervate neurons in all layers, at least to some extent (in rat: Meyer et al., 2010). These new findings might lead to the re-evaluation of laminar functions, nevertheless traditionally the first steps of signal processing are considered to take place in L4 neurons. These neurons are highly interconnected as shown in the rat (Feldmeyer et al., 1999). Similarly, in the mouse L4-L4 connections have ~24% connection probability, which is one of the highest synaptic connections in a barrel column (Lefort et al., 2009). In the rat, the synaptically coupled L4 neurons form their connections on secondary to quaternary dendritic branches, mostly in the proximity of the soma (Feldmeyer et al., 1999). Predominantly the connections are formed between neurons of the same barrel, and the connections are established within the barrel. Compared to other cortical connections, L4-L4 connections have low variability (coefficient of variance of evoked EPSP amplitude around 0.4) and low failure rate (approx. 6%). These properties enable L4 neurons to amplify and distribute incoming thalamic inputs within the cortical column (Feldmeyer et al., 1999). L4 neurons also give prominent projections to L2/3, and to a lesser extent to other cortical layers within the column (Lefort et al. 2009). In addition to the connections within the barrel, some axon collaterals, especially in L5 and L6, project to adjacent cortical columns (in rat: Lübke et al., 2000). Nevertheless, barrels are traditionally thought to be functionally independent (in rat: Laaris and Keller, 2002; Petersen and Sakmann, 2001).

From L4 the information reaches the supragranular layers (Armstrong-James et al., 1992). In rat, most of the L4 projections stay confined within the boundaries of the barrel column, and project only partly to neighboring columns (in rat: Feldmeyer et al., 2002). Approximately 90% of the connections of L4 neurons are made with L2/3 neurons (in rat: Lübke

et al., 2000). Although these connections are relatively reliable (failure rate is around 5%), the evoked EPSPs have relatively small (around 1 mV) amplitude (all values are for rat from Feldmeyer et al., 2002). Thus, a given degree of convergence of L4 inputs is necessary to drive action potential (AP) firing in L2/3 neurons. The superficial L2 receives a strong projection from L5A in the septal column (Shepherd et al., 2005; Lefort et al., 2009), thus it is part of the paralemniscal system (see section 1.1.2.). L2/3 neurons form strong connections to other L2/3 neurons, and also project to L5. However, they hardly connect to L4 and L6 (Lefort et al., 2009). The lateral projections are not confined to the barrel column but can extend to a distance of several barrels (in rat: Gottlieb and Keller, 1997), predominantly along the row (Bernardo et al., 1990; Petersen et al. 2003a).

Based on morphology, electrical properties, and the projection patterns, L5 can be subdivided into L5A and L5B (in rat: Ahissar et al., 2001; Manns et al., 2004; Mercier et al., 1990; Schubert et al., 2006). L5B cells get collateral projections from VPM afferent targeting L4. In contrast, L5A neurons get projections from POm and provide projection to L2, thus they are part of the paralemniscal circuit (Shepherd and Svoboda, 2005). L5 neurons provide extended projections laterally which can span over several barrel columns (Manns et al., 2004). L5 neurons establish connections within the same layer, but they also project to L2/3 and L6 (Lefort et al 2009).

L6 neurons receive connections from L5 and L4, and it provides connections to itself and L5 (Lefort et al 2009). L6 neurons have diverse morphology (Pichon et al., 2012), and those projecting within and out of cortex have been shown to have different morphological an electrical properties (in rat: Kumar and Ohana, 2008). Moreover, corticothalamic neurons in L6 seem to receive strong direct connections from L4 (in rat: Tanaka et al., 2011).

1.1.3.4. Morphology of L2 and L4 excitatory neurons in mouse S1

In L2 the main excitatory type of neurons are pyramidal cells. However, L2 pyramidal cells are morphologically different as compared to the typical pyramidal cells of L5 (DeFelipe and Farinas, 1992). They lack or have only short apical dendrite, and the soma is often polygonal, similar to shape of L4 stellate cells, however L2 somata are larger. Mouse L2 neurons

have their apical dendrite bifurcating in proximity to the soma. The apical branches project in diagonal or horizontal directions, and they often branch extensively in L1 (Feldmeyer et al 2006).

L4 of the rodent wS1 shows high cell density and compact dendritic and axonal plexus (Feldmeyer et al., 1999). Three types of excitatory neurons were identified: spiny stellate cells, star pyramids and pyramids. Spiny stellate cells have small spherical cell bodies, which makes them both geometrically and electronically more compact then pyramidal cells (Mainen and Sejnowski, 1996). Unlike in the visual cortex, where spiny stellate cells were described as multipolar neurons with radially symmetric dendritic field (in cat: Le Vay, 1973), in the barrel cortex these neurons have asymmetric dendritic tree oriented towards the center of the barrel (Woolsey et al., 1975; in rat: Lübke et al., 2000). Star pyramids (described by Simons and Woolsey, 1984 in wS1, and by Lund, 1984 in visual cortex) have apical dendrites which reach to L2/3, however, they lack an apical tuft (in rat: Feldmeyer et al 1999, Oberlaender et al 2011). The third group of excitatory neurons, the pyramids has apical dendrite reaching L1 and ending in apical tuft (Oberlaender et al., 2011). The majority of excitatory neurons in L4 are the spiny stellate cells (Lund 1984, Ahmed et al 1994, Hirsch 1995, Stratford et al 1996); however, the exact proportion of neuron types is not completely clear. In the rat, from the study by Oberlaender et al. (2011) one can estimate a proportion of 47% spiny stellate cells, 45% star pyramids and 8% pyramids. An earlier study (Feldmeyer et al., 1999), also in the rat, reported 70% spiny stellate cells and 15% star pyramids, with the rest being inhibitory neurons. Another study (Staiger et al., 2004) found 58% spiny stellate cells, 25 % star pyramids and 17 % pyramids in the rat. In the rat, different excitatory neurons tend to occur at different depths of L4 (Oberlaender et al., 2011).

1.2. The function of mouse S1

1.2.1. Receptive field properties of L2 and L4 neurons in mouse wS1

Receptive field of a neuron in a sensory system is, generally, the region of space where the presence of a stimulus alters the activity or state of that neuron. In case of the wS1, the receptive field of a neuron corresponds to the whiskers whose stimulation can evoke depolarization in that neuron. One can distinguish subthreshold and suprathreshold receptive fields. In case of subthreshold receptive field, the presence of a stimulus evokes changes in the membrane potential of the neuron without producing AP, while in case of suprathreshold receptive field, the presence of the stimulus drives the neuron to fire AP. As it will be discussed below, the subthreshold and suprathreshold receptive fields overlap, but can be different in size, usually with subthreshold receptive fields being larger. Moreover, the size of receptive field can change over time, a concept called "dynamic receptive field" (Brecht and Sakmann, 2002b; Petersen et al., 2003). Dynamic receptive field represents a reversed view on the signal propagation in the cortex. As it will be discussed in section 1.2.2., the stimulation of a single whisker produces depolarization in cortical neurons with different latency from the time of stimulation (Petersen et al., 2003). From the point of view of a single neuron with longer latency, at the beginning (when the depolarization has not reached the neuron) the receptive field of that neuron does not contain the stimulus, while later (when the neuron has depolarized) it does. The size of receptive field at any given time depends on other neurons that project and provide input to that neuron, and it is considered to be restricted by inhibitory connections.

Since most information on the receptive fields of neurons in wS1 was recorded in rats, the following description of receptive field properties of L4 and L2 neurons are from the literature on the rat. Here, the direction selectivity of receptive fields will not be considered. For further information on this topic, please see elsewhere, for example Hemelt et al. (2010).

To L4 neurons, as it was described in section 1.1.3.3., the majority of inputs arrive from the somatotopically corresponding regions of the thalamus and from other L4 neurons. On subthreshold level, receptive fields include the PW with short latency and fast rise times and

several (5-8) SWs with longer latency and slower rise times (Brecht and Sakmann, 2002b; Moore Nelson, 1998). The SW-evoked depolarization is assumed to reach L4 neurons through multi-whisker thalamocortical cells and single whisker thalamocortical cells that project to several barrel columns. On suprathreshold level, L4 neuron receptive fields are highly dominated by the PW, and include only few SWs (3-4) (Brecht and Sakmann, 2002b). Recently, the subcortical nature of mechanisms leading to multi-whisker receptive fields in L4 was confirmed (Roy et al., 2011), by blocking cortical activity with $GABA_A$ agonist muscimol.

As for L2/3 neurons, their input mainly originates from L4 neurons, both vertically and diagonally, and other L2/3 neurons (Lübke et al., 2003). Specifically in L2, neurons which reside above the barrel get their input from L4, while neurons above the septa get their input preferentially from L5A (Shepherd and Svoboda, 2005). Since L5 neurons have projections over several barrels (see section 1.1.3.3.), it is not surprising that the signal reaching L2 carries information on multiple whiskers. Indeed, the subthreshold receptive field of L2 neurons comprises, beside the PW, a relatively large number of SWs (around 8-13) (Brecht et al., 2003, Moore and Nelson; Zhu and Connors, 1999). Similarly to L4, a difference was detected between the time courses of PW and SW evoked depolarization. On suprathreshold level, compared to L4 neurons, the receptive field includes a larger number of SWs (3-5) (Brecht et al., 2003).

Altogether for both L4 and L2 neurons the subthreshold receptive field changes dynamically, exceeds the suprathreshold receptive field, and contains multiple whiskers. In both layers, the suprathreshold receptive field is dominated by the PW, but also includes other whiskers. On subthreshold level, the size of the receptive field of L2 neurons clearly exceeds those of L4 neurons.

1.2.2. Touch representation in the mouse S1

Touch representation can be described as the consecutive and/or parallel activation of neurons. One of the consequences of the consecutive activation of neuron populations is the aforementioned dynamic receptive field. However, touch representation seems to depend on

cortical state and whether the whisker is passively deflected or it is actively moved by the mouse.

The generally accepted course of activation describes the flow of excitation in response to passive whisker deflections. L4 is considered to be the main input site of sensory information to the cortex. On the one hand this is supported by anatomical reconstructions showing that the majority of thalamocortical projections target L4 (for example in rat Oberlaender et al., 2011). On the other hand, electrophysiological recordings also show that L4 neurons in the principal barrel activated first in response to stimulation. In the rat, within 10 ms after the stimulation of a single whisker, only these neurons were excited (Armstrong-James et al., 1992). From L4, the activation is distributed throughout the cortex. Considering the vertical signal transmission, L3, L2 and L5A neurons responded 2 ms, 3 ms and 3.2 ms after the activation of L4. L5B neurons fired with short latencies similar to L4, and in all cases L6 was activated at last. Considering the horizontal transmission, neighboring barrels were also activated within 10 ms after whisker stimulation. Finally, more than 20 ms after whisker deflections, responses could be recorded from 6-8 barrel territories.

The above mentioned results were gained based on the suprathreshold responses (AP firing) of neurons in various layers. To study the propagation of subthreshold activation, another method, voltage-sensitive dye (VSD) imaging can give useful insights (Grinvald et al., 1984). VSD-imaging gives information on entire populations (single cells cannot be distinguished) and gives superior time resolution to calcium imaging (Orbach et al., 1985). The VSD signal corresponds mainly to the subthreshold activity of neurons (Yuste et al., 1997; Petersen et al., 2003). To visualize the flow of excitation throughout the rat cortex, VSD imaging can be performed on cortical slices, and whisker stimulation can be substituted by current injection to L4 (Petersen and Sakmann, 2001). L2/3 was activated in a similar time course as previously mentioned. However, the activation was mostly confined to a barrel-related column. Contrary to these results, when VSD imaging was performed in vivo and the whisker was deflected with at least middle strength, activation spread from L4 to supragranular layers above (within 10-12 ms) and further away from the barrel (in rat: Petersen et al., 2003). Moreover strong deflection resulted in the spread of signal over the whole barrel cortex 40 ms after

whisker deflection, at least in L2/3, and persisted up to 100 ms (in rat: Petersen et al., 2003). It is worthwhile to note that in in vivo conditions, the VSD signal originates mainly from the supragranular layers (Kleinfeld and Delaney, 1996).

The sensory signal flow was shown to be influenced by the spontaneous state of the cortex (Petersen et al., 2003b). Cortical neurons exhibit spontaneous subthreshold membrane potential changes (in cat: Steriade et al., 1993, in rat: Cowan and Wilson, 1994). The hyperpolarized state is called “down state”, while the slight depolarization of the membrane potential for prolonged time intervals (typically around 100-300 ms, Cowan and Wilson, 1994) is called “up state”. In the up state of L2/3 neurons, the single whisker deflection evoked smaller responses both on subthreshold and suprathreshold level compared to sensory stimulus reaching the neurons in their down state (Petersen et al., 2003b). Similarly, the size of the activated area was markedly smaller.

In addition to up and down states, the wakefulness of mice also influences the propagation of sensory signals. For example, L2/3 neurons showed a more prolonged depolarization over a larger cortical area when the mice were awake compared to when they were anesthetized (Ferezou et al., 2006). However, when comparing the stimulation evoked signals when the mouse was quiet or actively whisking, both the signal duration and the activated area was smaller when the sensory stimulus was delivered during active whisking (Ferezou et al., 2006). Similarly, the signal reaching other cortical areas was influenced by the behavior. If whisker deflection initialized active whisking behavior in awake animals, large depolarization could be observed over the wS1 and M1 areas. However, if the whisker deflection did not trigger whisking, or the stimulus was delivered during active whisking, the evoked signal was highly restricted and generated only weak depolarization in M1 (Ferezou et al., 2007). On cellular level, the passive stimuli during quiet wakefulness produced large-amplitude membrane potential changes, while during active whisking, when the membrane potential was dominated by fast fluctuations, the sensory stimuli evoked small amplitude, highly variable responses (Crochet and Petersen, 2006). A possible explanation comes from the observation that during quiet wakefulness neighboring neurons showed highly correlating subthreshold activity which was taken over by desynchronized membrane potential

fluctuations during active whisking (Poulet and Petersen, 2008). The desynchronized membrane potential changes during active behavior were found to be the result of increased action potential firing in the thalamus (Poulet et al., 2012).

Along with the variability in signal flow exerted by the behavior, touch representation is also characterized by sparse coding and trial to trial variability. Two-photon calcium imaging of bulk loaded neurons (Stosiek et al., 2003) is a widely used method to study suprathreshold population responses with single cell resolution. With this method in L2/3 of the rat wS1, the response probability of PW-related and SW-related neurons was estimated to be 20% and 15%, respectively (Kerr et al., 2007). Within the PW-related column the response probabilities decreased steadily with distance from the column center (Kerr et al., 2007). Additionally, single whisker deflections were sparsely represented. On average 20% of PW-related neurons and 16% of SW-related neurons were activated upon single deflection (Kerr et al., 2007). Surprisingly, the subset of activated neurons changed from trial to trial (Kerr et al., 2007). Another group with similar methods found the response probability to be around 0.32 for PW stimulation and around 0.2 for SW stimulation (Sato et al., 2007a). They also found that although whisker selectivity smoothly changed over the cortex, neighboring neurons could have different whisker selectivity.

Similarly to passive whisker deflection in anesthetized animals, active touch performed by awake mice is also sparsely represented. O'Connor et al. (2010) showed that across all layers 10% of neurons fired 50% of spikes. Moreover, the firing rates differed significantly. L2/3 and L6 were firing at low rates, on average at 0.18 Hz and 0.48 Hz, respectively, while L4 (3.48 Hz) and L5 (9.13 Hz) fired with higher frequencies. [The spontaneous firing rate of L2 neurons is around 0.1 Hz (Brecht and Sakmann, 2003b) and the spontaneous firing frequency for L4 neurons 0.05 Hz (Brecht and Sakmann, 2002).] Another study (Crochet et al., 2011) on L2/3 neurons found that active touch drove AP in approximately 10% of the neurons. They suggested that sparse coding was due to the cell-specific reverse potential for the touch response.

Taken together, the stimulation of a single whisker causes the activation of neuron groups in an ordered manner, and the signal can propagate over large cortical areas. However, the size of cortical area activated by the sensory stimulation is affected the by the arousal state

of the animal and the cortical state. Additionally, the sensory representation involves only a subset of neurons in the corresponding cortical area, and the group of actual neurons participating in the sparse code changes from trial to trial.

1.3. Methods for studying synaptic connections in vitro and in vivo

This section gives a short overview without specific details on some of the techniques applicable to study synaptic connections. For more details and other methods please refer elsewhere.

1.3.1. Anatomical reconstructions

The anatomy of neuronal connections can be reconstructed in several ways. One method involves the direct visualization of single neurons and the description of the projection patterns. Such technique is the silver impregnation of the Golgi staining, which was the earliest reconstruction technique to visualize individual neurons with their projections. To correlate neuronal morphology and physiological properties neurons can be filled with Neurobiotin or biocytin through patch pipettes with the juxtacellular labeling method (Pinault, 1996). The labeled neuron can be visualized with avidin-conjugated labels (chromogenic or fluorescent) post hoc. Horseradish peroxidase can be as well filled into neurons and visualized in a similar way. Neurons and their projections can also be visualized with anterograde (e.g. Phaseolus Vulgaris Leucoagglutinin PHA-L, radioactive amino acids) or retrograde labeling (e.g. horseradish peroxidase, Fast Blue, Fluoro-Gold, cholera toxin subunit B) where the tracer molecule entering the neuron at one pole (i.e. at the soma in anterograde or at the axon in retrograde labeling) is redistributed to the whole neuron.

To identify neurons which are synaptically coupled the method of transneuronal viral tracing can be used. Here infectious viruses (e.g. herpes simplex virus types or pseudorabies virus types) are injected to the brain and are taken up by nerve terminals innervating that region. The virus replicates within the neuron and then get transported across synapses thus

marking the neurons projecting to the infected neuron (retrograde labeling). Recently anterograde transsynaptic labeling was also achieved (Lo and Anderson, 2011).

Finally, the recent technique of Brainbow makes use of the variety fluorescent proteins with different spectral properties (Livet et al., 2007). The combinatorial expression of fluorescent proteins in neurons creates virtually individual color tag for each neuron. This enables the tracking of individual neuronal projections among other labeled neurons. For review see Lichtman et al. (2008).

The above mentioned techniques investigated connectivity at cellular level. However, to achieve higher resolution in order to study the sites of connections other means of microscopy are necessary. One possibility is electron microscopy which makes use of the shorter wavelength of electrons thus increasing resolution. The increased resolution enabled, for example, the detailed description of morphological properties of synapses leading to the differentiation of type I and type II synapses in the cerebral cortex of the rat (Gray, 1959). Since type I and type II synapses are considered to be excitatory and inhibitory connections, respectively, the electron microscopic analysis of neurons could provide information on the ratio and preferential connection site of excitatory and inhibitory projections. Another potential solution is promised by the new techniques of super-resolution light microscopy (e.g. stimulated emission depletion microscopy). These techniques enable high-resolution structural imaging in living samples and might contribute to clarifying the morphology of synaptic connections in the future. For review on super-resolution microscopy, please refer to Leung and Chou (2011).

Finally, the recent method of serial block-face imaging combines the high-resolution electron microscopy imaging with automated data acquisition, as well as automated neuronal tracing to gain fine structural information over large brain volumes (Denk and Horstmann, 2004; Jurrus et al., 2009; Helmstaedter et al., 2011). This technique was applied, in conjunction with two-photon microscopy, to map the connection of interneurons and ganglion cells in the mouse retina (Briggman et al., 2011). A similar approach was used to trace the local connectivity of excitatory and inhibitory neurons in the mouse primary visual cortex (Bock et al., 2011).

1.3.2. Electrophysiological pair recordings

In electrophysiological pair recordings simultaneous whole-cell recordings are established on 2-4 neurons. Usually one of neurons is depolarized to fire action potentials and the evoked changes in the membrane potentials of the other neuron(s) are monitored. With this technique it can be determined whether there is any functional connection between the recorded neurons. If the neurons are functionally connected, the strength of the connection, the latency of activation (monosynaptic or disynaptic connection), the failure rate and the receptor component of the transmission can be measured (for example Feldmeyer et al., 1999; Feldmeyer et al., 2002; Feldmeyer et al., 2006). The combination of this technique with biocytin staining can reveal the morphology of synaptically coupled neurons. Electrophysiological pair recordings can be used in vivo, even in awake animals. For example, Gentet et al. (2010) used double recordings to simultaneously monitor the membrane potential changes of excitatory and inhibitory L2/3 neurons in the barrel cortex of the awake mouse.

1.3.3. Photostimulation

1.3.3.1. Optogenetics

Optogenetic tools introduce light-sensitive channels to the genome of the neurons of the interest. Genetic targeting can be achieved with viral vectors (for example lentivirus, in Dittgen et al., 2004; or adeno-associated virus, in Kuhlman and Huang, 2008; for review on viral vectors see Osten et al., 2007), or direct construction of transgenic mice which contain the genetic information to produce the light-sensitive molecules under their own promoter-enhancer regions (for example Thy1::ChR2-EYFP mouse lines, Arenkiel et al., 2007; Wang et al., 2007). After the expression of the light-sensitive channels, the channel-expressing neurons can be activated (as in case of e.g. ChR2) or inhibited (e.g. Arch) by shining light on them. For more details on the technique please refer to the recent review by Yizhar et al. (2011). An example application is the “subcellular ChR2-assisted circuit mapping” which combines whole-cell recordings with optogenetic stimulation to map the origin of inputs reaching different regions of a neuron (Petreanu et al., 2009).

1.3.3.2. Glutamate uncaging

This technique uses glutamate chemically bound to another compound ("caged") and biologically inactive. The caged glutamate can be activated by using light of the appropriate wavelength to cleave off (in case of irreversible caged neurotransmitters, for example Wilcox et al., 1990) or switch (in case of reversibly caged neurotransmitters, for example Volgraf et al., 2007) the protecting group. The activated glutamate acts as synaptically released glutamate, causing EPSP or AP firing in the neurons nearby. When glutamate uncaging is combined with whole-cell recording, a high resolution map of the sources providing functional inputs to the neuron can be gained (Callaway and Katz 1993, Dantzker and Callaway 2000). Moreover, if glutamate uncaging is restricted to sufficiently small spatial volumes (i.e. single spines), by spatiotemporally varying the activation sequence of single spines, the features of dendritic integration can be studied (Branco et al., 2010; Branco and Hausser, 2011).

1.3.4. Two-photon calcium imaging

Studying the in vivo functional connection among neurons in the intact brain became possible with the construction of two-photon microscope (Denk et al., 1990). The principle of two-photon effect is the excitation of a fluorophore molecule with the simultaneous absorption of two low-energy photons. Since the simultaneous absorption of two photons depends on the second power of light intensity and light intensity quadratically decreases with distance, the spatial volume of excited fluorophores is restricted to the focus of illumination. Thus all fluorescent photons are assumed to be emitted from the focus point, and can be collected for image construction. Two-photon microscopy allows the visualization and manipulation of neurons in the scattering tissue of living brain up to a depth of 1 mm. This superior feature lies in the above mentioned characteristics (i.e. the use of less scattering red/near infrared light for excitation, the restricted spatial extent of excitation and the fact that all detected photons can contribute to the signal).

Two-photon calcium imaging (Yuste and Denk, 1995) records the change of intracellular calcium concentration within the neurons. Cytosolic calcium is an important second messenger

and participates in multiple signaling pathways. The calcium concentration in the cytosol can increase through various mechanisms, among which the calcium entry through voltage-gated calcium channels and NMDA receptors are the most relevant for this study.

To detect the changes in intracellular calcium concentration, special molecules which change their fluorescent properties upon calcium binding should be introduced to the neurons. These molecules can be synthetic indicators or genetically encoded proteins. Synthetic calcium indicators, such as the Oregon Green BAPTA-1, have the advantage of higher sensitivity and ease of introduction to neurons. However, genetically encoded calcium indicators, such as the Yellow Cameleon 3.60, can be targeted to specific cell types or cell compartments and allow chronic imaging experiments (for example Minderer et al., 2012).

Although generally in vivo two-photon calcium imaging is used to follow the dendritic activation of individual neurons (for example Svoboda et al., 1999) or the population activity of several neurons (Kerr et al., 2007), recently it was applied to map excitatory synaptic inputs on dendrites in the visual cortex (Jia et al., 2010) and spines in the auditory cortex (Chen et al., 2011). In both studies in vivo two-photon calcium imaging was combined with whole-cell recording, thus suprathreshold and subthreshold activation of dendrites and spines could be dissected apart. The subthreshold activation was shown to correspond synaptic activity, thus this method was suitable to visualize the projection pattern of neurons upstream from the recorded cell. However, the identity of the projection neurons was not revealed. In this study a similar method (see Materials and Methods and Results) was used to identify the dendritic activation pattern of neurons in the wS1.

Please refer elsewhere for more details on the principles of two-photon microscopy (e.g. Helmchen and Denk, 2005; Svoboda and Yasuda, 2006), calcium-sensitive dye properties (e.g. Paredes et al., 2008), properties of genetically encoded calcium indicators (Yamada et al., 2011) and general calcium imaging in vivo (e.g. Grienberger and Konnerth, 2012; Helmchen and Waters, 2002; Kerr and Denk, 2008).

1.4. Dendrites and spines

Neurons are polarized structures with multiple dendrites to receive information from other neurons and a single axon to transmit information to other neurons. Traditionally dendrites were considered to be passive structures with features predicted by the cable theory. However, they were shown to contain ion channels for the active conduction of signal. Spines are small protrusions on the dendrites of excitatory neurons, and are considered to be the sites of excitatory signal transmission. In the following the main features of dendrites and spines will be very shortly summarized. As in case of the other parts of the introduction, readers are referred elsewhere for more details.

The dendrites of pyramidal neurons were shown to contain, among others, voltage-gated sodium (Huguenard et al., 1989) and calcium channels. The voltage-gated calcium channels can be subdivided into several subtypes (L-, N-, P/Q-, R-type, see Markram et al., 1995). APs actively invade the dendritic tree via the activation of voltage-gated sodium channels (Stuart and Sakmann, 1994). This depolarization triggers calcium influx through the voltage-gated calcium channels (Markram et al., 1995). In fact, the backpropagating AP evoked calcium transients are widely used indicators for neuronal firing (e.g. Svoboda et al., 1997) and for the frequency of AP firing (Helmchen et al., 1996). Backpropagating APs are also present in in vivo conditions (Svoboda et al., 1997). The invasion of backpropagating APs occured to be distance dependent both under in vitro (Schiller et al., 1995) and in vivo (Svoboda et al., 1999) conditions. Subthreshold activation (EPSP) was also shown to produce dendritic calcium signal in vitro (Markram and Sakmann, 1994), and recently in vivo (Jia et al., 2010). However, in the first study the dendritic signal was shown to originate from EPSP activated voltage-gated calcium channels, while in the latter in vivo study the dendritic signal was attributed to synaptic activation of NMDA receptors. The backpropagating AP evoked calcium signal had different amplitude in different subcellular compartments (Schiller et al., 1995). Finally, both in vitro and in vivo conditions, supralinear calcium influx was observed in the tuft of pyramidal neurons when backpropagating AP was paired with synaptic input (Waters et al., 2003). Here some of the features of the dendrites of neocortical pyramidal neurons were collected, however

dendrites of hippocampal pyramidal neurons, cerebellar Purkinje cells and various interneurons are also in the focus of research. For review see for example Higley and Sabatini (2008), Johnston et al. (1996), Regehr and Tank (1994).

Similarly to dendrites, spines are studied extensively. The dendritic spine head also contains active conductances, such as NMDA receptors (Schiller et al., 1998), voltage gated calcium channels (N-, P/Q- and T-subtypes, see Schiller et al., 1998; in hippocampus Kovalchuk et al., 2000; Sabatini and Svoboda, 2000) and AMPA receptors (in cortex Takahashi et al., 2003; in hippocampus Takumi et al., 1999). NMDA and AMPA receptors are ionotropic glutamate receptors. Similarly to dendrites, AP invades spines as well (in hippocampal CA1 pyramidal neurons Yuste and Denk, 1995; in pyramidal neurons Schiller et al., 1998; in spiny stellates Nevian and Sakmann, 2004). In resting state, the conductance of NMDA receptors is blocked by an extracellular magnesium ion (Nowak et al., 1984). During depolarization, due to either backpropagating AP or synaptic input through AMPA receptors, the magnesium block is relieved and the current can flow. The current through the NMDA receptor is a mixture of sodium, potassium and calcium ions. This calcium entry can be detected with calcium-sensitive dyes (e.g.in hippocampal CA1 pyramidal neurons Yuste and Denk, 1995; for protocol see Yasuda et al., 2004). However, until recently the in vivo separation of backpropagating AP and synaptic input evoked calcium signal met some difficulties (Chen et al., 2011). Studying subthreshold events evoked calcium signals in spines showed the localization of the signal to individual spines without affecting the neighboring dendritic parts (in hippocampus Guthrie et al., 1991; Müller and Connor, 1991; Yuste and Denk, 1995). The spatial restriction of the signal can function as biochemical and/or electrical compartment providing specificity to synaptic changes. The spine neck is considered to be one of the major contributors to compartmentalization (Araya et al., 2006a; Araya et al., 2006b; in hippocampus Svoboda et al., 1996). Moreover, the diffusion through the spine neck is regulated by neuronal activity (Bloodgood and Sabatini, 2005). The calcium dynamics in spines were shown to be influenced by the spine neck, the surface to volume ratio of the spine head, and internal buffer and extrusion mechanisms (Sabatini et al., 2002), additionally the position of the spine on the dendritic tree also can also have a significant effect (Holthoff et al., 2002). Finally, the interaction between subthreshold and suprathreshold

signals can produce supralinear calcium accumulations in spines only if the subthreshold precedes the suprathreshold signal by a short time interval (in L5 neurons: Koester and Sakmann, 1998; Schiller et al., 1998; in spiny stellates: Nevian and Sakmann, 2004). These properties might have implications in synaptic plasticity (e.g. Nevian and Sakmann, 2006). For reviews on spine imaging and spine function, see, among others, Bloodgood and Sabatini (2007); Denk et al. (1996); Higley and Sabatini (2008); Rochefort and Konnerth (2012); Siegel and Lohmann (2012); Yuste (2011).

At last the phenomenon of dendritic spikes should be mentioned. Dendritic spikes are the simultaneous all-or-none activation of dendrites and spines in a localized region, and are supposed to facilitate signal transmission to the soma. Dendritic spikes are associated with supralinear calcium summation in the activated region. Dendritic spikes were described in vitro in the basal dendrites of L5 neurons (Schiller et al., 2000; as NMDA-spikes), in the distal tuft of L5 neurons (Larkum et al., 2009; as NMDA-spikes), and in the apical dendrites of L2/3 neurons (Larkum et al., 2007).

2. Aims

The aim of the present study was to identify the spatial properties of whisker stimulation evoked excitatory synaptic inputs reaching L2 and L4 excitatory neurons in the barrel cortex of the mouse with two-photon calcium imaging. This spatial map could help to clarify the following points.

1. Since L4 is traditionally considered to be the layer where sensory information enters the cortex and L2 is associated with higher order cortical functioning (see section 1.1.3.3.), comparing the spatial distribution of inputs reaching neurons in these layers could help to understand whether there is a difference of input organization in layers with different function.
2. Comparing the distribution of PW- and SW-stimulation evoked synaptic inputs could help to understand the receptive field properties of neurons (see section 1.2.1.).
3. The previous studies mapping synaptic inputs were performed in cortical regions without clear columnar organization and found no obvious spatial structure of the inputs (Jia et al., 2010 and Chen et al., 2011). Studying the input distribution in neurons located in a brain region with cortical columns (see section 1.1.3.) could help to clarify the effect of cortical columns on cellular functioning.

3. Materials and methods

All experimental procedures were performed in accordance with institutional animal welfare guidelines and were approved by the state government of Bavaria, Germany.

The materials and methods sections for L2 experiments were previously published (Varga et al., 2011).

3.1. Animals and surgical procedures

3.1.1. L2 experiments

C57BL/6 mice of both sexes were used for in vivo dendrite (n=12, P27-38) and spine (n=4, P29-38) imaging experiments. Mice were bred under standard caging conditions.

Anesthesia was induced by 1.5% isoflurane (Curamed, Karlsruhe, Germany) vaporized in pure oxygen. After reaching deep anesthesia level (negative tail pinch reflex), the animals were put on pre-heated heating plates. Throughout the surgery, the animals' body temperature was monitored and kept at 37 °C. Eye ointment (Bepanthen, Bayer) was applied on both eyes to prevent dehydration.

With the exception of 2 whiskers (C2 and E2, D2, C4 or C1) on the right side of the snout, all macrovibrissa were plucked with forceps and all visible microvibrissa were cut by scissors on both sides under dissecting microscope. The flexible tips of the whiskers were cut to aid insertion into glass pipettes used for whisker stimulation.

Lidocaine (Xylocaine, 2%, AstraZeneca) was locally applied to the head by injection subcutaneously. The dorsal part of the skull was exposed by removing the skin with surgical scissors. The periosteum was removed with scalpel blade and the surface of the bone was dried and abraded with sand paper (P80). Custom-made recording chamber (Garaschuk et al., 2006) was attached to the left side of the skull with cyanoacrylic glue (UHU, Germany).

The position of the cortical barrel columns related to the spared whiskers was determined with intrinsic signal optical imaging (see section 3.3). During intrinsic signal optical

imaging body temperature was kept at 37.5°C and breathing rate was set to 100-130 beat per minute (bpm) with reducing isoflurane concentrations (0.8-1%).

Following intrinsic signal optical imaging the animal was transferred back to the dissection station and the depth of anesthesia was increased with increasing isoflurane concentrations (1.1-1.3%). The skull was thinned by drilling, and a small craniotomy (~ 0.8 x 0.6 mm) was opened above one of the identified barrels (usually C2) with a 30G injection needle (Sterican, B.Braun). The exposed cortical region was covered with 2-3% agarose gel dissolved in Ringer solution (~ 1-2 mm thick) to reduce vibrations of brain tissue.

The animal was transferred to the imaging setup and the recording chamber was perfused with warm (37°C) Ringer solution containing: 125 mM NaCl, 26 mM $NaHCO_3$, 4.5 mM KCl, 2 mM $CaCl_2$, 1.25 mM NaH_2PO_4, 1 mM $MgCl_2$, 20 mM glucose, pH 7.4 when bubbled with carbogen. The isoflurane concentration was reduced to 0.8-1% to achieve lighter anesthesia (breathing rate ranged between 100-120 bpm) during recordings. Throughout the recordings the animal's body temperature was maintained at 37.5°C.

3.1.2. L4 experiments

For L4 experiments C57/BL6 of both sexes were used. The age of animals ranged from P27 to P38. Caging conditions and surgical procedure were identical to those in L2 experiments, except for the size of the craniotomy. The size of craniotomy was approximately twice as large as for L2 experiments to allow longer penetration tracks of the pipettes. Whiskers C2 and E2 were spared on the right side of the snout neurons with dendritic imaging. For a subset of experiments only whisker C2 was spared.

3.2. Whisker stimulation protocol

3.2.1. L2 experiments

The whisker stimulation protocol was identical during intrinsic signal optical imaging and two-photon calcium imaging. Whiskers were inserted in glass capillaries attached to piezo actuators and deflected approximately 30° in rostrocaudal direction. A pulse stimulator (Model

2100, A-M systems) delivered for each trial a train of voltage pulses (10 pulses, 50 ms, 10 Hz) driving the piezoelectric actuators. In each trial only one whisker was stimulated. During the 8-second sessions of two-photon calcium imaging, the train of whisker stimulation started 3 seconds after the start of image acquisition ("pre-set mode", see section 3.6.1.).

3.2.2. L4 experiments

The whisker stimulation procedure and the stimulation protocol during intrinsic signal optical imaging were identical to those used in L2 experiments. However during two-photon calcium imaging, instead of a train of deflections, the sensory stimulus was a single 2-second deflection of individual whiskers. One recording session lasted for 30 second, and contained 3-6 deflections at time points chosen by the experimenter online ("arbitrary event mode", see section 3.6.2.).

3.3. Intrinsic signal optical imaging

3.3.1. L2 experiments

The location of the barrel columns related to the spared whiskers was mapped on the cortex with intrinsic signal optical imaging through the intact skull. The intrinsic signal optical imaging setup was mounted on the two-photon microscope. During intrinsic signal imaging, one of the oculars was replaced by a camera (National Instruments smart camera, NI-1744, pixel resolution cropped to 1024 x 1024), and the microscope objective was replaced by a camera lens (Olympus, 50 mm / f3.5) inversely oriented (back focal plane on the cortex). The field of view was 1.1 x 1.1 mm. Illumination was provided by a green (515-530 nm) and a red (620-625 nm) LED-array attached to the camera lens. Green light was used to acquire the blood vessel map of the cortical surface; red light was used to record the functional map of the barrels. Images were acquired with custom-made acquisition software in LabView of an image acquisition frequency of 10 Hz. Acquired images were spatially filtered with a Gaussian kernel of 5x5 pixels. Image acquisition protocol consisted of two 1-second acquisition period repeated 10 times. The first acquisition period was just after the offset of whisker stimulation, the second

(baseline) was at 16 second after the stimulation. Relative reflectance changes were calculated as the summed images acquired during stimulation divided by the summed baseline images. The two whiskers were mapped in consecutive sessions.

3.3.2. L4 experiments

For L4, intrinsic signal optical imaging procedure and protocol were identical to those in L2 experiments, except that the field of view was increased to 2.2 x 2.2 mm.

3.4. Filling the neurons with calcium-sensitive dye

3.4.1. L2 experiments – two-photon targeted whole-cell configuration

Whole-cell recordings of L2/3 neurons were established with the "shadow patching" approach (Kitamura et al., 2008) in the column C2 of the barrel cortex. Patch pipettes with resistances of 5-8 MΩ were pulled from borosilicate glass capillaries on a vertical puller (PC-10, Narishige). The intracellular patch solution contained 112 mM K-gluconate, 10 mM HEPES, 8 mM KCl, 10 mM Na-Phosphocreatine, 4 mM Mg-ATP, 0.3 mM Na2-GTP, 2 mg/ml biocytin, 100 µM Oregon Green 488 BAPTA-1 hexapotassium salt, 25 µM Alexa Fluor 594 hydrazide sodium salt.

3.4.2. L4 experiments – two-photon targeted single cell electroporation

L4 neurons in column C2 of the barrel cortex were electroporated with an ELC-03XS (NPI) amplifier triggered with a pulse stimulator (Model 2100, A-M systems). The electroporation pipettes were pulled from borosilicate glass capillaries on a vertical puller (PC-10, Narishige), and had a resistance of 5-6 MΩ. The electroporation solution contained 18 mM Oregon Green 488 BAPTA-1 hexapotassium salt dissolved in 130 mM NaCl solution. When approaching L4, 60 nA bias current was applied to the electrode to keep dye in the pipette and allow only a slight leak. The dye leaking out of the pipette was used to visualize the "shadows" of neuronal somata (similarly to "shadowpatching" in Kitamura et al., 2008) Individual neuronal somata located

420-460 µm below the pial surface were electroporated with two 50-ms pulses of -500 nA current applied to the electrode.

3.5. Electrophysiological recordings

3.5.1. L2 experiments – whole-cell recordings

In L2 experiments the dye delivery method of whole-cell configuration provided a convenient method for the monitoring of electrical activity of neuron. Current-clamp recordings were acquired with an EPC-9 HEKA amplifier through software Pulse. Signals were filtered at 3 kHz and digitized at 10 kHz. Series resistances ranged from 20-60 MΩ. During two-photon calcium imaging the cells were slightly hyperpolarized to prevent backpropagating action potential evoked global calcium changes. For this purpose, negative current was injected through the patch pipette in steps of -10 pA, until action potential firing vanished. Over the course of the recording the injected current level was adapted to the condition of the neurons, and, if necessary, more negative current was injected. Neurons were not hyperpolarized below -85 mV. The hyperpolarized and non-hyperpolarized membrane potential values were in the range of resting potentials reported previously in the rat L2/3 neurons (-85 mV to -60 mV, Svoboda et al., 1999).

3.5.2. L4 experiments – loose cell-attached recordings

Having the cell filled with dye, the electroporation pipette was retracted, and a cell-attach pipette was inserted into the same track targeting the electroporated neuron. The pipette resistance ranged between 5-6 MΩ. The cell-attach pipette contained 12.5 or 25 µM Alexa Fluor 594 hydrazide sodium salt dissolved in extracellular solution (140 mM NaCl, 5 mM KCl, 2 mM $CaCl_2$, 1 mM $MgCl_2$, 10 mM HEPES, pH 7.4). Once reaching the electroporated neuron, a seal of 20-50 MΩ was established. Because of the loose seal the electrode picked up both the electrical activity of the attached neuron and an LFP component of a larger area.

3.6. Synchronization of electrical recordings with calcium imaging and stimulation timing

3.6.1. L2 experiments – "pre-set mode"

The FPGA module in the image scanning control system was programmed to generate a 'startup' trigger signal (TTL pulse of 5 μs) at the first pixel of the first image frame to be recorded. This signal instantaneously triggered the data acquisition of electrical recordings as well as the pre-set timer (typically 3 seconds) of whisker stimulation device. Both imaging and electrical recordings sessions stopped at a pre-set time (typically 8 seconds), and then the experimenter commanded to start the next session.

3.6.2. L4 experiments – "arbitrary event mode"

The 'startup' signal was generated the same way as in the previous mode, and it triggered the electrical recording device. However, instead of using a pre-set timer, the stimulation device executed stimulation command upon additional trigger signals that were sent by the experimenter at any arbitrary time during the session of imaging. Multiple stimulation events were generated within one recording session (3 to 6 events in 30-second long session). The exact time of whisker stimulation was registered by both the imaging system (as frame numbers) and the electrical recording system (as pulse waveforms in the second channel).

3.7. Two-photon calcium imaging

3.7.1. L2 experiments

Two-photon calcium imaging was performed on a custom built setup which was similar to that used in previous study (Jia et al., 2010). A resonant scanner unit (GSI Lumonics) including one fast axis of 12 kHz resonant mirror and one slow axis of standard galvanometric mirror was mounted on upright microscope chassis (BX51, Olympus) with long working distance water-immersion objective (Nikon 40x / 0.8). Fluorescent excitation light was delivered by pulsing infrared laser (wavelength 800 nm, pulse width 100 fs, repetition rate 80 MHz) equipped with pre-chirper (model "Mai-Tai DeepSee", Spectra-Physics). Laser power was

modulated by a Pockels cell (Conoptics Inc.). For visualizing multiple dendrites in one field-of-view, the power under the objective was typically 30-40 mW. Emitted fluorescent photons were separated by a beamsplitter mirror at 570 nm (F33-572, AHF Analysentechnik) and detected by high-sensitivity photomultiplier tubes (H-7224, Hamamatsu) and analog current amplifiers (DHPCA-100, FEMTO Messtechnik). The laser scanning, image acquisition and stimulation triggering were controlled by a real-time PXI computer (PXIe-1082, National Instruments) equipped with FPGA I/O board (PXI-7831R) and high-speed digitizer (PXI-5122). The user interface software was developed in LabVIEW (v2009) on an 8-core PC connected to the PXI computer. Full frame images consisted of 512 lines, and were scanned at 40 Hz repetition rate. Each line had 1041 raw pixels that were digitized at 25 MHz (100 MHz internal sampling rate) and reconfigured into 512 pixels according to the sinusoidal trajectory of the resonant mirror. Neurons were imaged in 6-11 focal planes distributed across the whole depth of the dendritic tree. The actual width of the field-of-view (controlled by the amplitude of scanning mirror rotation) ranged between 100-200 μm, depending on the layout of dendrites in the focal plane. Each focal plane was probed with 10 trials of PW and 10 trials of SW stimulation. Trials were interlaced (5 PW trials followed by 5 SW trials, repeated twice) with variable time intervals (10-20s) between two consecutive trials. For display purposes (Fig. 7; and for spines, Fig.10), the trials with the same whisker stimulation were grouped together. Z-stack images were taken at the largest possible field-of-view (300 μm x 300 μm) with a step size 0.5 μm.

The same two-photon imaging setup was used for the imaging of single spines. For the implementation of the low power temporal oversampling (LOTOS) procedure (Chen et al., 2011), the scanner was configured for the following mode: the number of lines was reduced to 64, the number of pixels in each line resampled to 256, and the image repetition speed increased to 200 Hz. The width of field-of-view was accordingly reduced to the range of 27-42 μm. Altogether, the spatial oversampling was 2x2 fold and temporal oversampling was 5 fold, compared to the mode for dendritic imaging as described above. Laser power was reduced to 15-25 mW during spine imaging. Recording protocol for the spine imaging was the same as for the dendritic imaging, except that only C2-E2 whisker configuration was used. Z-stack images of the spines were taken with step size 0.2 μm

3.7.2. L4 experiments

For L4 experiments the same two-photon imaging setup was used as for L2 experiments. The scanner configuration for L4 spine imaging was identical to that for L2 spine imaging (number of lines 64, pixel number in each line 256, image repetition speed 200 Hz). The width of field of view on both axes ranged approximately between 15-40 µm. The wavelength of laser was set to 920 nm to improve imaging quality in deeper tissue. Laser power ranged from approximately 30-120 mW, depending on the actual size of the field-of-view and the depth of the focal plane. In experiments with 1 or 2 whiskers each focal plane was imaged for 300 or 600 seconds in 30-second sessions, respectively. In 2-whisker experiments the sessions for the 2 whiskers was interlaced (150 second intervals, repeated twice). At the end of each experiment, Z-stack images were taken with a field of view of 300x300 µm and step size 0.5 µm.

3.8. Drug application

3.8.1. L4 experiments

1 mM D-AP5 (D-(-)-2-Amino-5-phosphonopentanoic acid, Tocris) dissolved in AF594 containing extracellular solution (described section 3.5.2) was applied to dendrites of L4 neurons. The drug solution containing pipette was inserted to reach the proximity of the electroporated neuron under visual control. Drug solution was pressure injected for few seconds (approximately 3 seconds with 150 mbar) directly before imaging.

3.9. Post-hoc procedures

3.9.1. L2 experiments

The exact location of each neuron recorded was documented by epifluorescence imaging and marked on the map of barrels aligned by the blood vessel map.

After the two-photon calcium imaging of the patched neuron, mice were overdosed with Ketamine/Xylazine and perfused with 0.1 M phosphate buffered saline followed by 4%

paraformaldehyde. Brains were removed and post-hoc fixed in 4% paraformaldehyde overnight. Slices of 100 µm thickness were cut with a Leica VT 1000S vibratome. Barrels were stained with cytochrome-c staining (Wong-Riley, 1979), and the patched neuron was visualized through biocytin-avidin reaction (Lubke et al., 1996). Stained slices were mounted on slides in the mounting medium Eukitt (Fluka, Sigma-Aldrich).

3.10. Data analysis

3.10.1. L2 experiments

The structural reconstruction was performed using the WCIF-ImageJ software (open access from http://www.uhnresearch.ca/facilities/wcif/imagej/), the whole-cell recordings were analyzed in Igor (Igor Pro v5.0.1.0, Wavemetrics Inc.) and the calcium imaging recordings were analyzed by custom-written programs in LabVIEW (version 2009, National Instruments). Statistical tests were performed in SPSS (version 17.0, IBM). Z-stack images of spines were deconvolved in Huygens (version J27.14, Scientific Volume Imaging BV) and volume rendered in Amira (version 5.3.3, Visage Imaging Inc.).

3.10.1.1. Reconstruction of dendritic trees. The projections for top-views and side views were generated from the z-stack images from the Alexa-channel of the two-photon microscope. The lengths of dendrites for each recorded focal plane were measured by the internal scale function in ImageJ.

3.10.1.2. Calculation of whisker-evoked subthreshold membrane potential depolarization. For each neuron and each whisker, 100 trials of subthreshold membrane potential recordings were averaged and aligned to the baseline of 0.2 second before stimulation onset. The stimulation evoked depolarization was defined as the mean value of membrane potential of the 1 second of stimulation time window subtracting the mean value of the baseline. To compare the result among neurons, the SW-evoked depolarization was normalized to the maximum value of PW-evoked depolarization.

3.10.1.3. Spatial-temporal filtering of calcium imaging data and transformation into Δf/f image sequences. First, each image from the Oregon Green-channel was convolved with a Gaussian

spatial filter kernel (size: 1 μm). The temporal sequence of images was processed with exponentially-weighted averaging, and transformed into a new temporal sequence of Δf/f images representing the time-dependent relative change of each pixel. This calculation was similar as described previously (Jia et al., 2011) except that it was performed for every pixel instead of manually chosen regions-of-interest. Static color-coded images in Fig. 6 were taken as the maximum projections of Δf/f image sequence for the stimulation time window and rendered by a color lookup table. For display purpose in figures, we used square ROIs to indicate the location of active hotspot sites.

3.10.1.4. Calculation of global dendritic calcium signals. For each trial, the Δf/f image temporal sequence was projected for the entire stimulation time window and thresholded at the Δf/f value of 0.3. All pixels above threshold appeared as isolated patches of dendrites, and were taken together as one region-of-interest (ROI). The Δf/f trace of this ROI was calculated by the same algorithm as in the previous point. To normalize the Δf/f trace of all trials for the same whisker for one neuron, each trace was multiplied by the number of above-threshold pixels in the corresponding hotspot and then summed. The peak value of the summed trace for PW trials was taken as 100% for normalization.

3.10.1.5. Detection and categorization of dendritic hotspot sites. For each stimulation (1-second duration), every 4 frames (100-millisecond duration) of the Δf/f image temporal sequence were maximum-projected as one image. These projected Δf/f images were thresholded at the value of 0.3. Patches with above-threshold pixels were registered to separate ROIs according to the position of the pixels. The time course of Δf/f for these ROIs was re-calculated for 8 seconds (including 3 seconds before stimulation onset and 4 seconds after stimulation offset). If the peak amplitude of Δf/f trace in the stimulation time window was greater than 4 times standard deviation of the trace in the non-stimulation time window, the signal was considered as a response event. Hotspot sites were defined by overlaying response events over all trials. The response probability for hotspot sites was defined as the number of response events occurred at one site divided by the total number of trials. A hotspot site is defined as PW-specific if the PW-response probability is 3 times higher than SW-response probability, and vice versa as for SW-specific hotspot site. If the response probabilities to both whiskers are non-zero and to

neither whisker is 3 times higher than to the other whisker, the hotspot site is defined as shared.

3.10.1.6. Calculation of calcium signals of individual spines (applies to 200 Hz spine imaging only). For each focal plane, the dendritic shaft was segmented with consecutive square box-like ROIs (about 1 µm) and, in addition, ROIs were drawn for each discernible spine. The calcium signals of the ROIs were calculated as indicated above. The categorization in whisker-specific and shared spines was the same as that for the dendritic hotspot sites.

3.10.2. L4 experiments

3.10.2.1. Reconstruction of dendritic trees. The projections were generated from the z-stack images from the Oregon Green-channel of the two-photon microscope. The lengths of dendrites for each recorded focal plane were measured by the internal scale function in ImageJ.

3.10.2.2. *Automatic recognition of stimulation evoked responses*. For each visible spine, a circle best fitting with the spine head was defined manually as ROI for that spine. Fluorescence change in these ROIs were calculated as Δf/f for all recording sessions and cut into 2500 ms segments around the time of stimulation (500 ms before stimulation, 2000 ms after stimulation). Evoked transients were recognized as following. First, the median Δf/f value of 250 ms before stimulation onset was subtracted from the Δf/f values of the 2500 ms segments to compensate for baseline drifts or incomplete decay of a preceding transient. Second, a noise band was calculated as root-mean-square of the high-pass filtered (cut-off 3.5 Hz) Δf/f trace. Third, a peak point (local maximum) was identified in the time-window of 400 ms from start of stimulation. If the amplitude to the peak point was five times higher than the amplitude of the noise band, the trial was recognized as responsive trial in that given spine.

3.10.2.3. Calculation of response onset time. For each spine with at least 4 responsive trials, a common onset time of the responses was calculated. The common time of onset was defined as the time point 5 ms (i.e. 1 frame) before the point where the Δf/f values were significantly higher than the Δf/f values at 0 ms (i.e. the time of stimulation). Significance was tested with paired t-test (cut-off $p < 0.05$).

3.10.2.4. Calculation of subthreshold response probabilities. For each spine, the number of responsive subthreshold trials (identified as described in section 3.10.2.2.) divided by the total number of subthreshold trials. If the total number of subthreshold trials was less than five, the whole focal plane was discarded. In the Results section response probabilities are expressed in percentage by multiplying the above calculated number with 100.

3.10.2.5. Classification of short latency spines. A spine was identified as a short latency spine if the response onset time was 10 ms.

4. RESULTS

4.1. L2 neurons

4.1.1. Imaging dendrites of L2 neurons in the mouse wS1

This study characterizes the spatial and temporal organization of inputs to single neurons. To achieve this, a recent technique (Jia et al., 2010; Chen et al., 2011) of simultaneous in vivo whole-cell recording and calcium imaging was performed on L2 neurons in the barrel cortex of anesthetized mice. L2 neurons were patched in the C2 barrel related column (Fig.1.A), and the responses evoked by the stimulation of single whiskers (C2, the PW and another SW) were mapped on the dendrites of the patched neuron with two-photon calcium imaging. The whole-cell configuration allowed the filling of the neuron with calcium-sensitive dye Oregon Green BAPTA-1 hexapotassium (see Materials and methods section 3.4.1.), as well as monitoring and manipulating the membrane potential of the neurons. The whisker stimulus started 3 seconds after the start of recording and consisted of 10 deflections in 1 second (Fig.1.B). The 3-second recording before stimulation was necessary to establish stable baseline.

To assure that recordings were performed in C2 whisker related column, intrinsic signal optical imaging was used to map the whiskers on the cortical surface. In mice, intrinsic signal optical imaging could be accomplished through the intact skull (Fig.2.A-B). Using the blood vessel pattern as marker, the location of the C2 related column could be identified prior to craniotomy. Thus, the opening of the skull could be targeted to a specific region. As a result, the size of the craniotomy could be decreased and pulsation induced movements were reduced. For each neuron both PW and SW were mapped on the cortex, allowing to measure the distance of the neuron to both whisker related columns. To verify that recorded neurons were indeed in the C2 related column, two post-hoc methods were applied. After each experiment, the whole-cell recording pipette was gently retracted to keep the neuron alive, and a wide-field fluorescent image was taken to identify the exact location of the neuron recorded previously (Fig.2.C). Again with the help of the blood vessel pattern, the relation of the barrel column

position and the neuron location could be identified. Finally, for a subset of experiments (n = 3), mice were perfused and after fixation, 100 µm thick coronal slices were cut. Biocytin-filled neurons were recovered, and barrels were stained (Fig.2.D). In all animals, the biocytin-filled neuron was located above the C2 barrel.

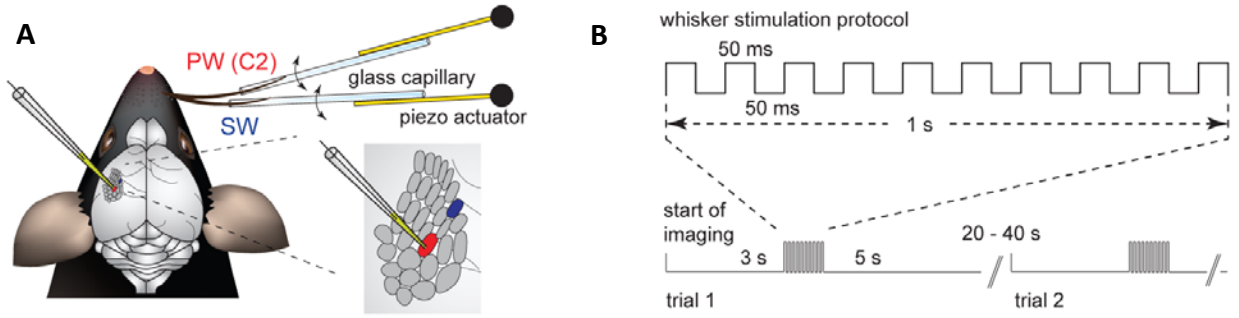

Fig.1. *Overview of experiment design.* ***(A)*** *L2 neurons in the C2 related column in the barrel cortex were filled with a patch pipette containing calcium sensitive dye. The PW and another SW was deflected separately to map the stimulation evoked inputs.* ***(B)*** *Whisker stimulation protocol used during the experiment. In each trial, a train of 10 Hz deflections followed the acquisition of baseline. Figure part A was published in Varga et al. (2011).*

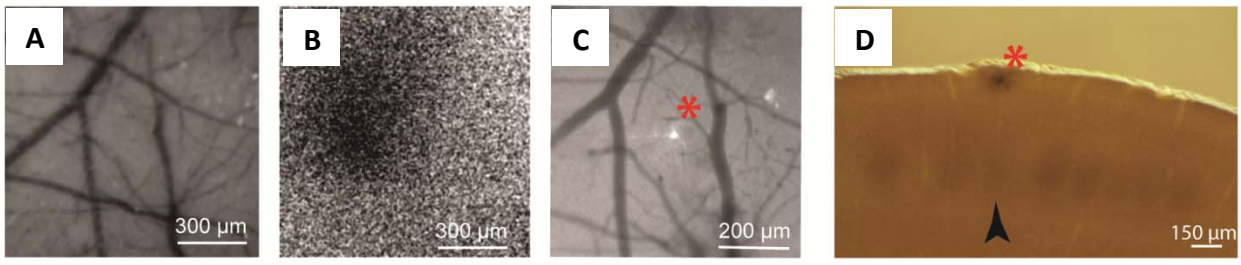

Fig.2. *Targeting neurons in C2 barrel related column.* ***(A)*** *Blood vessel pattern through the intact skull of a P27 mouse under green illumination.* ***(B)*** *The functional map of the C2 whisker on the cortex under red illumination.* ***(C)*** *Post-hoc wide-field fluorescence image of the L2 neuron recorded in the C2 barrel related column. Red asterisk marks the neuron.* ***(D)*** *Coronal slice of the barrel cortex. Black arrow head indicates the DAB-stained C2 barrel, red asterisk mark the biocytin-filled neuron.*

Neuron morphology could be reconstructed from the fluorescent z-stack images acquired after the recordings. An example reconstructed neuron can be seen in figure 3. The recorded neurons lacked any apparent apical dendrite, and they were located at an average depth of 126.5 µm (± 22.48 µm SD, n = 12 neurons) below the pia. These features classify the recorded neurons as L2 pyramidal cells. Overlaying the reconstruction of neuron morphology with the recorded focal planes allowed the identification of the dendrites that were mapped with two-photon imaging (Fig.3.A-B). Recorded dendrites were distributed along the whole dendritic tree and ranged from subpial depths -235 µm to -40 µm (with most dendrites being located between -170 µm and -70 µm). Dendrites were recorded on all sides of the neuron except for the region shaded by the patch pipette. For each neuron approximately 6-11 focal planes were recorded, which is approximately 20-30 % of the dendrites recovered from fluorescent z-stack images.

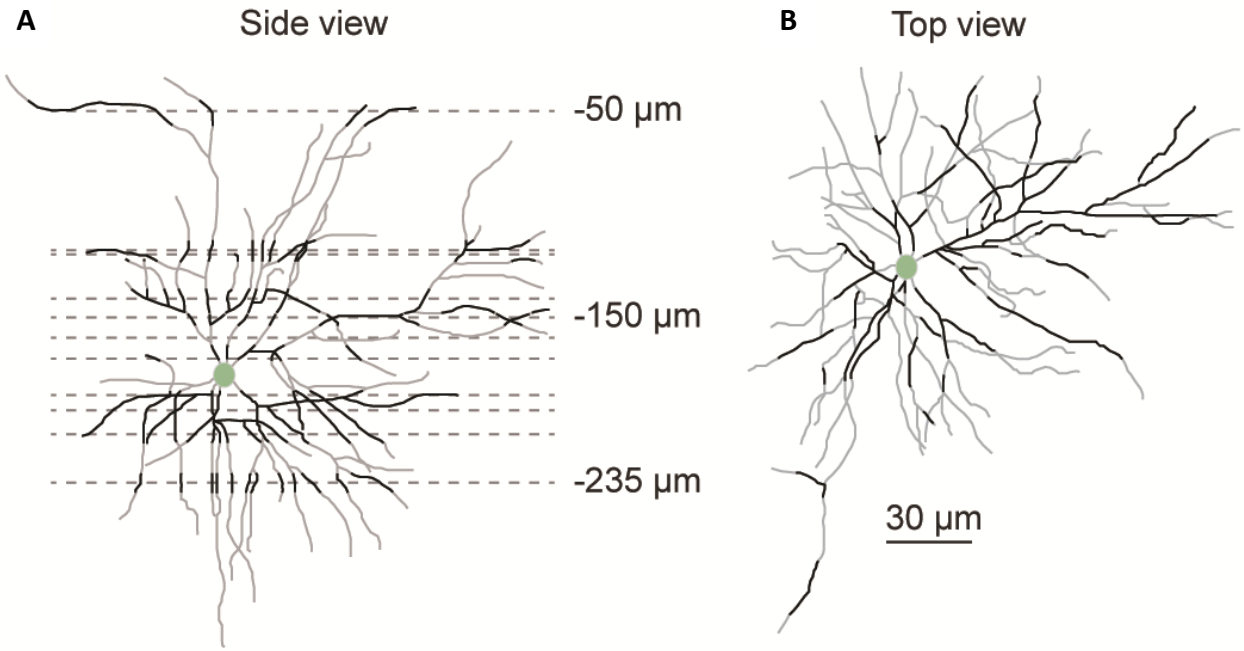

Fig.3. *Neuron morphology reconstructed from fluorescent z-stack images.* ***(A)*** *Side-projection of a reconstructed neuron. Green disc indicates soma, grey lines are dendrites and black lines are dendrites which were recorded with whisker stimulation. Gray dotted lines are depths of the focal planes.* ***(B)*** *Z-projection of the same neuron. Notations are the same as for (A). Figure parts A-B were previously published in Varga et al. (2011).*

Altogether, the neurons which will be further analyzed in the next sections belong to L2 pyramidal neurons, and they were located in the C2 barrel related column of the mouse wS1. The following results emerged from a fraction of all dendrites of the neurons, and these dendrites were located all over the dendritic tree.

4.1.2. Distance dependence of electrical and global calcium signals

To map the sensory stimulation evoked inputs, whole-cell recordings were established on L2 pyramidal neurons in wS1. In addition to filling the neurons with calcium-sensitive dye, the whole-cell configuration permitted the electrical monitoring of membrane potential as well. The average firing frequency in response to PW stimulation was 1.93 Hz (± 1.72 SD, n = 12 neurons, ranging from an average 0.05 Hz to 5.6 Hz with some trials producing APs, others not). The average firing frequency in response to SW stimulation (irrespective of the distance of SW to the neuron) was 1.56 Hz (± 1.58 SD, n = 12 neurons, ranging from an average 0 Hz to 5.4 Hz). The number of evoked APs in one trial ranged from 0 to 16 for both PW and SW.

In order to detect the calcium entry through NMDA-receptors (synaptic input), the calcium entering through voltage-gated calcium channels in response to backpropagating AP should be minimized. For this purpose, neurons were slightly hyperpolarized stepwise until no AP was detected when whiskers were deflected. The average membrane potentials for the 12 cells were -58.5 mV (SEM ±1.5 mV) and -58.4 (SEM ± 1.4 mV) in trials of PW and SW stimulation, respectively. The average hyperpolarized membrane potentials were -67.3 mV (SEM ± 2.2 mV) and -67.4 mV (SEM ± 2.3 mV) in trials of PW and SW stimulation, respectively. Neither the non-hyperpolarized nor the hyperpolarized membrane potentials were significantly different across PW and SW trials (paired *t*-test, p=0.993 for non-hyperpolarized, p=0.848 for hyperpolarized membrane potentials; Kolmogorov-Smirnov test for normality, p=0.200). Thus, neurons were hyperpolarized by an average 8.85 mV. However, for individual neurons the amount of hyperpolarization ranged between 0 and 20 mV, with 67% of neurons were hyperpolarized by 8-12 mV and 25% by 0-3 mV. Even in the hyperpolarized condition, the membrane potential of

individual neurons were in the range of resting membrane potentials previously described (Svoboda et al., 1999) for L2/3 neurons in the rodent barrel cortex (-85 to -60 mV).

As previously mentioned, different SWs were mapped to single neurons in different experiments. Specifically, the immediate neighbor in the row (C1) and in the arc (D2), and the second neighbor in the row (C4) and in the arc (E2) were tested versus the PW. However, since the exact location of the neurons relative to the PW barrel column center varied over experiments, the distance between the neuronal somata and the SW barrel column center depended on both the neuron location and the SW identity. Figure 4 shows the individual neuron distances to both the PW and the SW barrel column center.

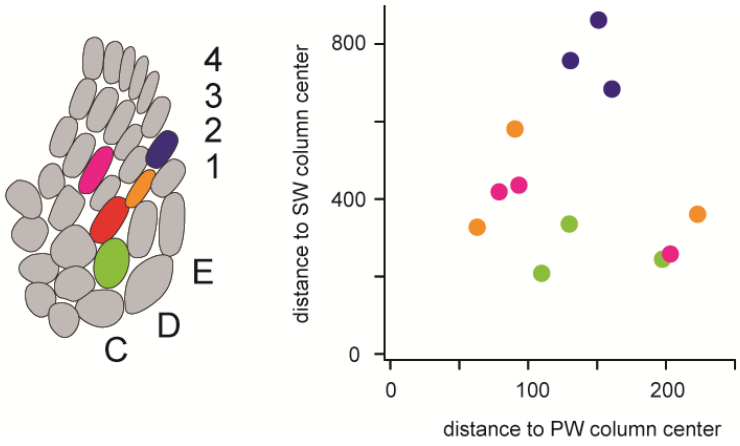

Fig.4. *The location of neuron somata relative to the PW and the SW barrel column center. The left part of the figure is a schematic representation of the barrels. The right part of the figure shows the distances of individual neurons to both the PW and the SW barrel column center. Colors on the left and the right part indicate which SW was tested for the neuron. Blue, orange, green and magenta corresponds to whiskers E2, D2, C1 and C4, respectively. The red barrel in the left figure part represents the PW C2.*

Independently of the distance to the barrel column centers, both PW and SW whisker deflections produced subthreshold depolarization in all neurons. Comparing the area under the curve of average depolarization evoked by PW and SW, whiskers E2, C4, D2 and C1 evoked depolarization that on average occupied 24 % (± 13% SD, n = 3 neurons), 60 % (± 10% SD, n = 3

neurons), 90 % (± 12% SD, n = 3 neurons) and 92 % (± 35% SD, n = 3 neurons) of the area of PW evoked depolarization, respectively. Figures 5 A-B show an example comparing the depolarization evoked by a proximal and a distant whisker. Figure 5 E plots the proportion of SW evoked depolarization in function of distance for individual neurons. The correlation between distance and depolarization was significant (Pearson correlation r = 0.66, p = 0.03).

Similarly, whisker deflections evoked subthreshold calcium transient in all neurons. These calcium transients were localized to distinct regions and were distributed over the dendrites (Fig.5.C). Adding up all calcium signals detected over trials and in different focal planes described the global input reaching the cell upon a virtual PW or SW stimulation (See Materials and Methods section 3.10.1.4 and Fig.5.C). Comparing the PW and SW evoked global signals showed that, similarly to the average membrane potential, the SWs further away evoked smaller calcium signals. An example of a proximal and a distant SW evoked calcium signal relative to the PW evoked calcium signal is shown in Figure 5 D. The correlation between distance and global dendritic calcium signal (Fig.5.F) was significant (Pearson correlation r = 0.62, p = 0.04).

Altogether, in addition to the PW, the SWs which were tested also evoked responses in each neuron. This response was detected as both electrical and calcium signals. Both the electrical and the calcium signal showed distance dependence.

4.1.3. Distribution of inputs to L2 neurons

The calcium transients detected in distinct dendritic regions are called hotspots (Jia et al., 2010). First, an overview will be given on the features of these hotspots, and then their response probabilities will be characterized. The first point is based on characteristics of hotspots evoked by PW stimulation, the second point includes properties of both PW and SW evoked hotspots.

During dendrite imaging, generally one field of view contained several dendrites with various lengths (Fig.6.A). When whisker stimulation was applied, multiple hotspots were readily detected on single dendritic branches within the same trial (Fig.6.B). These hotspots were

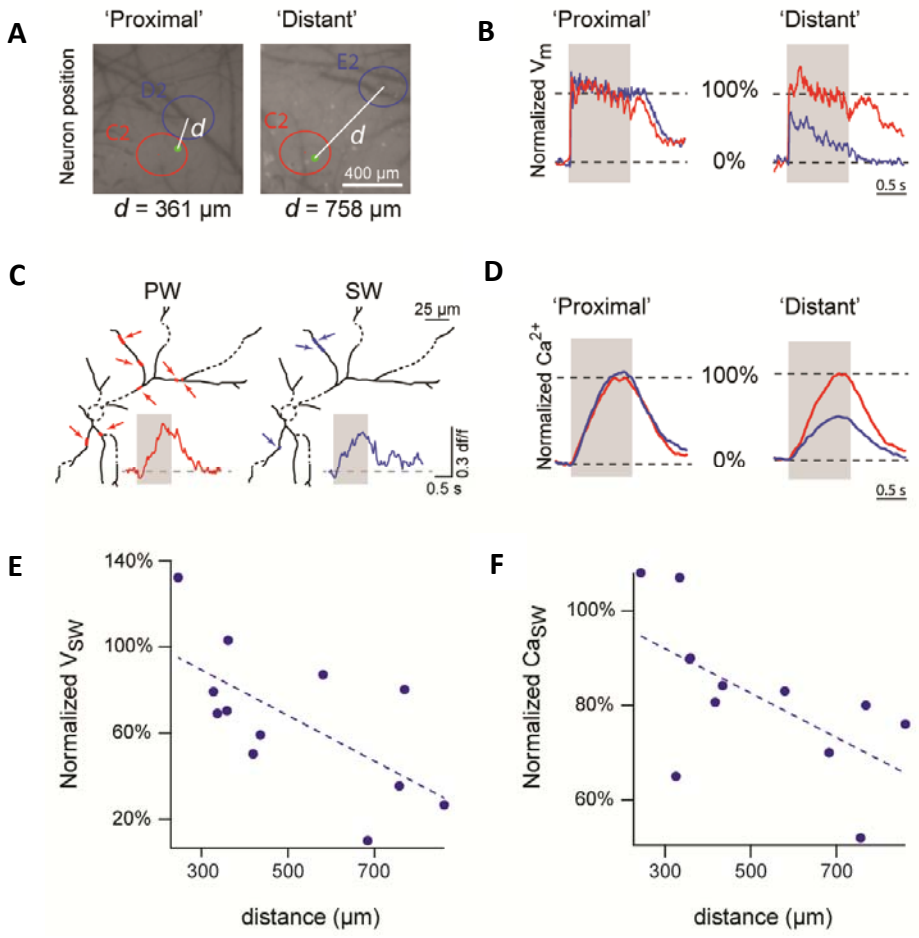

Fig.5. *Distance dependence of electrical and calcium signals.* ***(A)*** *Cortical location of the two example neurons which were mapped for proximal or distant SW. Red and blue circles represent the PW and SW barrel columns, respectively. Green discs mark the location of the neurons. The distance between the neuron and the center of the SW barrel column is denoted with d.* ***(B)*** *The PW and SW evoked depolarization for the example neurons. Red and blue traces indicate the depolarization evoked by PW and SW, respectively. Gray shades mark the time of stimulation.* ***(C)*** *Train of whisker deflections evokes subthreshold calcium transients in the dendrites. Red and blue segments highlighted with arrows are the locations where calcium signals were detected when PW and SW was stimulated, respectively. The calcium transients at the bottom are the sum of the input signals.* ***(D)*** *The PW and SW evoked subthreshold global calcium signals for the example neurons. Notations are the same as for (B).* ***(E)*** *SW-evoked depolarization plotted against the distance between the neuron and the SW barrel column center. Blue discs indicate single neurons; dotted line is the linear fit.* ***(F)*** *SW-evoked global dendritic calcium signal plotted against the distance between the neuron and the SW barrel column center. Notations are the same as for (E). Figure parts A-F were previously published in Varga et al. (2011).*

found to be confined to restricted dendritic regions with both the conventional segmentation method (as described in Jia et al., 2010) and with the color mapping technique (see Materials and methods section 3.10.1.3).

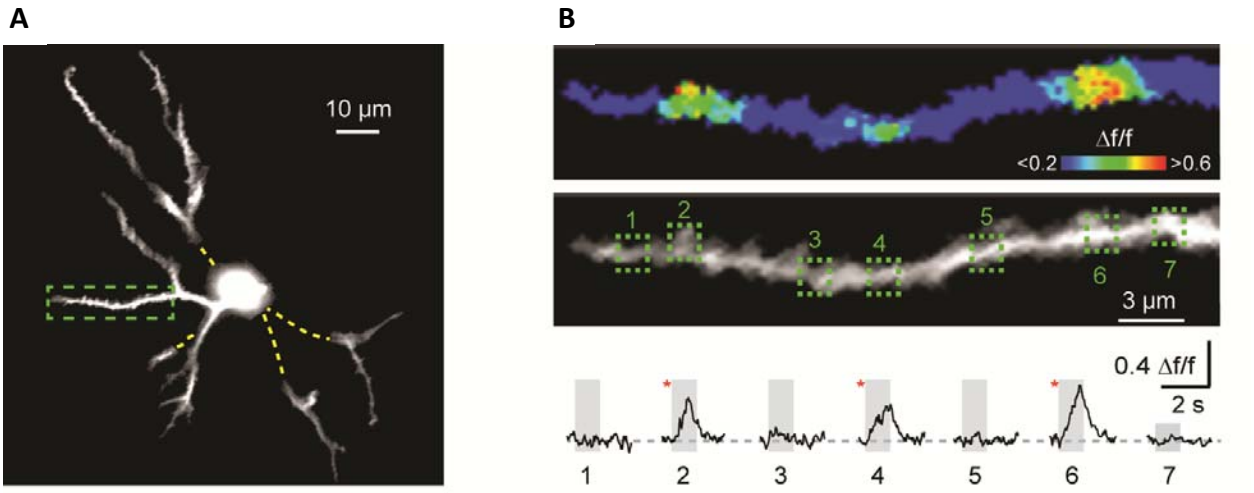

Fig.6. *Single dendritic branches contain multiple hotspots.* ***(A)*** *A typical field of view with multiple dendrite branches in the Alexa channel (average of 280 frames). Yellow dotted lines mark dendrites out of field of view, green box indicates the dendrite shown in (B).* ***(B)*** *The upper panel shows the relative fluorescent change over the 1 second stimulation in the Oregon Green-channel in pseudocolor. The middle panel the average grayscale image of 280 frames in Oregon Green-channel. Green boxes mark dendritic segments corresponding to location of the calcium signals in the lower panel. In the lower panel, red asterisks mark the detected transients and gray shades indicate the time of whisker stimulation. Figure parts A-B were previously published in Varga et al. (2011).*

Following the activity of hotspot sites (i.e. the dendritic region where a hotspot event occurred) showed marked variability over trials (Fig.7.A-B). On the one hand, from trial to trial different hotspot sites were activated within the same focal plane. On the other hand, as a consequence of the pattern variability, the activation of single hotspot sites also varied over trials (Fig.7.C). Thus, from the point of view of the whole neuron, there was a spatial variability in which hotspot sites would activate, and from the point of view of an individual hotspot site, there was a temporal variability in when it would activate. As a result of this variability, many

hotspot sites showed low response probability (Fig.7.D). The response probability distributions for PW and SW evoked responses were similar.

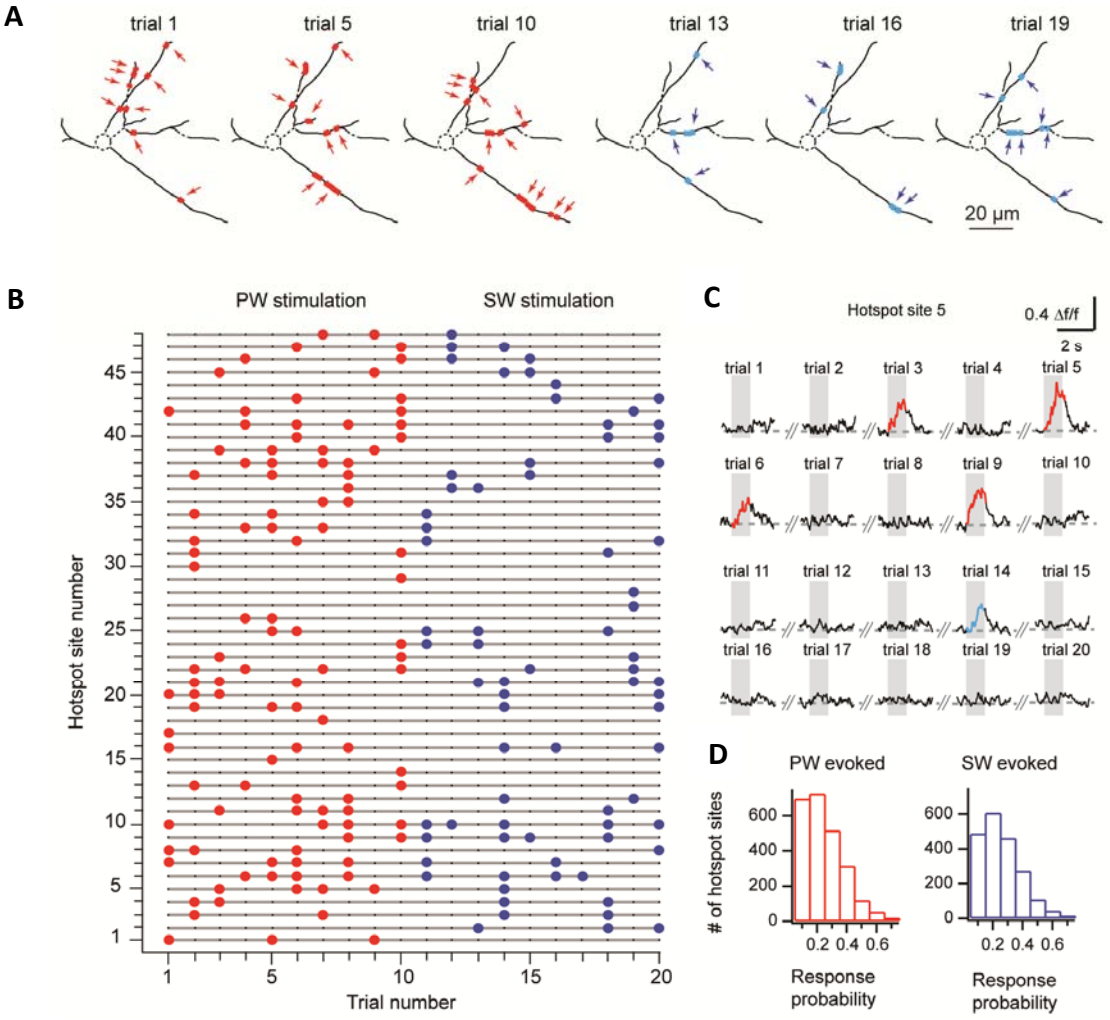

Fig.7. *The activation pattern of hotspots shows marked variability.* ***(A)*** *Example activation pattern of hotspots in response to PW and SW stimulation. Red and blue segments highlighted with arrows are active hotspots where calcium transients were detected.* ***(B)*** *The activation pattern of all hotspot sites in the focal plane shown in (A). Red and blue dots represent hotspot site activated by PW and SW stimulation, respectively.* ***(C)*** *The calcium signals detected in a single hotspot site over trials. Signals highlighted with red and blue are calcium transients detected in response to PW and SW stimulation, respectively. Gray shades represent the time of stimulation.* ***(D)*** *Response probability distributions of hotspots evoked by PW and SW stimulation. Figure parts A-D were previously published in Varga et al. (2011).*

Comparing the activation pattern of individual hotspot sites showed that a large number of hotspot sites were activated by both PW and SW stimulation (Fig.7.B and Fig.8). These sites were denoted as shared hotspot sites. PW-specific, SW-specific and shared hotspot sites were intermingled.

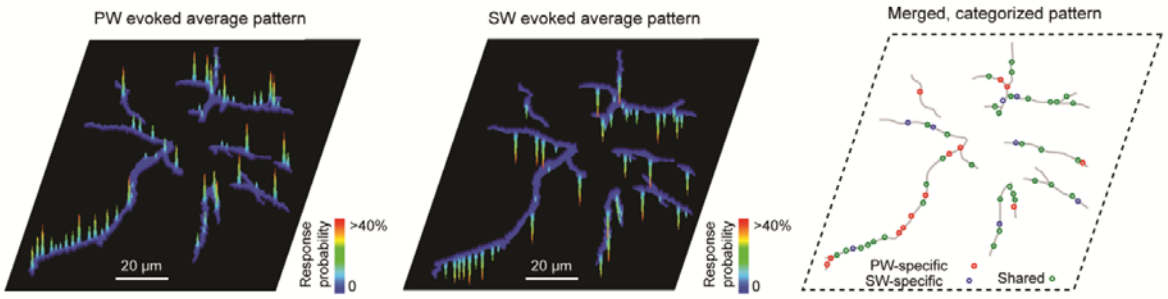

Fig.8. *Shared hotspot sites are activated by both PW and SW stimulation. The left and middle images show the average activation pattern of hotspots in response to PW and SW stimulation, respectively. The right image contains the same sites categorized into PW-specific (red), SW-specific (blue) and shared hotspot sites (green). Figure was previously published in Varga et al. (2011).*

4.1.4. Distance dependence of the number of inputs to L2 neurons

In analogy to the distance dependence of the SW stimulation evoked depolarization and global subthreshold calcium signal described in section 4.1.2., the number of evoked hotspots was also quantified in function of distance. The average number of PW evoked hotspots was 5.36 hotspots/100 µm (± 0.87 SD for n = 12 neurons) of dendrites. No significant correlation was found between the number of PW-specific hotspots and distance (Pearson correlation r = 0.26, p = 0.42). However, the number of SW evoked and shared hotspots depended on the distance between the neuron somata and the center of the SW barrel column. The number of SW evoked and shared hotspot sites is plotted in figure 9 in function of distance. The correlation between the number of hotspots and distance was significant for both SW-specific and shared hotspots (Pearson correlation r = - 0.72, p = 0.008 for SW-specific; r = -0.72, p = 0.009 for shared hotspots). Thus, the distance of SW to the neuron directly affected the number of inputs evoked by SW.

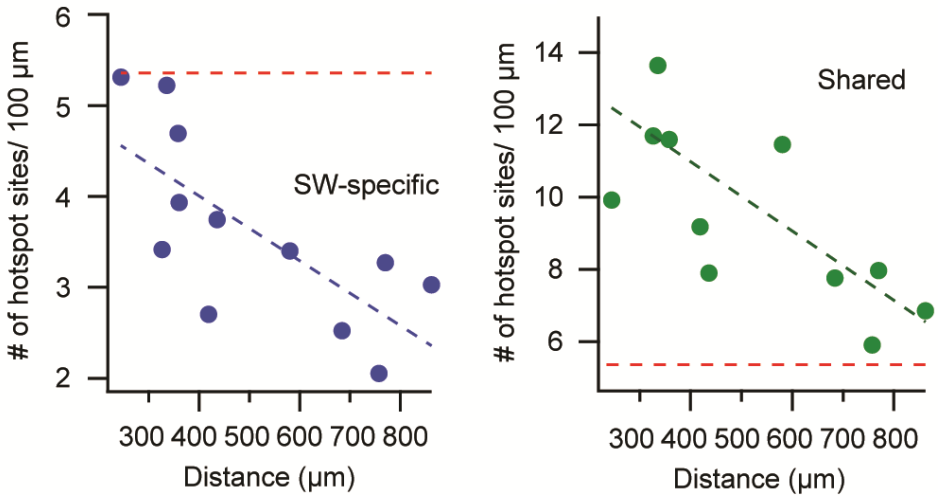

Fig.9. *The number of SW evoked and shared hotspot sites depends on the distance. Blue and green dots represent the SW evoked and shared hotspot values for single neurons, respectively. Red dotted lines represent the average number of PW-specific hotspots. Blue and green dotted lines are linear fittings for the number of SW-specific and shared hotspots, respectively. Figure was previously published in Varga et al. (2011).*

4.1.5. Spine imaging reveals shared spines

Theoretically, shared hotspots could be the result of either non-whisker-specific inputs or closely located PW-specific and SW-specific spines. To distinguish between the two cases, two-photon calcium imaging was performed with spine resolution in the same setup with 200 Hz sampling frequency.

To resolve spines, the sides of the field of view were reduced by 4-5x compared to the field of view used in dendritic imaging (Fig.10.A-B, and see Materials and methods section 3.7.1.). Only spines which had a large cross section of their heads in the focal plane (i.e. spines which protrude to the sides from the dendrite) could be clearly identified (Fig.10.B). Spines below or above the dendrite could not be reconstructed (Fig.10.C). Nevertheless, calcium signals could be detected from single spines (Fig.10.D).

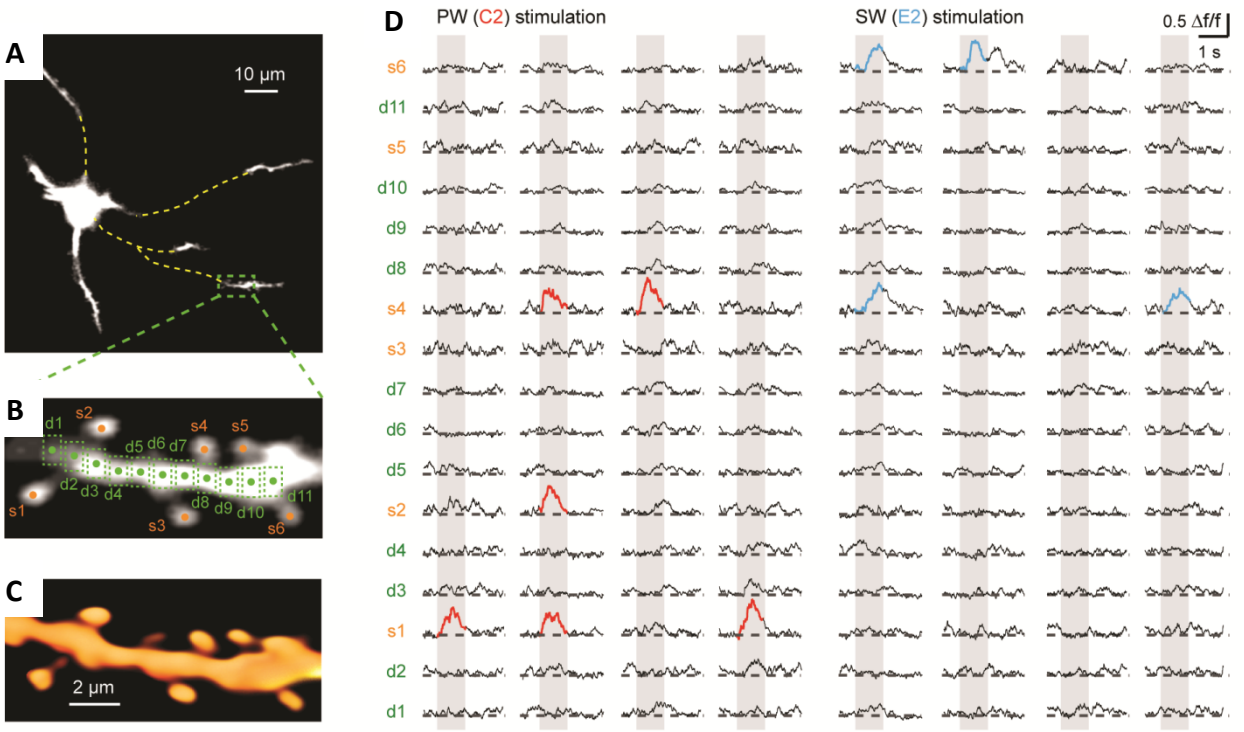

Fig.10. *In vivo spine imaging in L2 neurons in the mouse wS1.* ***(A)*** *Two-photon average image (280 frames) of a layer 2 neuron recorded at full frame at 40 Hz. Yellow dashed lines indicate dendrites out of focal plane, green box mark the dendritic portion shown in (B).* ***(B)*** *Two-photon average image (1400 frames) of a dendritic portion with spine resolution 158 µm below the pia. Orange dots indicate spines and green boxes highlighted with green dots mark ROIs on the dendritic branch.* ***(C)*** *Volume-rendered reconstruction of the same dendritic portion as in (B) from z-stack images.* ***(D)*** *Calcium signals calculated from the ROIs indicated in (B). Signals marked with red and blue are calcium transients detected in response to PW and SW stimulation, respectively. Gray shades indicate the time of whisker stimulation. Figure parts A-D were previously published in Varga et al. (2011).*

Comparing the calcium signals detected in spines and dendritic shafts showed that for the majority of spines the calcium signal was confined to the spine and no signal was detected in the adjacent dendritic shaft (Fig.11.A and C). However, for approximately one third of the spines a small amplitude signal was detected in the directly adjacent dendritic shaft (Fig.11.B and C). The amplitude of calcium signals in the spines was significantly larger than in the shaft (paired t-test, $p<0.001$; Fig.11.D). Backpropagating AP evoked calcium transients in both spines and dendritic shaft (Fig.11.A-B).

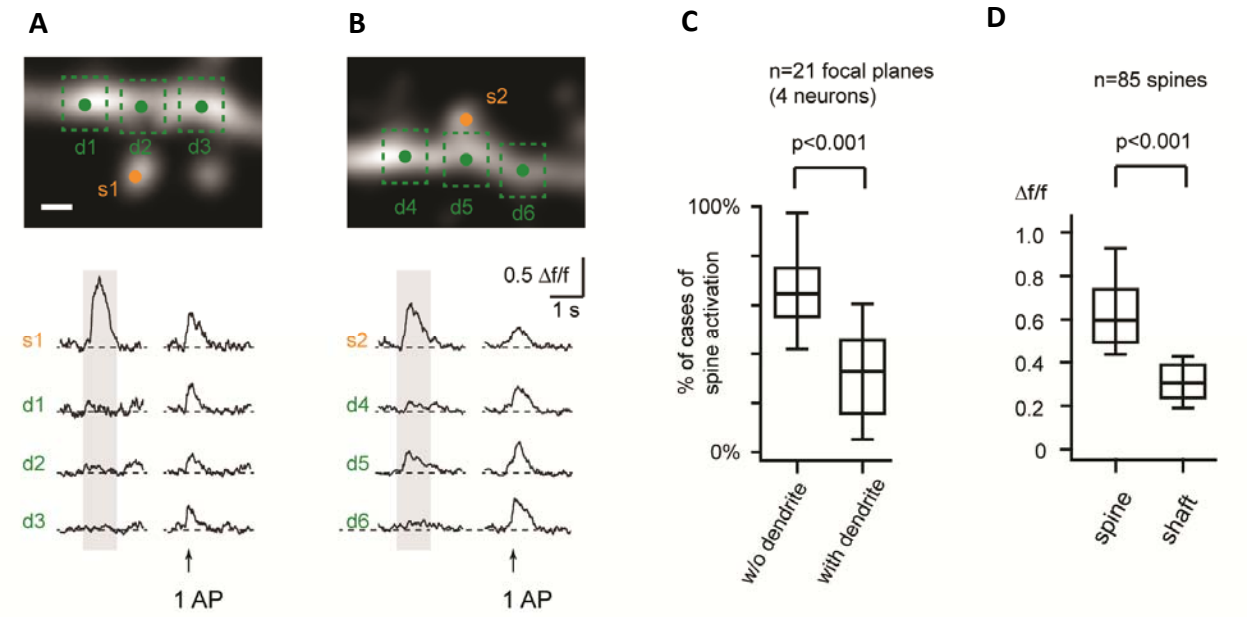

Fig.11. *Comparison of calcium signals in spines and dendritic shaft.* ***(A)*** *Example for a calcium signal confined to a single spine. The upper part is a maximum projection of a z-stack of dendritic portion from a L2 neuron. Orange dot marks the active spine, green boxes highlighted with green dots mark dendritic ROIs used for calcium signal calculations shown below. Scale bar corresponds to 1 µm.* ***(B)*** *Example for a calcium signal intruding to the dendritic shaft. Notations are the same as for (A).* ***(C)*** *The proportion of spine activation events without or with dendritic involvement. Middle bar is the median, box edges are 25 and 75 percentiles, error bars are 10 and 90 percentiles.* ***(D)*** *The amplitude of calcium signals in spines and dendritic shaft in case of shaft involvement. Notations are the same as in (C). Figure parts A-D were previously published in Varga et al. (2011).*

Following the activation pattern of single spines over trials showed that some spines were activated only by PW, others were activated only by SW, and a fraction of spines were activated by both PW and SW. These spines were denoted as shared spines. Figure 12.A shows an example for the spine activation pattern of a dendritic segment over trials. Similarly to dendritic hotspots, overlapping the PW pattern with SW pattern yielded three groups of active spines: PW-specific, SW-specific and shared spines (Fig.12.B). Comparably to dendritic hotspots, whisker-specific and shared spines were intermingled and located throughout the whole dendritic tree. The number of PW-specific, SW-specific and shared spines are plotted in Fig.12.C. In spine imaging experiments, only E2 whisker was tested as SW. Therefore, considering the distance dependence described in section 4.1.4., the calculated shared spine number might

underestimate the number of shared spines when the distance between the neuron and the SW barrel column is smaller.

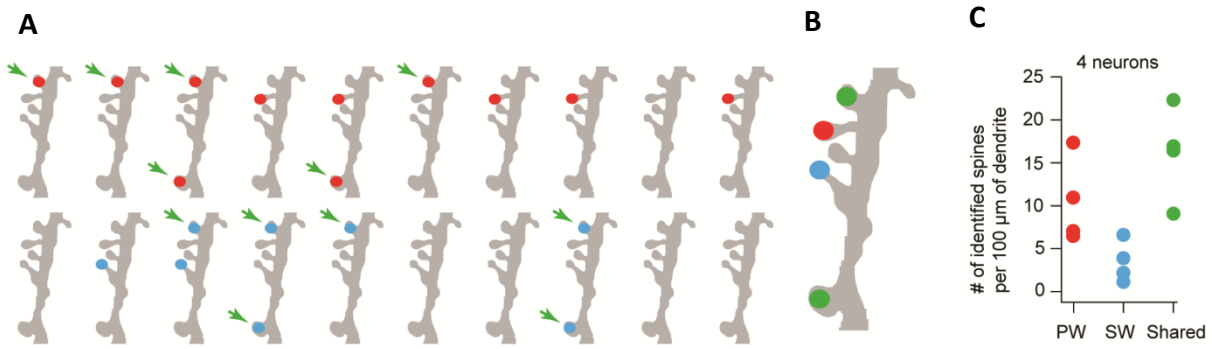

Fig.12. *Both PW and SW stimulation activate shared spines.* ***(A)*** *Cartoon of a dendritic segment with active spines. Red and blue dots indicate spines activated by PW and SW stimulation, respectively. Green arrows highlight spines which were active in response to stimulation of both whiskers.* ***(B)*** *Categorization of spines from the dendritic segment shown in (A). Red is a PW-specific spine, blue is an SW-specific spine and green spines are shared by both whiskers.* ***(C)*** *Number of PW-specific (red), SW-specific (blue) and shared spines per 100 µm dendrite length. Each colored dot indicates the value for one neuron. Figure parts A-C were previously published in Varga et al. (2011).*

Finally, the response probability of the spines was tested (Fig.13.A-D). For shared spines the response probabilities for both whiskers were calculated. The distributions of spine response probabilities were similar to those of hotspots. Thus, both for hotspots and spines the low reliability events dominated and highly reliable responses had lower probability.

Altogether, dendritic spine calcium signals were readily detected in L2 neurons. The calcium signals derived predominantly from spines, dendritic shafts had only minor contribution. Based on the response properties, whisker specific and shared spines could be distinguished. Thus, at least a fraction of shared hotspots could be accounted for innervation sites which are activated by multiple whiskers. The putative sources of shared innervation sites will be discussed in section Discussion.

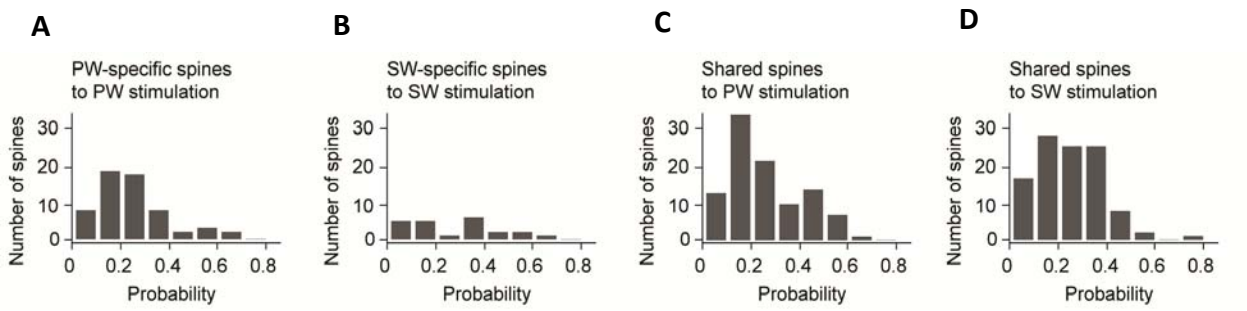

Fig.13. *Response probability distributions of active spines.* ***(A)*** *Response probability distribution of PW-specific spines in response to PW stimulation.* ***(B)*** *Response probability distribution of SW-specific spines in response to SW stimulation.* ***(C)*** *Response probability distribution of shared spines in response to PW stimulation.* ***(D)*** *Response probability distribution of shared spines in response to SW stimulation. All distribution histograms were calculated from 4 neurons. Figure parts A-D were previously published in Varga et al. (2011).*

4.1.6. Summary of the results of L2 experiments

This study addressed the question how inputs originating from multiple peripheral sensory organs (two whiskers) are mapped on the dendrites of a single neuron in the mouse wS1. In 12 neurons dendritic two-photon calcium imaging was performed to record the so-called hotspots which are assumed to be the location of synaptic events, and in 4 neurons calcium signals were detected with spine resolution.

In the dendrite imaging experiments, the whisker stimulation evoked subthreshold depolarization and the global calcium signals were shown to be distance dependent. These measures estimate the global input to a neuron in response to stimulation. Thus, surround whiskers which were further away seemed to be less effective in providing input than closer ones. When looking at the inputs on a smaller scale, hotspots were found to be distributed throughout the whole-dendritic tree, with multiple hotspots on single dendrites. However, the activation pattern of dendritic hotspots showed high variability, with most hotspots having relatively low response probability. Comparing the activation pattern evoked by PW and SW showed that some hotspots were specific to a single whisker, while others showed response to the stimulation of both whiskers. The whisker-specific and shared hotspots were intermingled and showed no clustering in specific parts of the dendritic tree. Nevertheless, the number of

SW-specific and shared spines continuously decreased with increasing distances to the SW barrel column.

In the spine imaging experiments synaptic calcium signals were shown to originate from single spines, with only minor contribution from dendritic shafts. Similarly to dendritic hotspots, active spines could be categorized into whisker-specific and shared spines. Whisker-specific and shared spines were intermingled, and showed low response probabilities.

4.2. L4 neurons

4.2.1. Two-photon calcium imaging of spines in L4 neurons in the mouse wS1

To establish good quality whole-cell recording for extended time periods in L4 was found to be challenging. The typical time course of the above described L2 experiments involved approximately 30 - 40 minutes filling of the neurons with the calcium sensitive dye followed by 1.5 - 2 hour recording session. However in L4 neurons, presumably because of the small size of somata (DeFelipe and Farinas, 1992) and the dense packing of the neuropil (Feldmeyer et al., 1999), the quality of the patch was not sufficient to achieve adequate filling and/or stable recordings over longer time periods. Nevertheless, whole-cell recordings without calcium imaging were used to test pharmacological properties of neuron responses. These recordings lasted only about 20 - 30 minutes.

Therefore to perform calcium imaging in L4 neurons another approach was applied. The calcium sensitive dye was filled into neurons with the technique of single cell electroporation (see Materials and methods section 3.4.2.). After electroporation, a new patch pipette was inserted, and the electroporated neuron was loosely attached. Thus, calcium imaging and suprathreshold electrical information could be acquired simultaneously from a single neuron. The lack of active control over the membrane potential did not prevent the identification of subthreshold calcium signaling events because of low AP firing properties of L4 neurons (see Results section 4.2.2.). Moreover, the practice of using loose cell-attached configuration instead of whole-cell recordings extended the recording time up to 4 hours after electroporation (typically 2.5 - 3 hours). This prolonged time period and the change in the whisker stimulation protocol (see Materials and methods sections 3.2.1. and 3.6.2.) allowed a remarkable increase in the number of trials used to test whisker deflection evoked responses. While in L2 experiments, typically each whisker was tested 10 times for a given focal plane, for L4 neurons this number was over 40. Thus, although whisker deflection could evoke AP in L4 neurons, there were a substantial number of trials where subthreshold responses could be identified.

Previously three types of excitatory neuron types were described in L4 of the rodent wS1 (see Introduction section 1.1.3.4.): spiny stellate cells, star pyramids (Fig.14.) and

pyramidal neurons. In the present study the morphology of neurons was recovered from the z-stack images, as described for L2 neurons. Although in initial experiments few pyramidal neurons were also identified, in late experiments the neurons belonged to spiny stellate cells and star pyramids. Therefore the calcium imaging results presented below were based on the analysis of recordings from 9 spiny stellate cells and 6 star pyramids. In experiments without calcium imaging the morphology of the neuron could not be recovered, and the identity of the neuron type could not be provided.

The neurons were targeted to the C2 barrel with intrinsic signal optical imaging as described previously for L2 neurons (see section 4.1.1.) However, because of the longer travelling distances of the pipette along the ~ 40° insertion axis, craniotomies were made larger compared to L2 experiments. Nevertheless the imaging quality did not decrease significantly due to the expected increase in pulsation artifacts, possibly because of the stabilization effect of depth. The average soma depth was 444 µm (± 29 µm SD, n = 15 neurons) below the pia, and the depth of imaged dendritic spines ranged from -310 to -520 µm, with the majority of spines located between -390 to -470 µm.

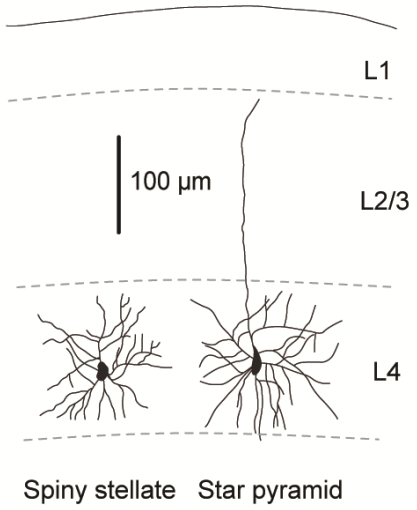

Fig.14. *Morphology of L4 neurons. The reconstructions were made from the x-y projections of the z-stacks of a spiny stellate and a star pyramid. Neuron schemes were manually overlaid on the scheme of the neocortex.*

The average length of dendrite recorded with two-photon calcium imaging was 173.5 µm (± 71.1 µm SD, n = 9 neurons; median = 170.8 µm) for spiny stellate cells, and 264.5 µm (± 124.3 µm SD, n = 6 neurons; median = 284.6 µm) for star pyramids. The average number of identified and analyzed spines was 75 (± 53 SD, n = 9 neurons; median = 51) for spiny stellate cells, and 82 (± 34 SD, n = 6 neurons; median = 89) for star pyramids. The average spine density was 42.25 spines/100 µm dendrite (±15.22 SD, n = 9 neurons; median = 42.6) for spiny stellate cells, and 31.98 spines/100 µm dendrite (±3.75 SD, n = 6 neurons; median = 31.37) for star pyramids. None of the above mentioned values was significantly different across groups (unpaired t-test $p = 0.0930$ for dendrite length, $p = 0.7804$ for the number of identified spines, and $p = 0.1332$ for spine density).

Altogether, compared to the L2 experiments a different approach (electroporation + loose cell-attached) was used to image dendritic spines in L4 neurons. The majority of neurons belonged to spiny stellate cells and star pyramids. On average, the density of spines recorded with calcium imaging was not significantly different between cell types.

4.2.2. Characterization of whisker stimulation evoked inputs to L4

Compared to L2 experiments, in L4 experiments a different whisker stimulation protocol was used (see Materials and methods, section 3.2.2.) The 2-second deflection of the PW produced distinct EPSPs. However, the fine structure of the evoked EPSPs varied from trial to trial (Fig.15.A). Nevertheless, when averaging over trials (Fig.15.B.) and over neurons (Fig.15.C), a common fast component became apparent, and the fluctuations on the slow component averaged out. The time course of the first fast component (Fig.15.D) showed approximately 10 ms latency to the onset (Fig.16.) and was over in about 50-60 ms. Due to the conservative fast component and the variable slow component, in further analysis only the time window of the fast component was considered. Specifically, for quantifying AP responses, only AP generated within 50 ms from stimulation were included (Fig.17. and Fig.18.). For the imaging analysis, spines which had 10 ms onset latency were classified as short latency spines. This criteria was chosen, because the latency distribution of stimulation evoked EPSPs (Fig.16.) showed that

most EPSP has latency around 10 ms. Thus, from circuit properties these short latency spines are assumed to receive thalamocortical input (see Discussion section 5.4.1.).

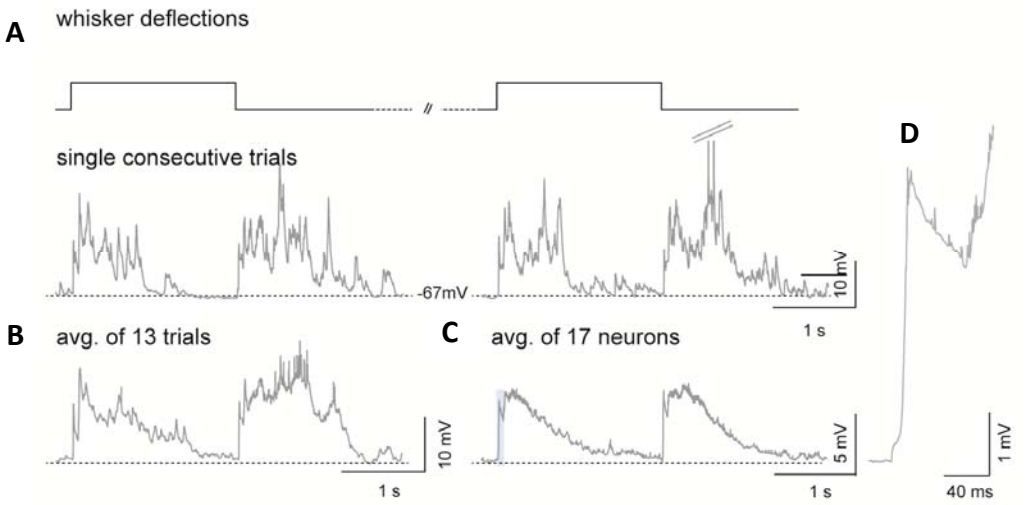

Fig.15. *The deflection of PW evokes EPSPs with 2 components.* ***(A)*** *Upper panel shows the whisker deflection protocol, the lower panel shows the evoked consecutive trials.* ***(B)*** *The average EPSP of 13 trials from the same neuron as in (A).* ***(C)*** *The grand average EPSP from 17 neurons. Blue shade indicates the fast component magnified in (D).* ***(D)*** *The zoomed-in fast component of the grand average EPSP in (C).*

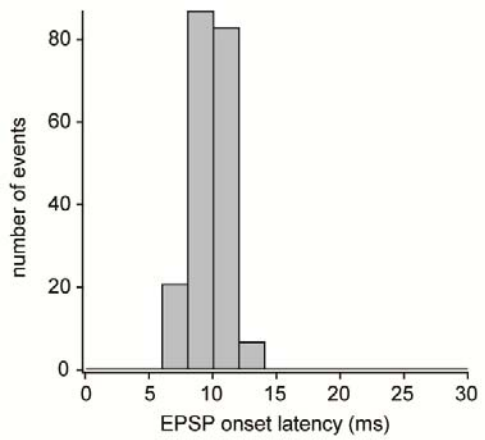

Fig.16. *Whisker stimulation evoked EPSP latency distribution. The distribution was calculated from 50 sensory stimulation (PW deflection) trials of 4 neurons.*

The firing probability (% of trials with AP firing within 50 ms) in response to whisker deflection was estimated from the loose cell-attached and whole-cell recordings. First, all neurons were pooled together, independently of their morphology if it was available (recordings from electrical only and from imaging experiments together). In this way the median firing response probability was calculated to be 1.57% (n = 23) from cell-attached recordings, and 1.43% from whole-cell recordings (n = 17). The distributions were not significantly different (Mann-Whitney U-test p = 0.498), thus the overall median firing probability in response to whisker stimulation was 1.5% (Fig.17.A). The firing response probability was also calculated for a smaller subset of neurons with known morphology. Here, the median firing response probability was 2.1% (n = 9 neurons, 25 percentile = 1.27, 75 percentile = 9.91) for the spiny stellate cells, and 1.1% (n = 6 neurons, 25 percentile = 0.66, 75 percentile = 1.57) for the star pyramids (Fig.17.B). Nevertheless the difference between the two morphological groups was not significant (Mann-Whitney U-test, p = 0.237).

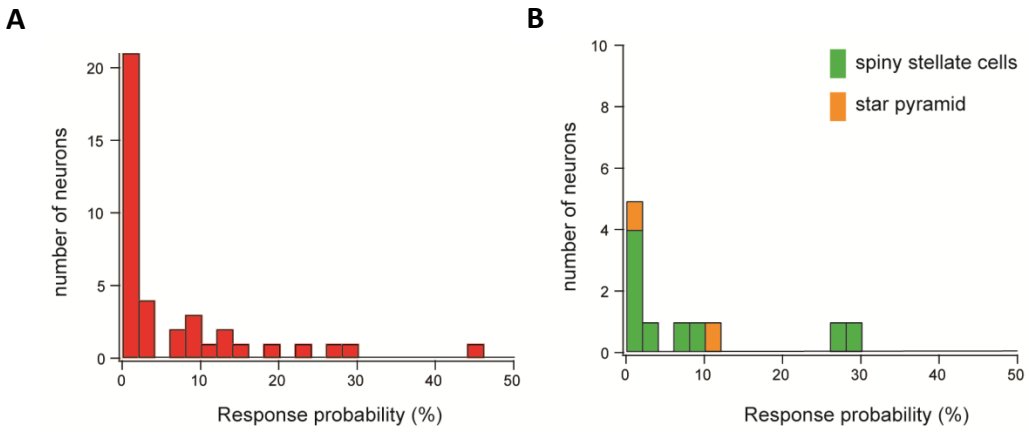

Fig.17. *The probability distribution of subthreshold responses.* ***(A)*** *The probability distribution of all neurons recorded with both whole-cell and cell-attached techniques.* ***(B)*** *The probability distribution of spiny stellate cells (green) and star pyramids (orange).*

To test the role of NMDA-receptors in the sensory stimulation evoked signaling in L4 neurons, the NMDA antagonist AP5 was locally applied during whisker deflections (see Materials and methods, section 3.8.). In whole-cell recordings AP5 significantly reduced the amplitude of the fast component of evoked EPSPs (Fig.18.A-B). In both loose cell-attached

recordings and whole-cell recordings AP5 completely blocked the AP firing in the first 50 ms after sensory stimulation (Fig. 18.C-D).

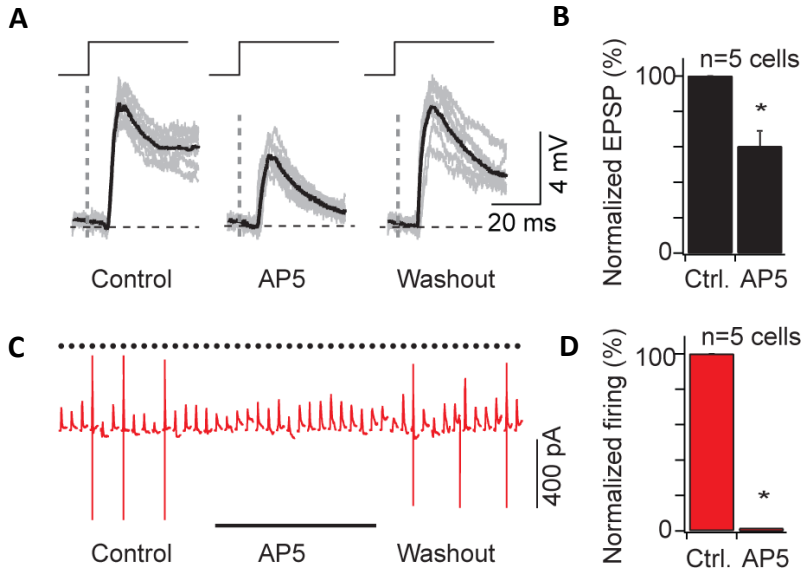

Fig.18. *The effect of AP5 on electrical recording.* ***(A)*** *AP5 application reversibly decreases the sensory stimulation evoked EPSP amplitudes. The stimulation protocol is shown above the electrical traces. Gray traces indicate single trials, black traces indicate the average (n = 8 trials).* ***(B)*** *Normalized EPSP amplitudes for 5 neurons under control (Ctrl.) and AP5 condition.* ***(C)*** *AP5 application reversibly blocks sensory stimulation evoked AP firing. Black dots above electrical traces mark the first 50 ms period of individual trials.* ***(D)*** *Normalized firing probability in response to whisker stimulation under control (Ctrl.) and AP5 condition.*

Two-photon calcium imaging was performed on the spiny dendrites of L4 neurons. L4 neurons, specifically spiny stellates, showed asymmetric dendritic tree with dendrite branches projecting toward the center of the barrel (Fig.19.A). Dendritic segments confined to single focal planes were chosen to record the activity of individual spines (Fig.19.B). Spines were identified by eye. In a single spine whisker stimulation could evoke subthreshold calcium transients (Fig.19.C). Occasionally sensory stimulation also evoked AP firing. In the following analysis, trials where AP firing was evoked are not included.

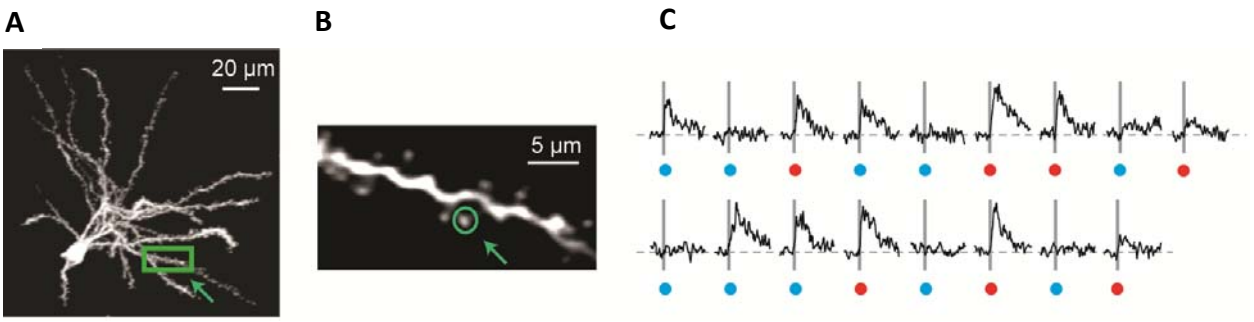

Fig.19. *Calcium signaling of individual spines in L4 neurons.* ***(A)*** *Z-projection of a spiny stellate neuron. Green box highlighted with green arrow marks the dendrite shown in (B).* ***(B)*** *A spiny dendritic segment at -468 µm below the pial surface. Green circle highlighted with green arrow marks the spine from which the calcium transients in (C) were calculated.* ***(C)*** *Whisker stimulation evoked calcium transients from a single spine (marked in B). Blue dots indicate subthreshold responses, while red dots indicate trials where AP firing occurred. Gray bars mark the start of whisker stimulation.*

The calcium transients recorded in single spines had different latencies (Fig.20.A-C). Here, only transients fulfilling the criteria under 3.10.2.2 were considered. The rise time of the subthreshold calcium transients identified in single spines were typically not instantaneous, presumably due to the multiple AP firing of the presynaptic neuron and channel kinetics.

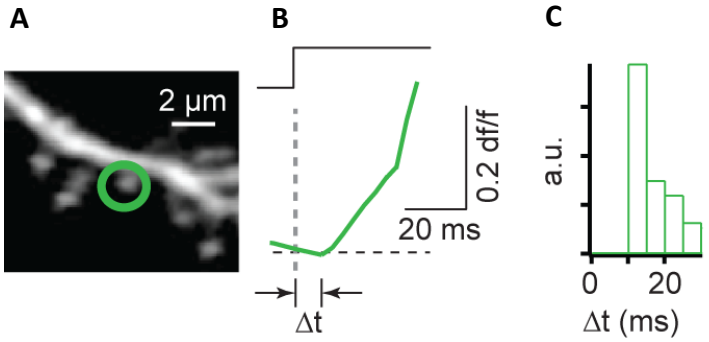

Fig.20. *The latency distribution of spine calcium signals in the time-window of the fast EPSP component.* ***(A)*** *Spiny dendritic segment at -410 µm below pia. Green circle indicate the spine from which the rise time of the calcium transient in (B) was calculated.* ***(B)*** *The latency of a single subthreshold signal in a single spine.* ***(C)*** *The distribution of subthreshold spine calcium signals in the early phase of stimulation evoked response for 15 neurons (n = 388 spines).*

The local application of AP5 had similar effect on calcium signaling as on electrical recordings. The sensory stimulation evoked subthreshold calcium signals in single spines were blocked by AP5 (Fig.20.A). This effect was reversible, as after the washout of the drug from the extracellular space, the sensory stimulation evoked subthreshold signals recovered. The difference in the amplitude of calcium transients in the control and in the drug conditions was significantly different (Fig.20.B; $p < 0.001$, $n = 24$ spines, paired t test).

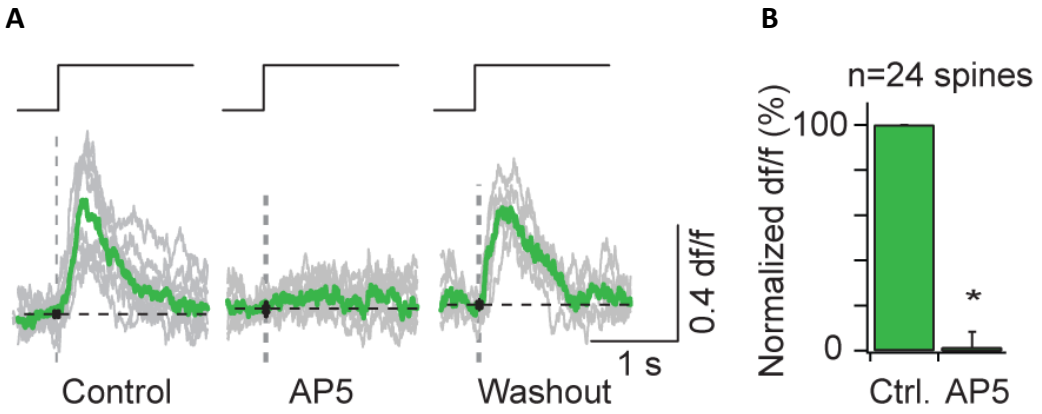

Fig.20. *AP5 blocks sensory stimulation evoked subthreshold calcium signaling.* ***(A)*** *AP5 application reversibly blocks sensory stimulation evoked subthreshold calcium transients. The stimulation protocol is shown above the calcium traces. Gray traces indicate single trials, black traces indicate the average (n = 6 trials).* ***(B)*** *Normalized calcium transient amplitudes for 24 spines under control (Ctrl.) and AP5 condition.*

Figure 21. shows a spiny dendritic segment where calcium traces of spines were calculated as described in Materials and methods section 3.10.2.2. From the indicated spines, spine 1, spine 3, spine 8 and spine 9 were recognized as short latency spines using the criteria described in Materials and methods section 3.10.2.3. Short latency spines were identified on 60 out of 84 dendritic segments. The spines with short latency onset time had various response probability (Fig.22.) with a median response probability of 15.66% (n = 194 spines). Thus, the majority of short latency spines had low response probabilities.

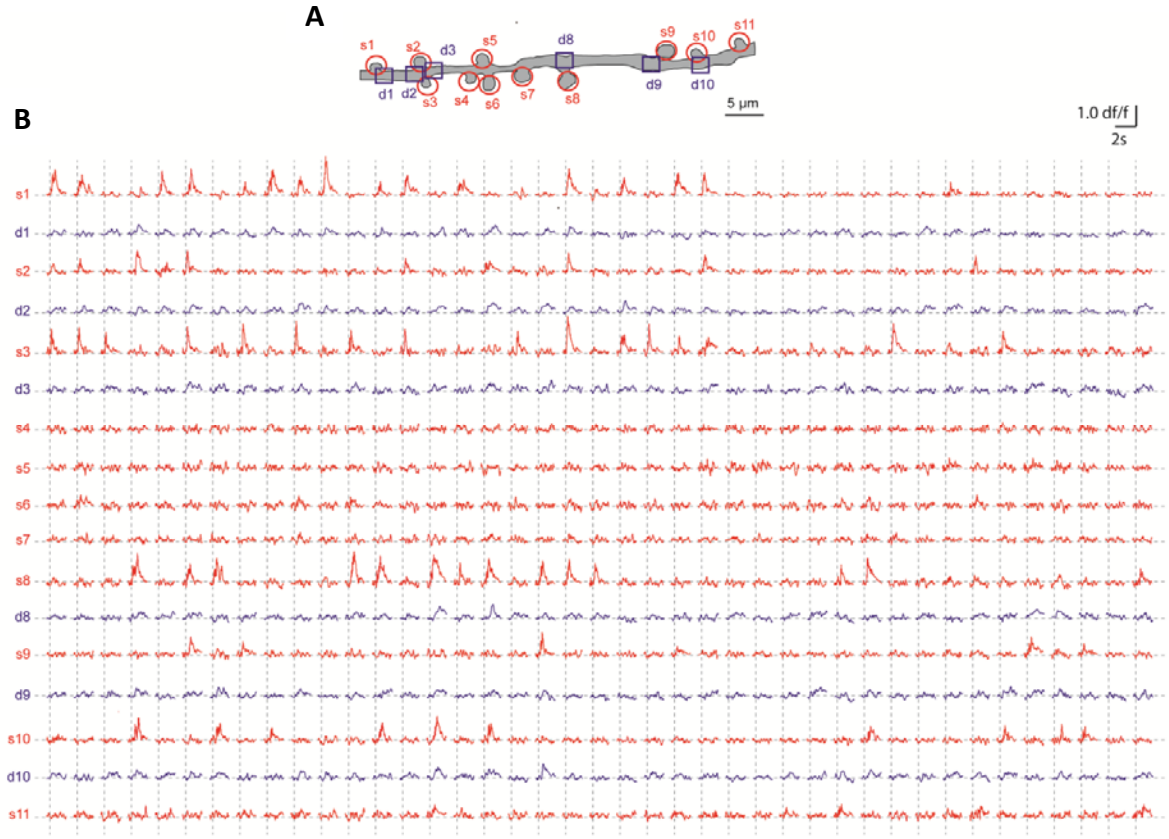

Fig.21. *Examples L4 spines with different response reliability.* ***(A)*** *A schematic representation of a spiny dendritic segment 415 µm below the pial surface. Red circles ROIs for visible spines, blue boxes mark the ROIs for dendritic segments.* ***(B)*** *Calcium traces calculated from the ROIs indicated in (A). Each vertical dotted line indicate a whisker stimulation trial.*

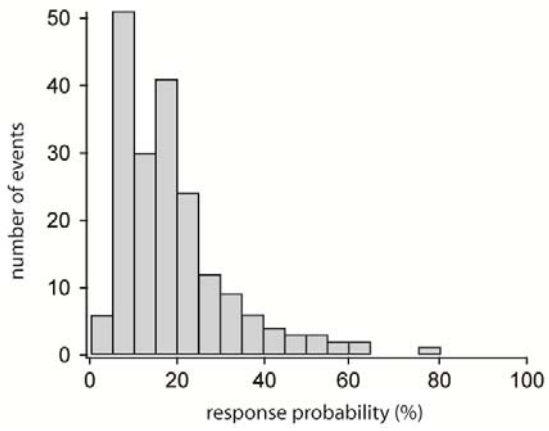

Fig.22. *Response probability of short latency spines. The histogram is calculated form the response probability values of n = 194 spines.*

Finally, the SW (E2) stimulation did not evoke significant number of calcium transients fulfilling the above mentioned criteria. The effect of SWs closer to the PW (C2) related barrel was not tested. Thus, in the further analysis, only the PW evoked responses will be considered.

Altogether, whisker deflection evoked reliable EPSPs in L4 neurons in the corresponding barrel with a latency of about 10 ms. In most neurons the whisker stimulation did not evoke very reliable suprathreshold responses. The amplitude of the sensory stimulation evoked EPSP was sensitive to the NMDA receptor blocker AP5. AP5 also blocked stimulation evoked AP firing. Similarly, the sensory stimulation evoked subthreshold calcium transients were also blocked by AP5. Short latency spines were identified based on the onset latency of their calcium transients. Short latency spines were identified on the majority of dendritic segments. Most of the short latency spines had low response reliability.

4.2.3. Spatial distribution of short latency spines

The spatial distribution of subthreshold calcium transients was mapped on both spiny stellates and star pyramids. In the analysis only spines with short latency transients were considered as active spines, thus the resulting maps were expected to represent the distribution of thalamocortical inputs. For the horizontal distribution (Fig.23.A-B), neurons with identical class morphology (i.e. either spiny stellate or star pyramid) were overlaid and rotated so that the direction to the barrel center is identical to all neurons. The directions and the rotation angles were calculated from the coordinates of intrinsic signal optical imaging and those of the neurons. In the new, common coordinate system the location of all identified spines were calculated. For the quantification, normalized input densities were calculated for both cell types separately (Fig.24.A-B). Normalized input densities were calculated as the number of active spines in a given distance bin divided by the number of all visible spines in that bin. In spiny stellates the input density decreases with distance from the soma center, while in star pyramids no such relation was found. Moreover, the highest input density was calculated for the perisomatic region of spiny stellates. The spine density values for star pyramids were comparable to the values outside the perisomatic region of spiny stellates.

Spiny stellates have two morphological subgroups. One subgroup of spiny stellates has asymmetric morphology with the dendrites oriented toward a barrel center. These spiny stellates are located in the side of the barrels. The other subgroup contains spiny stellates that have symmetric dendritic morphology with dendrites projected to all sides. These spiny stellates are located in the middle of the barrel. Thus, in principle, the two subgroups could have different input distributions when considering the anatomy of thalamocortical projections (see Introduction section 1.1.3.1.). Therefore the input densities were also calculated for the two morphological subgroups. For both the asymmetric and symmetric spine stellates, the input density depended on the distance from the soma center, thus the density of inputs in the perisomatic region was the highest for all spiny stellates, independently from their morphology.

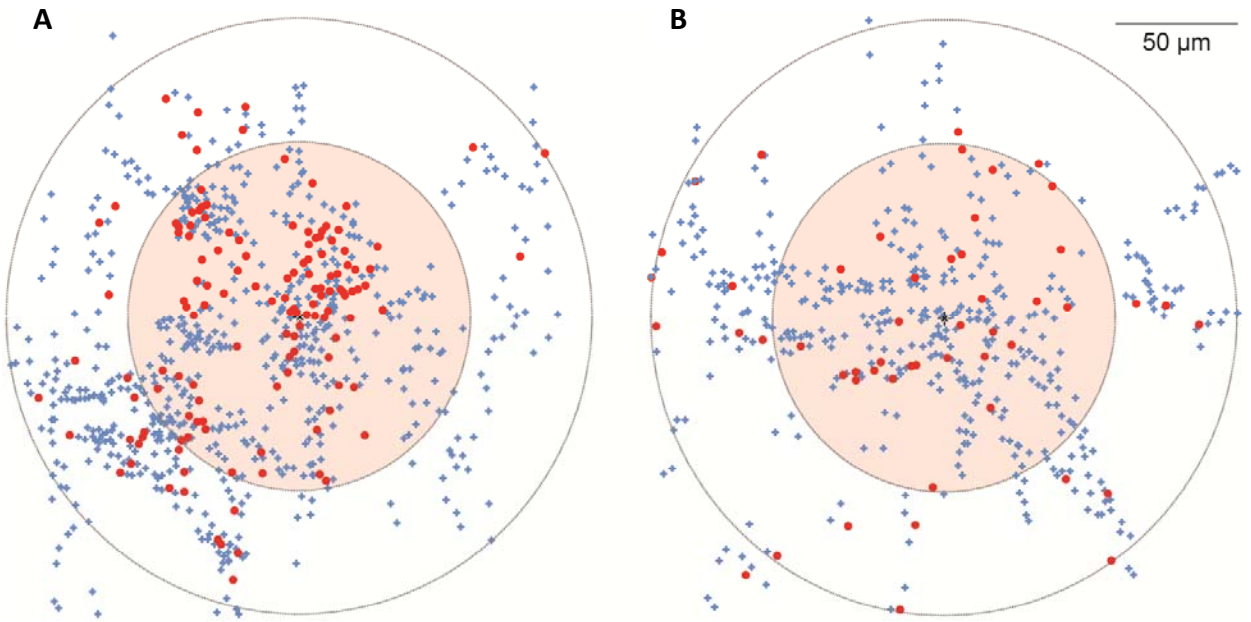

Fig.23. *The x-y distribution of spines receiving thalamocortical input.* ***(A)*** *The overlay of spine locations of 9 spiny stellates. The spiny stellates were rotated so that for each the barrel center is located to left of the figure. Red dots indicate spines receiving thalamocortical input, blue dots indicate other spines. Red and white concentric circles mark 70 µm and 120 µm distance from soma.* ***(B)*** *The overlay of spine locations of 6 star pyramids. The star pyramids were rotated so that for each the barrel center is located to the left of the figure. Notations are the same as for (A).*

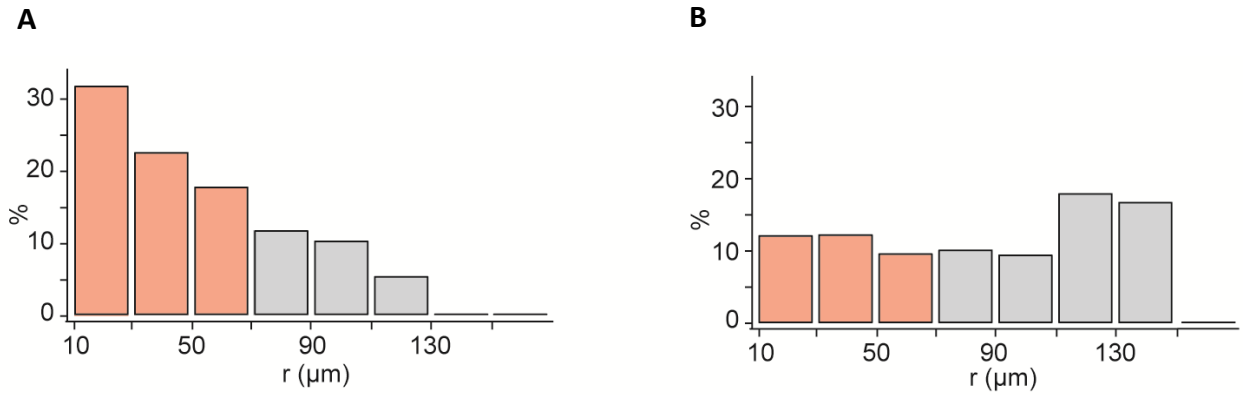

Fig.24. *Normalized input density to L4 neurons in the function of distance from soma center.* ***(A)*** *Normalized input density in spiny stellates (n = 9). Red bars indicate the bins within 70 µm from soma center (identical to red circle in Fig.23.).* ***(B)*** *Normalized input density in star pyramids (n = 6). Notations are the same as in (A).*

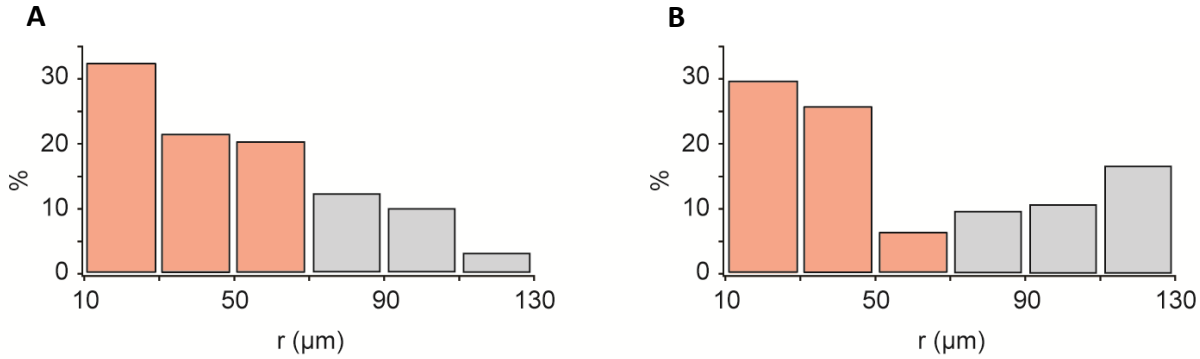

Fig.25. *Normalized input density to morphological subgroups of spiny stellates in the function of distance from soma center.* ***(A)*** *Normalized input density in asymmetric spiny stellates (n = 6). Red bars indicate the bins within 70 µm from soma center (identical to red circle in Fig.23.).* ***(B)*** *Normalized input density in symmetric spiny stellates (n = 3). Notations are the same as in (A).*

Altogether, the spines which respond to whisker deflection with short latency (i.e. spines which presumably receive thalamocortical input) are more densely packed around the soma and their density is decreasing with distance in case of spiny stellates. No similar relation between the density of active spines and distance was found for the star pyramids.

4.2.4. Summary of the results of L4 experiments

Although L4 experiments and their analysis are not complete, they can give useful insights on the features of sensory input reaching the cerebral cortex. Here 9 spiny stellates and 6 star pyramids were recorded with spine resolution to identify the location of inputs reaching these cell types.

Two-photon calcium imaging was used to detect subthreshold calcium transients in single spines of L4 neurons. Due to technical difficulties the electrical monitoring of L4 neurons were achieved with loose cell-attached recordings instead of whole-cell recordings which were previously used in L2 experiments. Nevertheless, due to the relatively low number of APs and the modified stimulation protocol, the number of subthreshold trials was sufficient to identify responsive spines.

Here, the spines receiving thalamocortical inputs were identified based on the latency of calcium responses evoked by the sensory stimulation. Spines active with short latency were identified in all recorded neurons. The sensory stimulation evoked calcium transients, similarly to AP firing, were reversibly blocked by the NMDA-receptor antagonist AP5. AP5 also reversibly decreased the amplitudes of evoked EPSPs. These results indicate that the subthreshold calcium transients recorded in single spines of L4 neurons are indeed of synaptic origin.

The spatial location of spines active with short latency was mapped on both spiny stellates and star pyramids. The two cell types showed different distributions of active spines. In case of spiny stellates the density of short latency spines decreased with distance from the soma center, while in case of star pyramids the density values were similar over all distances.

Finally, in case of L4 neurons no sufficient number of spines active with short latency in response to SW stimulation was identified when stimulating an SW that was two rows away from PW.

5. Discussion

In this study the properties of sensory stimulation evoked inputs were investigated in the L2 and L4 of the mouse wS1 with in vivo two-photon calcium imaging in dendrites and spines. Although previously similar studies were performed in the visual (Jia et al., 2010) and in the auditory (Chen et al., 2011) cortices, those studies were restricted to superficial layers of the neocortex. Here the more deeply located L4 neurons were also included to expand the view on sensory processing. Generally, L4 is considered to be the cortical region where sensory inputs enter the cortex, and L2 is considered to participate in higher order processing of sensory inputs. Thus, this study explores sensory processing in two consecutive, functionally different levels. In addition, this is the first time demonstration of in vivo two-photon calcium imaging with spine resolution in deeper layers.

In vivo two-photon calcium imaging allows the identification of sensory input sites on dendrites and spines (Jia et al., 2010; Chen et al., 2011), thus the spatial and the temporal organization of inputs to individual neurons can be studied. With the help of this technique, in this study the following results were acquired. L2 neurons invariably received sensory information from PW. Additionally, they received inputs from a number of SWs. The amount of input evoked by SW depended on the distance of the SW from the PW. Whisker stimulation evoked inputs were distributed throughout the whole dendritic tree, and the inputs from different whiskers were intermingled. Several input sites could be identified on single dendritic branches. However, the activation of these input sites had relatively low reliability. Additionally, input sites activated by multiple whiskers were found on both dendritic and spine level. Predominantly, the subthreshold calcium signals were restricted to the spines.

In L4 neurons the synaptic origin of subthreshold calcium transients was confirmed with the local application of the NMDA-receptor blocker AP5. The early phase of stimulation evoked response was assumed to represent the direct thalamocortical input due to the properties of the circuitry. The presumed thalamocortical inputs were distributed throughout the whole dendritic tree, and several input sites could be identified on single dendritic branches. However,

in spiny stellates the density of inputs was the highest around the soma, and it decreased with distance from the soma center. Such relation between input density and distance was not observed for star pyramids. Finally, in all recorded L4 neurons the inputs were clearly dominated by PW, and they did not receive substantial amount of input from SW.

In the following some of the technical aspects and implications of the results will be discussed.

5.1. Technical advances and aspects

5.1.1. Common coordinate system of intrinsic signal optical imaging and two-photon calcium imaging

Intrinsic signal optical imaging and two-photon calcium imaging requires different instrumentation. Although the alignment of the intrinsic signal map and the blood vessel map recorded with the intrinsic signal optical imaging system could give enough information to target a specific barrel, the continuous monitoring of the cortical region where the pipette passes through, could be useful, especially when aiming at deep layers. To achieve this, the 0 position of the motorized table was set to the position where the middle of the principal barrel was in the center of the field of view. Thus when approaching the targeted region, the position of the pipette tip relative to the barrel center could be estimated. This approach was essential in determining the relative position of L4 neurons to the barrel center, since the deep location hindered the post hoc confirmation of location with epifluorescent imaging (see Materials and methods section 3.9.1). However, since the 0 position of the motorized table was identified manually based on the blood vessel map, and the precise spatial profile of the intrinsic signal could change over trials (thus shifting the center of the signal), the precision of the coordinate system was estimated to be around 50 μm. Nevertheless, this precision was sufficient to reliably target neurons in the barrel or the barrel related column as confirmed with histology in case of L2 neurons (see Fig.2.D).

5.1.2. Dye filling approaches

In L2 experiments the calcium sensitive dye Oregon Green BAPTA-1 was introduced to the neurons through whole-cell patch pipette. In L4 experiments, due to technical issues, the shadow electroporation approach was applied (see Materials and methods section 3.4. and Results section 4.2.1.). The whole-cell approach had the advantages of using a single pipette for dye filling and electrical recording, and the ability of active control of the membrane potential. In L2 experiments, the membrane potential of the neurons was slightly hyperpolarized (see Materials and methods section 3.5.1.) if it was necessary to prevent AP firing. In principle, the injection of negative current could interfere with channel kinetics and recruitment. However, the hyperpolarized membrane potential values recorded at the soma were in the range of non-hyperpolarized membrane potential values previously reported (Svoboda et al., 1999). Moreover, the effect of current injection is expected to be smaller in dendrites further away because of the imperfect spatial clamp.

The shadow electroporation approach used in L4 experiments also had several advantages. First, besides the introduction of the calcium sensitive dye, there was no constant interference with the intracellular milieu of the cell. Second, the high success rate of the method eliminated the need to approach the target region several times, thus highly reduced the background signal resulting from the excess dye accumulating in the extracellular space. This point was essential to perform spine imaging in the deep, because relatively good signal to noise ratio is necessary to perform imaging with reduced power levels. Third, the lack of need for a tight contact between the neuron membrane and the pipette allowed re-attaching the neuron with the same pipette several times over the course of experiment if it was necessary, for example when the contact was lost due to movement. This extended the recording time. Although in these neurons the membrane potential could not be controlled, the extended recording time allowed sufficient number of trials with only subthreshold activation.

In case of L4 experiments, a few number of whole-cell recordings were also performed without calcium imaging. The firing response probability calculated under whole-cell and loose cell-attached recordings was not significantly different (see Results section 4.2.2.), which could also imply that input integration was not influenced (or influenced in a similar way) by the

recording method per se. Although L2 neurons were occasionally slightly hyperpolarized, since the slight hyperpolarization was assumed not to substantially influence the input properties (see above), the results on the mapping of inputs in L2 and L4 neurons were expected to be comparable.

5.1.3. Whisker stimulation protocols

In L2 and L4 experiments different whisker stimulation protocols were used (see Materials and methods section 3.2.). The main difference between the two protocols was that in case of L2 experiments the stimulus was a 1-second train of 10 deflections, while in case of L4 experiments the whisker was deflected only once for 2 seconds. A train of deflections was initially chosen because the physiological frequency of whisking is around 8 Hz (for review see for example Deschenes et al., 2012). However, this stimulation was quite strong presumably causing considerable amount of corticocortical activation. To isolate inputs reaching the cortex from intracortical activation, the stimulation protocol was reduced to a single-step stimulation in case of L4 experiments. This difference in stimulation protocol should be considered when interpreting the distribution of inputs in the two sets of experiments.

5.1.4. Morphology reconstructions from z-stacks

In both L2 and L4 experiments the morphologies of neurons were reconstructed from the z-stack images recorded at the end of the experiments. This approach was preferred to reconstruction from post hoc histology because the similar recording features allowed easy identification of the location of the spines and dendrites recorded. Although reconstructions from z-stacks have not been quantitatively compared to reconstructions from histological processing, they contained the dendrites that could be visualized with two-photon calcium imaging (thus all the dendrites that could be potentially recorded). This was sufficient to identify the morphology of neurons and also to measure the distance of spines and dendrites from the soma center. Precise anatomical assessment, such as the absolute number of spines,

was not possible due to the inherent features of in vivo two-photon imaging (for example spines directly above or directly under the dendritic shaft could not be visualized). Similarly, in case of L4 neurons, the deep dendrites (dendrites below -500 µm) could not be reliably resolved due to lack of sufficient contrast. Finally, since only dendrites and spines in the same focal plane could be recorded within a single field of view, for any neuron, the distribution of dendrites and spines tested with sensory stimulation was discrete on the reconstruction. Overall, the reconstructions generated from z-stack projections were suitable for morphological categorizations and distance calculations without precise anatomical measurements.

5.1.5. Spatial resolution of hotspots in dendritic imaging

Dendritic and spine imaging were performed on the same setup with the same optical elements. Thus the spatial resolution depended only on the zoom factor used during imaging. To calculate calcium signals with sufficient signal-to-noise ratio, in dendrite imaging experiments the signal was integrated over 2 µm during analysis (see Materials and methods section 3.10.1.3). Dendritic hotspots are considered to be the representation of synaptic inputs (see Jia et al., 2010), presumably to dendritic spines. Thus, considering the above mention integration, any two spines had to be apart by at least 2 µm to contribute to fluorescence signals resolved as two separate hotspots. As a result, closely located spines were most likely attributed to single hotspot sites. Finally, the calcium signals recorded in hotspots was a combination of spine and dendritic shaft signals. Spine resolution imaging was essential to determine the contribution of these different dendritic compartments to the stimulation evoked subthreshold responses.

5.1.6. Temporal resolution to identify early responses

In spine imaging experiments the image acquisition was performed with repetition rate of 200 Hz (see Materials and methods section 3.7.2.). This equaled to a theoretical time resolution of 5 ms. However, based on the Nyquist-Shannon sampling theorem, the effective

time resolution was 10 ms. The criteria for short latency spines was to have an onset time of 10 ms after the stimulation. Thus the time resolution was sufficient to classify spines with this criterion.

5.2. Similar properties of inputs reaching L2 and L4 neurons

5.2.1. Calcium transients localized to spines

In L2 experiments in approximately two thirds of the spines the calcium signal was localized to the spine, and in approximately one third of the spines the calcium signal was also detected in the shaft directly neighboring the spine. The shaft signal in all cases was smaller than the spine signal. Although no such quantification was presented for the L4 for experiments, Figure 21. shows that for most spine activation no calcium signal was detected in the adjacent shaft. These results are in line with previous recordings in slice (Yuste and Denk, 1995).

5.2.2. Distributed inputs

Although the inputs recorded in L2 and L4 experiments were not of the same origin, in both cases inputs were identified on several dendrites of a single neuron. In L2 neurons the sources of the identified inputs were cortical, and because of the recording conditions, most likely many of them originated from the same layer. In case of the L4 experiments, because of the modified criteria, most of the identified inputs could be assumed to be of thalamic origin. Nevertheless, in both cases the inputs were distributed among the dendrites. Even in spiny stellates, where most of the inputs were identified on dendritic branches close to the soma, the inputs were dispersed among multiple branches. Moreover, in L2 neurons, where PW-specific, SW-specific and shared spines could be distinguished, these different spines were spatially interspersed and not separated. These properties are in agreement with the idea of distributed circuits (Yuste, 2011). The advantages of distributed circuits include that it is relatively easier to organize such circuits and they could allow for a higher degree of plasticity (Yuste, 2011).

5.2.3. Temporal variability of input activation

Similarly to the distributed feature of inputs, the temporal variability was also comparable in L2 and L4 experiments. In both layers, the majority of spines had low response probability (less than 30%). In case of the shared spines of L2 neurons, this low response probability is not surprising, if the intralaminar origin of shared inputs is assumed. Kerr et al. (2007) showed that L2/3 neurons in wS1 had large variation in their suprathreshold responses upon whisker stimulation (in any trial approximately 20% of neurons were activated, and from trial to trial the subset of active neurons varied). The low response probability of whisker-specific inputs could be explained with the relatively low suprathreshold response probability of L4 neurons (see this study, and Brecht and Sakmann, 2002b: less than 0.3 AP / PW deflection; DeKock et al., 2007: 0.41 AP / PW deflection) under the present experimental conditions. These values are comparable to spine response probability values. However, the explanation for low response probabilities in L4 neurons is not so obvious. In the VPM, neurons respond with approximately 0.56 AP / stimulation at the preferred location (Scaglione et al., 2011) under urethane anesthesia. However, under the same anesthesia with different stimulation protocol (100 stimuli of 0.5 Hz) 1.21 AP / stimulation was reported by Augilar et al. (2007). This suggests that stimulation protocol has substantial effect on the response probability of VPM neurons. Moreover, isoflurane has been shown to decrease excitatory drive in thalamocortical neurons of the VPM by increasing the strength of GABAergic inhibition (Detsch et al., 2002). Thus, it is not unlikely that the use of isoflurane and a different stimulation protocol together reduced the response probability of thalamocortical projections.

On the other hand, low response probabilities in the cortex could have other explanations. The theory of sparse coding suggests the information is encoded only small set of active neurons. Sparse representation of sensory inputs has been demonstrated in awake rodents. Sparse coding could occur at two levels. First, the number of neurons which fire reliably is low (for example O'Connor et al., 2010); or second, the number of emitted spikes is low (for example Jadhav et al., 2009). Both cases would result in the predominance of low probability input sites. The mechanism of sparse coding of L2/3 neurons has been demonstrated in awake behaving mice (Crochet et al., 2011). Neural representations with

sparse coding could, among others, aid memory storage and learning. For more details on the advantages of sparse coding please refer to the review Olshausen and Field (2004).

5.3. Specific properties of inputs reaching L2 neurons

5.3.1. Shared spines

In L2 experiments a substantial fraction of spines showed activation in response to both PW and SW stimulation. These shared spines were distributed among the whisker specific spines. In principle, there are three possibilities to explain the observation of shared spines. First, the spatial configuration of two closely located spines with different whisker specificity is so that they cannot be resolved as two different spines (for example they partially overlap each other). Second, two separate presynaptic neuron with different whisker specificity project to the same postsynaptic spine. Third, a single neuron with multi-whisker or non-specific response properties project to the spine. The possibility of the role of spine configuration cannot be excluded; however, due to the requirement of a specific spatial configuration, one would not expect that the majority of shared spines are of this sort. Similarly, the second possibility, two presynaptic neurons projecting to a single postsynaptic spine, cannot be excluded, but based on electron microscopy studies (in hippocampus: Harris and Stevens, 1989; Trommald and Hulleberg, 1997;) the contribution of such spines to the overall amount of shared spines could not be substantial. Thus the third possibility, i.e. shared spines are the input sites of neurons with multi-whisker or non-specific properties, is assumed to account for the majority of shared spines. Neurons with multi-whisker properties were described in the thalamus (Diamond et al., 1992), as well as in the cortex (for example Armstrong-James et al., 1992; Brecht and Sakmann, 2003;). Moreover, intracortical secondary activation could also recruit large number of non-specific neurons. The cortical location of the presynaptic neurons to the shared spines can be speculated based on previous studies. The majority of inputs to L2 neurons arrive from L2/3 neurons (Lefort et al., 2009;), with a considerable contribution from L5 neurons (Shepherd et al., 2005). Thus, neurons projecting to shared spines are most likely to reside in these layers.

In L4 experiments no shared spines were identified among the short latency spines. A possible explanation is that the different whisker stimulation protocol and the restriction to the early responses excluded spines responding to extent intracortical activation. Although neurons with multi-whisker suprathreshold properties were identified in the VPM (Brecht and Sakmann, 2002a), their response is still highly dominated by the PW, thus the potentially small number of AP fired by the multi-whisker VPM neurons could hinder the identification of spines with multi-whisker input properties.

5.3.2. Distance dependence of SW-specific and shared spines

The amount of SW-specific and shared spines depended on the distance of the SW from the PW (see Results section 4.1.5.). This was in parallel with the finding that more distant SWs were less efficient to evoke global depolarization and global subthreshold dendritic calcium signal in L2 neurons (see Results section 4.1.2.). The decrease in the global depolarization could be, in principle the result of inhibition. This would be not surprising in the view that the neocortex is highly innervated by dense inhibitory projections (Fino and Yuste, 2011). Similarly, close interaction was described between excitation and inhibition (Derdikman et al., 2003; Okun and Lampl, 2008; Wilent and Contreras, 2005). For review on the interaction between excitation and inhibition, please refer to Isaacson and Scanziani (2011). However, the decrease in the global subthreshold calcium signal and in the number of SW-specific and shared spines suggest that besides the compensatory effect of increased inhibition, the amount of excitation is also responsible for the reduction in evoked depolarization. Thus a combination of excitatory and inhibitory input features shape the response properties of distant neurons.

5.4. Specific properties of inputs reaching L4 neurons

5.4.1. Short latency inputs

In the present study inputs which had short latency were assumed to be mostly of thalamic origin. This assumption was based on the properties of the microciruitry in the wS1. As it was previously described in the Introduction section the majority of thalamocortical projections carrying information on whisker deflection terminates in the barrel region of L4. This and the low spontaneous activity of L4 neurons imply that the first EPSP in response to whisker stimulation should correspond to inputs arriving to the cortex through thalamocortical projections. In this study, most EPSPs had an onset latency around 10 ms (see Fig.16.), which is close to previously reported values (for example 8 ± 1.4 ms in Brecht and Sakmann, 2002). The slight difference could originate from the mechanical properties of the stimulator. Thus, the first EPSPs recorded in this study were likely to correspond to thalamocortical inputs. However, L4 neurons are highly interconnected (Lefort et al., 2009). As a result, the initial activation by the thalamocortical projection could recruit other neurons as well. Thus, APs riding on the first EPSP could already produce spine activation of cortical origin. However, as shown in Figure 17., under the present experimental conditions, most L4 neurons do not fire AP reliably in the first 50 ms after the whisker stimulation. Consequently, although thalamic and cortical input could not be strictly separated, one could assume that the majority of inputs detected in the short time window after stimulation was of thalamic origin.

5.4.2. Spatial distribution of short latency inputs to spiny stellates and star pyramids

The spatial distribution of short latency inputs was different in spiny stellates and in star pyramids. In spiny stellates the short latency inputs occurred with highest density around the soma and decreased with distance in the x-y projection of the neurons. In star pyramids the short latency inputs were distributed with equal density along the dendrites in the x-y projection of the neurons. The explanation for high density of short latency inputs around the soma of spiny stellates is not so clear. Most of the VPM projections terminate in the middle hollow part of the barrel (for example Oberlaender et al., 2011), and most of the spiny stellates were described with asymmetric dendritic field with the soma on the side and the dendrites

projecting to the middle of the barrel (Egger et al., 2008). Thus one would expect to have more connections on dendritic ends closer to the barrel center. Although some spiny stellates residing in the middle of the barrel have symmetric dendritic tree, in this experiment set the majority of spiny stellates had asymmetric dendritic morphology (6 out of 9). Moreover, when symmetric and asymmetric spiny stellates were separated, they still showed the perisomatic aggregation of inputs. A similar finding was reported in the auditory cortex slices, where thalamic projections ended preferentially on dendritic segments within 100 µm from the soma (Richardson et al., 2009).

In the visual cortex of the cat and the ferret, spiny stellates were shown to develop from neurons with pyramid morphology (cat: Vercelli et al., 1992; ferret: Callaway and Borrell, 2011). In development of the wS1, sensory inputs were found to be crucial to instruct the barrel formation (Narboux-Neme et al., 2012). When decreasing neurotransmission from thalamic projections, spiny stellate cells did not develop asymmetric morphology and stayed evenly distributed in the barrel. Thus, the aggregation of inputs near the soma in spiny stellates might reflect developmental features.

The functional consequences of the distribution of short latency inputs were not addressed in this study. From the passive cable theory of dendritic processes, it would follow that synapses closer the soma controlled the membrane potential more effectively (Rall, 1964). However, numerous studies suggested that more distant synapses had compensatory mechanisms thus leading to “synaptic democracy” (for overview see Hausser, 2001; Hausser and Mel, 2003; Williams and Stuart, 2003). Finally, another idea by Cash and Yuste (1998) proposed that the position of synapses had an effect on the interaction between EPSP and backpropagating AP.

5.5. Model circuitry

Based on the results acquired in this study and in previous work in the literature, a model for the excitatory information transmission in L4 and L2 in the mouse wS1 is put forward in Fig.26A-B. Here, the inputs conveying information on sensory stimulation is reaching the cortex by projecting to spiny stellate and star pyramid neurons in L4. In case of spiny stellates,

the inputs are preferentially distributed close to the soma, thus effectively driving stimulation evoked firing. The connections among L4 neurons themselves recruit more and more neurons, and the information is transmitted to supragranular layers. In L2 the sensory information spreads laterally, reaching neurons in columns related to neighboring columns. The lateral spread of excitation is decreasing with distance. Due to intralaminar L2-L2 connections most of the neurons are activated by multiple whiskers.

All these properties contribute to that information is effectively reaching the cortex and then transmitted for further contextual processing.

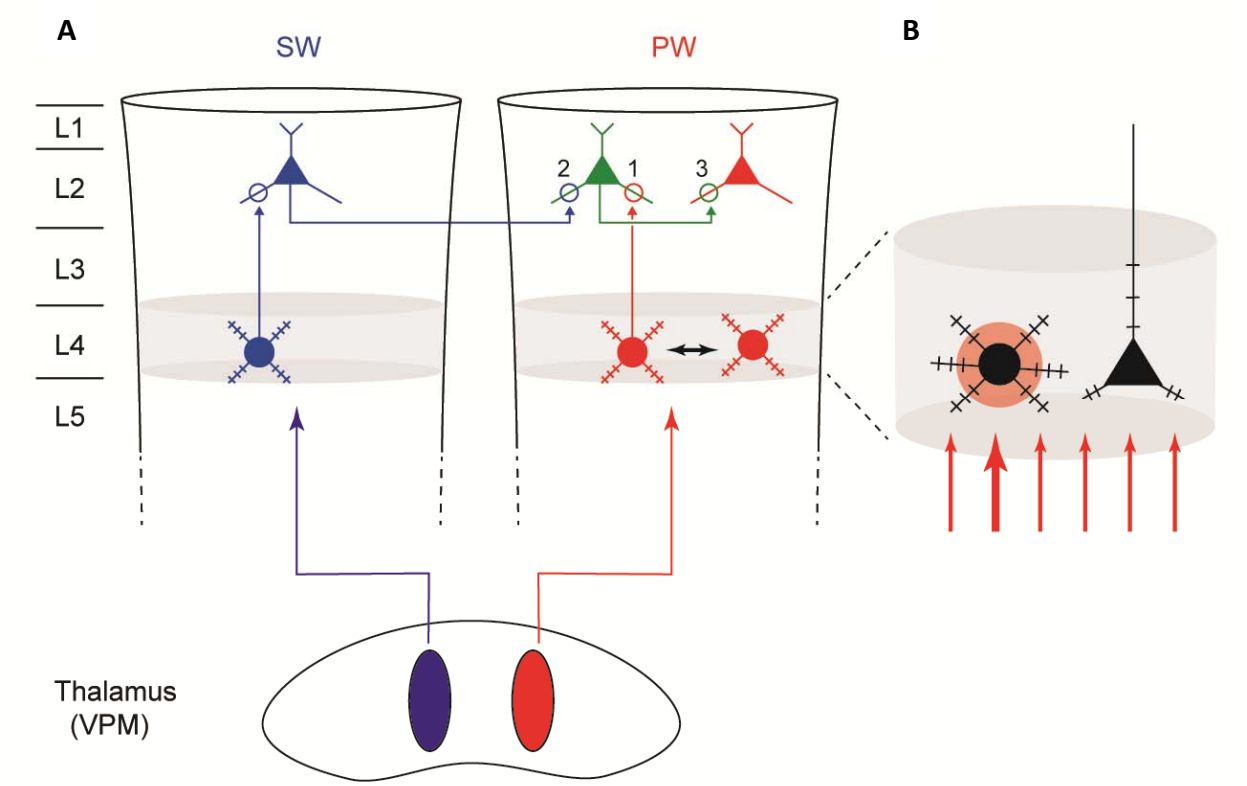

Fig.26. *Model circuit of sensory information processing in the upper half of wS1.* ***(A)*** *Scheme of projections. Red indicate PW-related projections, blue indicate SW-related projections. Green neuron is the potential source of projections to shared spines. Circles marked by the numbers of 1, 2 and 3 indicate PW-specific, SW-specific and shared spines, respectively.* ***(B)*** *Magnified view of L4. The perisomatic region of spiny stellates is reached by the most number of thalamocortical porjections.*

6. Summary

This study addressed the in vivo mapping of single synapses activated in response to sensory stimulation in the mouse wS1 to understand how sensory information is represented in the dendrites of neurons residing in an anatomically structured cortical area. To approach this question in vivo two-photon calcium imaging with single spine resolution was performed on L2 and L4 neurons. This is the first time demonstration of single spine signals from deep neurons of L4. Although the analysis on L4 experiments was not completed, the available results, in combination with the results of L2 experiments, give unique insight on the representation of sensory information in multiple cortical layers.

In L2 neurons, sensory information was found to be highly distributed on the dendrites, despite of the columnar structure of this cortical region. Neurons received inputs from multiple whiskers, and the spines receiving information from different whiskers were interspersed. Moreover, single spines that received information from multiple whiskers were also identified. These spines were also distributed among the spines that responded to a specific whisker and are likely to be the receiver partner of neurons with multi-whiskers properties. Similarly, in L4 neurons, active inputs were identified on multiple dendrite branches. Notably, in a morphological subtype of L4 neurons, in the spiny stellates the inputs accumulated around the somatic region. These results indicate that from the view of a single neuron, the structure of cortical columns does not impose functional polarization of the dendritic tree, but all branches could participate in the representation of sensory inputs. In both layers, the majority of spines had relatively low response probabilities, suggesting sparse coding a generally used strategy used for information coding.

Altogether, this study shed light on some of the features of sensory information coding in wS1. The main technical advance is the demonstration of in vivo functional imaging of spines of neurons located in deeper layers. This could be an essential step to further increase the cortical depth accessible for in vivo calcium imaging.

7. Abbreviations

AP: action potential

AP5: D-(-)-2-Amino-5-phosphonopentanoic acid

Bmp: beat per minute

EPSP: excitatory postsynaptic potential

GABA: γ-Aminobutyric acid

Hz: Hertz

L1-L6: cortical layers from layer 1 to layer 6

M1: primary motor cortex

mm: millimeter

mM: millimol

ms: millisecond

mV: millivolt

MΩ: megaohm

nA: nanoamper

NMDA: N-Methyl-D-aspartic acid

PMBSF: posteromedial barrel subfield

POm: posterior medial nucleus of the thalamus

PW: principal whisker

ROI: region of interest

SW: surround whisker

VPM: ventral posterior medial nucleus of the thalamus

VSD: voltage-sensitive dye

wS1: whisker representation part of the primary somatosensory cortex

wS2: whisker representation part of the secondary somatosensory cortex

µm: micrometer

8. References

Aguilar J, Morales-Botello ML, Foffani G. Tactile responses of hindpaw, forepaw and whisker neurons in the thalamic ventrobasal complex of anesthetized rats. Eur J Neurosci. 2008 Jan;27(2):378-87

Ahissar E, Sosnik R, Bagdasarian K, Haidarliu S. Temporal frequency of whisker movement. II. Laminar organization of cortical representations. J Neurophysiol. 2001 Jul;86(1):354-67

Alloway KD, Zhang M, Chakrabarti S. Septal columns in rodent barrel cortex: functional circuits for modulating whisking behavior. J Comp Neurol. 2004 Dec 13;480(3):299-309

Araya R, Jiang J, Eisenthal KB, Yuste R. The spine neck filters membrane potentials. Proc Natl Acad Sci U S A. 2006 Nov 21;103(47):17961-6

Araya R, Eisenthal KB, Yuste R. Dendritic spines linearize the summation of excitatory potentials. Proc Natl Acad Sci U S A. 2006 Dec 5;103(49):18799-804

Arenkiel BR, Peca J, Davison IG, Feliciano C, Deisseroth K, Augustine GJ, Ehlers MD, Feng G. In vivo light-induced activation of neural circuitry in transgenic mice expressing channelrhodopsin-2. Neuron. 2007 Apr 19;54(2):205-18

Armstrong-James M, Fox K, Das-Gupta A. Flow of excitation within rat barrel cortex on striking a single vibrissa. J Neurophysiol. 1992 Oct;68(4):1345-58

Armstrong-James M, Fox K. Spatiotemporal convergence and divergence in the rat S1 "barrel" cortex. J Comp Neurol. 1987 Sep 8;263(2):265-81

Aronoff R, Matyas F, Mateo C, Ciron C, Schneider B, Petersen CC. Long-range connectivity of mouse primary somatosensory barrel cortex. Eur J Neurosci. 2010 Jun;31(12):2221-33

Belford GR, Killackey HP. Vibrissae representation in subcortical trigeminal centers of the neonatal rat. J Comp Neurol. 1979 Jan 15;183(2):305-21

Berg RW, Kleinfeld D. Rhythmic whisking by rat: retraction as well as protraction of the vibrissae is under active muscular control. J Neurophysiol. 2003 Jan;89(1):104-17

Bernardo KL, McCasland JS, Woolsey TA, Strominger RN. Local intra- and interlaminar connections in mouse barrel cortex. J Comp Neurol. 1990 Jan 8;291(2):231-55

Bloodgood BL, Sabatini BL. Neuronal activity regulates diffusion across the neck of dendritic spines. Science. 2005 Nov 4;310(5749):866-9

Bloodgood BL, Sabatini BL. Ca(2+) signaling in dendritic spines. Curr Opin Neurobiol. 2007 Jun;17(3):345-51. Epub 2007 Apr 23

Bosman LW, Houweling AR, Owens CB, Tanke N, Shevchouk OT, Rahmati N, Teunissen WH, Ju C, Gong W, Koekkoek SK, De Zeeuw CI. Anatomical pathways involved in generating and sensing rhythmic whisker movements. Front Integr Neurosci. 2011;5:53

Bourassa J, Pinault D, Deschênes M. Corticothalamic projections from the cortical barrel field to the somatosensory thalamus in rats: a single-fibre study using biocytin as an anterograde tracer. Eur J Neurosci. 1995 Jan 1;7(1):19-30

Bureau I, von Saint Paul F, Svoboda K. Interdigitated paralemniscal and lemniscal pathways in the mouse barrel cortex. PLoS Biol. 2006 Nov;4(12):e382.

Branco T, Clark BA, Häusser M. Dendritic discrimination of temporal input sequences in cortical neurons. Science. 2010 Sep 24;329(5999):1671-5

Branco T, Häusser M. Synaptic integration gradients in single cortical pyramidal cell dendrites. Neuron. 2011 Mar 10;69(5):885-92

Brecht M, Preilowski B, Merzenich MM. Functional architecture of the mystacial vibrissae. Behav Brain Res. 1997 Mar;84(1-2):81-97

Brecht M, Sakmann B. Whisker maps of neuronal subclasses of the rat ventral posterior medial thalamus, identified by whole-cell voltage recording and morphological reconstruction. J Physiol. 2002 Jan 15;538(Pt 2):495-515

Brecht M, Sakmann B. Dynamic representation of whisker deflection by synaptic potentials in spiny stellate and pyramidal cells in the barrels and septa of layer 4 rat somatosensory cortex. J Physiol. 2002 Aug 15;543(Pt 1):49-70

Brecht M, Roth A, Sakmann B. Dynamic receptive fields of reconstructed pyramidal cells in layers 3 and 2 of rat somatosensory barrel cortex. J Physiol. 2003 Nov 15;553(Pt 1):243-65

Briggman KL, Helmstaedter M, Denk W. Wiring specificity in the direction-selectivity circuit of the retina. Nature. 2011 Mar 10;471(7337):183-8

Bock DD, Lee WC, Kerlin AM, Andermann ML, Hood G, Wetzel AW, Yurgenson S, Soucy ER, Kim HS, Reid RC. Network anatomy and in vivo physiology of visual cortical neurons. Nature. 2011 Mar 10;471(7337):177-82

Callaway EM, Katz LC. Photostimulation using caged glutamate reveals functional circuitry in living brain slices. Proc Natl Acad Sci U S A. 1993 Aug 15;90(16):7661-5

Callaway EM, Borrell V. Developmental sculpting of dendritic morphology of layer 4 neurons in visual cortex: influence of retinal input. J Neurosci. 2011 May 18;31(20):7456-70

Carvell GE, Simons DJ. Somatotopic organization of the second somatosensory area (SII) in the cerebral cortex of the mouse. Somatosens Res. 1986;3(3):213-37

Carvell GE, Simons DJ. Task- and subject-related differences in sensorimotor behavior during active touch. Somatosens Mot Res. 1995;12(1):1-9

Cash S, Yuste R. Input summation by cultured pyramidal neurons is linear and position-independent. J Neurosci. 1998 Jan 1;18(1):10-5

Chakrabarti S, Alloway KD. Differential origin of projections from SI barrel cortex to the whisker representations in SII and MI. J Comp Neurol. 2006 Oct 10;498(5):624-36

Chen X, Leischner U, Rochefort NL, Nelken I, Konnerth A. Functional mapping of single spines in cortical neurons in vivo. Nature. 2011 Jun 26;475(7357):501-5

Cowan RL, Wilson CJ. Spontaneous firing patterns and axonal projections of single corticostriatal neurons in the rat medial agranular cortex. J Neurophysiol. 1994 Jan;71(1):17-32

Crochet S, Petersen CC. Correlating whisker behavior with membrane potential in barrel cortex of awake mice. Nat Neurosci. 2006 May;9(5):608-10

Crochet S, Poulet JF, Kremer Y, Petersen CC. Synaptic mechanisms underlying sparse coding of active touch. Neuron. 2011 Mar 24;69(6):1160-75

Dantzker JL, Callaway EM. Laminar sources of synaptic input to cortical inhibitory interneurons and pyramidal neurons. Nat Neurosci. 2000 Jul;3(7):701-7

DeFelipe J, Farinas I. The pyramidal neuron of the cerebral cortex: morphological and chemical characteristics of the synaptic inputs. Prog Neurobiol. 1992 Dec;39(6):563-607

de Kock CP, Bruno RM, Spors H, Sakmann B. Layer- and cell-type-specific suprathreshold stimulus representation in rat primary somatosensory cortex. J Physiol. 2007 May 15;581(Pt 1):139-54

Denk W, Strickler JH, Webb WW. Two-photon laser scanning fluorescence microscopy. Science. 1990 Apr 6;248(4951):73-6

Denk W, Yuste R, Svoboda K, Tank DW. Imaging calcium dynamics in dendritic spines. Curr Opin Neurobiol. 1996 Jun;6(3):372-8

Denk W, Horstmann H. Serial block-face scanning electron microscopy to reconstruct three-dimensional tissue nanostructure. PLoS Biol. 2004 Nov;2(11):e329

Derdikman D, Hildesheim R, Ahissar E, Arieli A, Grinvald A. Imaging spatiotemporal dynamics of surround inhibition in the barrels somatosensory cortex. J Neurosci. 2003 Apr 15;23(8):3100-5

Deschênes M, Moore J, Kleinfeld D. Sniffing and whisking in rodents. Curr Opin Neurobiol. 2012 Apr;22(2):243-50

Detsch O, Kochs E, Siemers M, Bromm B, Vahle-Hinz C. Differential effects of isoflurane on excitatory and inhibitory synaptic inputs to thalamic neurones in vivo. Br J Anaesth. 2002 Aug;89(2):294-300

Diamond ME, Armstrong-James M, Ebner FF. Somatic sensory responses in the rostral sector of the posterior group (POm) and in the ventral posterior medial nucleus (VPM) of the rat thalamus. J Comp Neurol. 1992 Apr 22;318(4):462-76

Diamond ME, von Heimendahl M, Knutsen PM, Kleinfeld D, Ahissar E. 'Where' and 'what' in the whisker sensorimotor system. Nat Rev Neurosci. 2008 Aug;9(8):601-12

Dittgen T, Nimmerjahn A, Komai S, Licznerski P, Waters J, Margrie TW, Helmchen F, Denk W, Brecht M, Osten P. Lentivirus-based genetic manipulations of cortical neurons and their optical and electrophysiological monitoring in vivo. Proc Natl Acad Sci U S A. 2004 Dec 28;101(52):18206-11

Ebara S, Kumamoto K, Matsuura T, Mazurkiewicz JE, Rice FL. Similarities and differences in the innervation of mystacial vibrissal follicle-sinus complexes in the rat and cat: a confocal microscopic study. J Comp Neurol. 2002 Jul 22;449(2):103-19

Egger V, Nevian T, Bruno RM. Subcolumnar dendritic and axonal organization of spiny stellate and star pyramid neurons within a barrel in rat somatosensory cortex. Cereb Cortex. 2008 Apr;18(4):876-89

Erzurumlu RS, Murakami Y, Rijli FM. Mapping the face in the somatosensory brainstem. Nat Rev Neurosci. 2010 Apr;11(4):252-63

Feldmeyer D, Egger V, Lubke J, Sakmann B. Reliable synaptic connections between pairs of excitatory layer 4 neurones within a single 'barrel' of developing rat somatosensory cortex. J Physiol. 1999 Nov 15;521 Pt 1:169-90

Feldmeyer D, Lübke J, Silver RA, Sakmann B. Synaptic connections between layer 4 spiny neurone-layer 2/3 pyramidal cell pairs in juvenile rat barrel cortex: physiology and anatomy of interlaminar signalling within a cortical column. J Physiol. 2002 Feb 1;538(Pt 3):803-22

Feldmeyer D, Lübke J, Sakmann B. Efficacy and connectivity of intracolumnar pairs of layer 2/3 pyramidal cells in the barrel cortex of juvenile rats. J Physiol. 2006 Sep 1;575(Pt 2):583-602

Ferezou I, Bolea S, Petersen CC. Visualizing the cortical representation of whisker touch: voltage-sensitive dye imaging in freely moving mice. Neuron. 2006 May 16;50(4):617-29

Ferezou I, Haiss F, Gentet LJ, Aronoff R, Weber B, Petersen CC. Spatiotemporal dynamics of cortical sensorimotor integration in behaving mice. Neuron. 2007 Dec 6;56(5):907-23

Fino E, Yuste R. Dense inhibitory connectivity in neocortex. Neuron. 2011 Mar 24;69(6):1188-203

Fox, Kevin. Barrel cortex. Cambridge University Press. 2008

Garaschuk O, Milos RI, Konnerth A. Targeted bulk-loading of fluorescent indicators for two-photon brain imaging in vivo. Nat Protoc. 2006;1(1):380-6

Gentet LJ, Avermann M, Matyas F, Staiger JF, Petersen CC. Membrane potential dynamics of GABAergic neurons in the barrel cortex of behaving mice. Neuron. 2010 Feb 11;65(3):422-35

Gheorghita F, Kraftsik R, Dubois R, Welker E. Structural basis for map formation in the thalamocortical pathway of the barrelless mouse. J Neurosci. 2006 Sep 27;26(39):10057-67

Gibson JM, Welker WI. Quantitative studies of stimulus coding in first-order vibrissa afferents of rats. 1. Receptive field properties and threshold distributions. Somatosens Res. 1983;1(1):51-67

Gottlieb JP, Keller A. Intrinsic circuitry and physiological properties of pyramidal neurons in rat barrel cortex. Exp Brain Res. 1997 Jun;115(1):47-60

Gray EG. Axo-somatic and axo-dendritic synapses of the cerebral cortex: an electron microscope study. J Anat. 1959 Oct;93:420-33

Grienberger C, Konnerth A. Imaging calcium in neurons. Neuron. 2012 Mar 8;73(5):862-85

Grinvald A, Anglister L, Freeman JA, Hildesheim R, Manker A. Real-time optical imaging of naturally evoked electrical activity in intact frog brain. Nature. 1984 Apr 26-May 2;308(5962):848-50

Guthrie PB, Segal M, Kater SB. Independent regulation of calcium revealed by imaging dendritic spines. Nature. 1991 Nov 7;354(6348):76-80

Haidarliu S, Ahissar E. Size gradients of barreloids in the rat thalamus. J Comp Neurol. 2001 Jan 15;429(3):372-87

Harris KM, Stevens JK. Dendritic spines of CA 1 pyramidal cells in the rat hippocampus: serial electron microscopy with reference to their biophysical characteristics. J Neurosci. 1989 Aug;9(8):2982-97

Harvey MA, Bermejo R, Zeigler HP. Discriminative whisking in the head-fixed rat: optoelectronic monitoring during tactile detection and discrimination tasks. Somatosens Mot Res. 2001;18(3):211-22

Häusser M. Synaptic function: dendritic democracy. Curr Biol. 2001 Jan 9;11(1):R10-2

Häusser M, Mel B. Dendrites: bug or feature? Curr Opin Neurobiol. 2003 Jun;13(3):372-83

Helmchen F, Imoto K, Sakmann B. Ca2+ buffering and action potential-evoked Ca2+ signaling in dendrites of pyramidal neurons. Biophys J. 1996 Feb;70(2):1069-81

Helmchen F, Waters J. Ca2+ imaging in the mammalian brain in vivo. Eur J Pharmacol. 2002 Jul 5;447(2-3):119-29

Helmchen F, Denk W. Deep tissue two-photon microscopy. Nat Methods. 2005 Dec;2(12):932-40

Helmstaedter M, Briggman KL, Denk W. High-accuracy neurite reconstruction for high-throughput neuroanatomy. Nat Neurosci. 2011 Jul 10;14(8):1081-8

Hemelt ME, Kwegyir-Afful EE, Bruno RM, Simons DJ, Keller A. Consistency of angular tuning in the rat vibrissa system. J Neurophysiol. 2010 Dec;104(6):3105-12

Higley MJ, Sabatini BL. Calcium signaling in dendrites and spines: practical and functional considerations. Neuron. 2008 Sep 25;59(6):902-13

Hoffer ZS, Hoover JE, Alloway KD. Sensorimotor corticocortical projections from rat barrel cortex have an anisotropic organization that facilitates integration of inputs from whiskers in the same row. J Comp Neurol. 2003 Nov 24;466(4):525-44

Holthoff K, Tsay D, Yuste R. Calcium dynamics of spines depend on their dendritic location. Neuron. 2002 Jan 31;33(3):425-37

Hoogland PV, Welker E, Van der Loos H. Organization of the projections from barrel cortex to thalamus in mice studied with Phaseolus vulgaris-leucoagglutinin and HRP. Exp Brain Res. 1987;68(1):73-87

Hooks BM, Hires SA, Zhang YX, Huber D, Petreanu L, Svoboda K, Shepherd GM. Laminar analysis of excitatory local circuits in vibrissal motor and sensory cortical areas. PLoS Biol. 2011 Jan 4;9(1):e1000572

Huguenard JR, Hamill OP, Prince DA. Sodium channels in dendrites of rat cortical pyramidal neurons. Proc Natl Acad Sci U S A. 1989 Apr;86(7):2473-7

Isaacson JS, Scanziani M. How inhibition shapes cortical activity. Neuron. 2011 Oct 20;72(2):231-43

Izraeli R, Porter LL. Vibrissal motor cortex in the rat: connections with the barrel field. Exp Brain Res. 1995;104(1):41-54

Jadhav SP, Wolfe J, Feldman DE. Sparse temporal coding of elementary tactile features during active whisker sensation. Nat Neurosci. 2009 Jun;12(6):792-800

Jia H, Rochefort NL, Chen X, Konnerth A. Dendritic organization of sensory input to cortical neurons in vivo. Nature. 2010 Apr 29;464(7293):1307-12

Jia H, Rochefort NL, Chen X, Konnerth A. In vivo two-photon imaging of sensory-evoked dendritic calcium signals in cortical neurons. Nat Protoc. 2011 Jan;6(1):28-35

Johnston D, Magee JC, Colbert CM, Cristie BR. Active properties of neuronal dendrites. Annu Rev Neurosci. 1996;19:165-86

Jones LM, Lee S, Trageser JC, Simons DJ, Keller A. Precise temporal responses in whisker trigeminal neurons. J Neurophysiol. 2004 Jul;92(1):665-8

Jurrus E, Hardy M, Tasdizen T, Fletcher PT, Koshevoy P, Chien CB, Denk W, Whitaker R. Axon tracking in serial block-face scanning electron microscopy. Med Image Anal. 2009 Feb;13(1):180-8

Kerr JN, de Kock CP, Greenberg DS, Bruno RM, Sakmann B, Helmchen F. Spatial organization of neuronal population responses in layer 2/3 of rat barrel cortex. J Neurosci. 2007 Nov 28;27(48):13316-28

Kerr JN, Denk W. Imaging in vivo: watching the brain in action. Nat Rev Neurosci. 2008 Mar;9(3):195-205

Kitamura K, Judkewitz B, Kano M, Denk W, Häusser M. Targeted patch-clamp recordings and single-cell electroporation of unlabeled neurons in vivo. Nat Methods. 2008 Jan;5(1):61-7

Kleinfeld D, Delaney KR. Distributed representation of vibrissa movement in the upper layers of somatosensory cortex revealed with voltage-sensitive dyes. J Comp Neurol. 1996 Nov 4;375(1):89-108

Koester HJ, Sakmann B. Calcium dynamics in single spines during coincident pre- and postsynaptic activity depend on relative timing of back-propagating action potentials and subthreshold excitatory postsynaptic potentials. Proc Natl Acad Sci U S A. 1998 Aug 4;95(16):9596-601

Koralek KA, Olavarria J, Killackey HP. Areal and laminar organization of corticocortical projections in the rat somatosensory cortex. J Comp Neurol. 1990 Sep 8;299(2):133-50

Kuhlman SJ, Huang ZJ. High-resolution labeling and functional manipulation of specific neuron types in mouse brain by Cre-activated viral gene expression. PLoS One. 2008 Apr 16;3(4):e2005

Kumar P, Ohana O. Inter- and intralaminar subcircuits of excitatory and inhibitory neurons in layer 6a of the rat barrel cortex. J Neurophysiol. 2008 Oct;100(4):1909-22

Kwegyir-Afful EE, Keller A. Response properties of whisker-related neurons in rat second somatosensory cortex. J Neurophysiol. 2004 Oct;92(4):2083-92

Laaris N, Keller A. Functional independence of layer IV barrels. J Neurophysiol. 2002 Feb;87(2):1028-34

Land PW, Buffer SA Jr, Yaskosky JD. Barreloids in adult rat thalamus: three-dimensional architecture and relationship to somatosensory cortical barrels. J Comp Neurol. 1995 May 15;355(4):573-88

Larkum ME, Waters J, Sakmann B, Helmchen F. Dendritic spikes in apical dendrites of neocortical layer 2/3 pyramidal neurons. J Neurosci. 2007 Aug 22;27(34):8999-9008

Larkum ME, Nevian T, Sandler M, Polsky A, Schiller J. Synaptic integration in tuft dendrites of layer 5 pyramidal neurons: a new unifying principle. Science. 2009 Aug 7;325(5941):756-60

Larsen DD, Wickersham IR, Callaway EM. Retrograde tracing with recombinant rabies virus reveals correlations between projection targets and dendritic architecture in layer 5 of mouse barrel cortex. Front Neural Circuits. 2007;1:5

Lefort S, Tomm C, Floyd Sarria JC, Petersen CC. The excitatory neuronal network of the C2 barrel column in mouse primary somatosensory cortex. Neuron. 2009 Jan 29;61(2):301-16

Leiser SC, Moxon KA. Relationship between physiological response type (RA and SA) and vibrissal receptive field of neurons within the rat trigeminal ganglion. J Neurophysiol. 2006 May;95(5):3129-45

Leiser SC, Moxon KA. Responses of trigeminal ganglion neurons during natural whisking behaviors in the awake rat. Neuron. 2007 Jan 4;53(1):117-33

Lee KJ, Woolsey TA. A proportional relationship between peripheral innervation density and cortical neuron number in the somatosensory system of the mouse. Brain Res. 1975 Dec 5;99(2):349-53

Leung BO, Chou KC. Review of super-resolution fluorescence microscopy for biology. Appl Spectrosc. 2011 Sep;65(9):967-80

LeVay S. Synaptic patterns in the visual cortex of the cat and monkey. Electron microscopy of Golgi preparations. J Comp Neurol. 1973 Jul 1;150(1):53-85

Lichtman JW, Livet J, Sanes JR. A technicolour approach to the connectome. Nat Rev Neurosci. 2008 Jun;9(6):417-22

Livet J, Weissman TA, Kang H, Draft RW, Lu J, Bennis RA, Sanes JR, Lichtman JW. Transgenic strategies for combinatorial expression of fluorescent proteins in the nervous system. Nature. 2007 Nov 1;450(7166):56-62

Lo L, Anderson DJ. A Cre-dependent, anterograde transsynaptic viral tracer for mapping output pathways of genetically marked neurons. Neuron. 2011 Dec 22;72(6):938-50

Lübke J, Markram H, Frotscher M, Sakmann B. Frequency and dendritic distribution of autapses established by layer 5 pyramidal neurons in the developing rat neocortex: comparison with synaptic innervation of adjacent neurons of the same class. J Neurosci. 1996 May 15;16(10):3209-18

Lübke J, Egger V, Sakmann B, Feldmeyer D. Columnar organization of dendrites and axons of single and synaptically coupled excitatory spiny neurons in layer 4 of the rat barrel cortex. J Neurosci. 2000 Jul 15;20(14):5300-11

Lübke J, Roth A, Feldmeyer D, Sakmann B. Morphometric analysis of the columnar innervation domain of neurons connecting layer 4 and layer 2/3 of juvenile rat barrel cortex. Cereb Cortex. 2003 Oct;13(10):1051-63

Lübke J, Feldmeyer D. Excitatory signal flow and connectivity in a cortical column: focus on barrel cortex. Brain Struct Funct. 2007 Jul;212(1):3-17

Ma PM. The barrelettes--architectonic vibrissal representations in the brainstem trigeminal complex of the mouse. I. Normal structural organization. J Comp Neurol. 1991 Jul 8;309(2):161-99

Mainen ZF, Sejnowski TJ. Influence of dendritic structure on firing pattern in model neocortical neurons. Nature. 1996 Jul 25;382(6589):363-6

Manns ID, Sakmann B, Brecht M. Sub- and suprathreshold receptive field properties of pyramidal neurones in layers 5A and 5B of rat somatosensory barrel cortex. J Physiol. 2004 Apr 15;556(Pt 2):601-22

Mao T, Kusefoglu D, Hooks BM, Huber D, Petreanu L, Svoboda K. Long-range neuronal circuits underlying the interaction between sensory and motor cortex. Neuron. 2011 Oct 6;72(1):111-23

Markram H, Sakmann B. Calcium transients in dendrites of neocortical neurons evoked by single subthreshold excitatory postsynaptic potentials via low-voltage-activated calcium channels. Proc Natl Acad Sci U S A. 1994 May 24;91(11):5207-11

Markram H, Helm PJ, Sakmann B. Dendritic calcium transients evoked by single back-propagating action potentials in rat neocortical pyramidal neurons. J Physiol. 1995 May 15;485 (Pt 1):1-20

Matyas F, Sreenivasan V, Marbach F, Wacongne C, Barsy B, Mateo C, Aronoff R, Petersen CC. Motor control by sensory cortex. Science. 2010 Nov 26;330(6008):1240-3

Mercier BE, Legg CR, Glickstein M. Basal ganglia and cerebellum receive different somatosensory information in rats. Proc Natl Acad Sci U S A. 1990 Jun;87(11):4388-92

Meyer HS, Wimmer VC, Hemberger M, Bruno RM, de Kock CP, Frick A, Sakmann B, Helmstaedter M. Cell type-specific thalamic innervation in a column of rat vibrissal cortex. Cereb Cortex. 2010 Oct;20(10):2287-303

Minderer M, Liu W, Sumanovski LT, Kügler S, Helmchen F, Margolis DJ. Chronic imaging of cortical sensory map dynamics using a genetically encoded calcium indicator. J Physiol. 2012 Jan 1;590(Pt 1):99-107

Moore CI, Nelson SB. Spatio-temporal subthreshold receptive fields in the vibrissa representation of rat primary somatosensory cortex. J Neurophysiol. 1998 Dec;80(6):2882-92

Müller W, Connor JA. Dendritic spines as individual neuronal compartments for synaptic Ca2+ responses. Nature. 1991 Nov 7;354(6348):73-6

Narboux-Nême N, Evrard A, Ferezou I, Erzurumlu RS, Kaeser PS, Lainé J, Rossier J, Ropert N, Südhof TC, Gaspar P. Neurotransmitter release at the thalamocortical synapse instructs barrel formation but not axon patterning in the somatosensory cortex. J Neurosci. 2012 May 2;32(18):6183-96

Nevian T, Sakmann B. Single spine Ca2+ signals evoked by coincident EPSPs and backpropagating action potentials in spiny stellate cells of layer 4 in the juvenile rat somatosensory barrel cortex. J Neurosci. 2004 Feb 18;24(7):1689-99

Nevian T, Sakmann B. Spine Ca2+ signaling in spike-timing-dependent plasticity. J Neurosci. 2006 Oct 25;26(43):11001-13

Nowak L, Bregestovski P, Ascher P, Herbet A, Prochiantz A. Magnesium gates glutamate-activated channels in mouse central neurones. Nature. 1984 Feb 2-8;307(5950):462-5

Oberlaender M, de Kock CP, Bruno RM, Ramirez A, Meyer HS, Dercksen VJ, Helmstaedter M, Sakmann B. Cell Type-Specific Three-Dimensional Structure of Thalamocortical Circuits in a Column of Rat Vibrissal Cortex. Cereb Cortex. 2011 Nov 16.

O'Connor DH, Peron SP, Huber D, Svoboda K. Neural activity in barrel cortex underlying vibrissa-based object localization in mice. Neuron. 2010 Sep 23;67(6):1048-61

Okun M, Lampl I. Instantaneous correlation of excitation and inhibition during ongoing and sensory-evoked activities. Nat Neurosci. 2008 May;11(5):535-7

Olshausen BA, Field DJ. Sparse coding of sensory inputs. Curr Opin Neurobiol. 2004 Aug;14(4):481-7

Osten P, Grinevich V, Cetin A. Viral vectors: a wide range of choices and high levels of service. Handb Exp Pharmacol. 2007;(178):177-202

Orbach HS, Cohen LB, Grinvald A. Optical mapping of electrical activity in rat somatosensory and visual cortex. J Neurosci. 1985 Jul;5(7):1886-95

Paredes RM, Etzler JC, Watts LT, Zheng W, Lechleiter JD. Chemical calcium indicators. Methods. 2008 Nov;46(3):143-51

Paxinos G., Franklin KB. The mouse brain in stereotaxic cooridinates. Second Edition. 2001. Academic Press

Petersen CC, Sakmann B. Functionally independent columns of rat somatosensory barrel cortex revealed with voltage-sensitive dye imaging. J Neurosci. 2001 Nov 1;21(21):8435-46

Petersen CC, Grinvald A, Sakmann B. Spatiotemporal dynamics of sensory responses in L2/3 of rat barrel cortex measured *in vivo* by voltage-sensitive dye imaging combined with whole-cell voltage recordings and neuron reconstruction. J Neurosci. 2003 Feb 15;23(3):1298-1309

Petersen CC, Hahn TT, Mehta M, Grinvald A, Sakmann B. Interaction of sensory responses with spontaneous depolarization in layer 2/3 barrel cortex. PNAS. 2003 Nov 11;100(23):13638-43

Petersen CC. The functional organization of the barrel cortex. Neuron. 2007 Oct 25;56(2):339-55

Petreanu L, Huber D, Sobczyk A, Svoboda K. Channelrhodopsin-2-assisted circuit mapping of long-range callosal projections. Nat Neurosci. 2007 May;10(5):663-8

Pichon F, Nikonenko I, Kraftsik R, Welker E. Intracortical connectivity of layer VI pyramidal neurons in the somatosensory cortex of normal and barrelless mice. Eur J Neurosci. 2012 Mar;35(6):855-69

Pinault D. A novel single-cell staining procedure performed in vivo under electrophysiological control: morpho-functional features of juxtacellularly labeled thalamic cells and other central neurons with biocytin or Neurobiotin. J Neurosci Methods. 1996 Apr;65(2):113-36

Poulet JF, Petersen CC. Internal brain state regulates membrane potential synchrony in barrel cortex of behaving mice. Nature. 2008 Aug 14;454(7206):881-5

Poulet JF, Fernandez LM, Crochet S, Petersen CC. Thalamic control of cortical states. Nat Neurosci. 2012 Jan 22;15(3)

Rall W. Theoretical significance of dendritic trees for neuronal input-output relations. R.F. Reiss (Ed.), Neural Theory and Modeling, Stanford University Press. 1964.

Regehr WG, Tank DW. Dendritic calcium dynamics. Curr Opin Neurobiol. 1994 Jun;4(3):373-82

Rice FL, Mance A, Munger BL. A comparative light microscopic analysis of the sensory innervation of the mystacial pad. I. Innervation of vibrissal follicle-sinus complexes. J Comp Neurol. 1986 Oct 8;252(2):154-74

Richardson RJ, Blundon JA, Bayazitov IT, Zakharenko SS. Connectivity patterns revealed by mapping of active inputs on dendrites of thalamorecipient neurons in the auditory cortex. J Neurosci. 2009 May 20;29(20):6406-17

Rochefort NL, Konnerth A. Dendritic spines: from structure to in vivo function. EMBO Rep. 2012 Jul 13. doi: 10.1038/embor.2012.102

Roy NC, Bessaih T, Contreras D. Comprehensive mapping of whisker-evoked responses reveals broad, sharply tuned thalamocortical input to layer 4 of barrel cortex. J Neurophysiol. 2011 May;105(5):2421-37

Sabatini BL, Svoboda K. Analysis of calcium channels in single spines using optical fluctuation analysis. Nature. 2000 Nov 30;408(6812):589-93

Sabatini BL, Oertner TG, Svoboda K. The life cycle of Ca(2+) ions in dendritic spines. Neuron. 2002 Jan 31;33(3):439-52

Sarko DK, Rice FL, Reep RL. Mammalian tactile hair: divergence from a limited distribution. Ann N Y Acad Sci. 2011 Apr;1225:90-100

Sato TR, Gray NW, Mainen ZF, Svoboda K. The functional microarchitecture of the mouse barrel cortex. PLoS Biol. 2007 Jul;5(7):e189

Sato TR, Svoboda K. The functional properties of barrel cortex neurons projecting to the primary motor cortex. J Neurosci. 2010 Mar 24;30(12):4256-60.

Scaglione A, Moxon KA, Aguilar J, Foffani G. Trial-to-trial variability in the responses of neurons carries information about stimulus location in the rat whisker thalamus. Proc Natl Acad Sci U S A. 2011 Sep 6;108(36):14956-61

Schiller J, Helmchen F, Sakmann B. Spatial profile of dendritic calcium transients evoked by action potentials in rat neocortical pyramidal neurones. J Physiol. 1995 Sep 15;487 (Pt 3):583-600

Schiller J, Schiller Y, Clapham DE. NMDA receptors amplify calcium influx into dendritic spines during associative pre- and postsynaptic activation. Nat Neurosci. 1998 Jun;1(2):114-8

Schiller J, Major G, Koester HJ, Schiller Y. NMDA spikes in basal dendrites of cortical pyramidal neurons. Nature. 2000 Mar 16;404(6775):285-9

Schubert D, Kötter R, Luhmann HJ, Staiger JF. Morphology, electrophysiology and functional input connectivity of pyramidal neurons characterizes a genuine layer va in the primary somatosensory cortex. Cereb Cortex. 2006 Feb;16(2):223-36

Siegel F, Lohmann C. Probing synaptic function in dendrites with calcium imaging. Exp Neurol. 2012 Feb 21

Simons DJ. Response properties of vibrissa units in rat SI somatosensory neocortex. J Neurophysiol. 1978 May;41(3):798-820

Simons DJ, Woolsey TA. Morphology of Golgi-Cox-impregnated barrel neurons in rat SmI cortex. J Comp Neurol. 1984 Nov 20;230(1):119-32

Simons DJ. Temporal and spatial integration in the rat SI vibrissa cortex. J Neurophysiol. 1985 Sep;54(3):615-35

Shepherd GM, Svoboda K. Laminar and columnar organization of ascending excitatory projections to layer 2/3 pyramidal neurons in rat barrel cortex. J Neurosci. 2005 Jun 15;25(24):5670-9

Staiger JF, Flagmeyer I, Schubert D, Zilles K, Kötter R, Luhmann HJ. Functional diversity of layer IV spiny neurons in rat somatosensory cortex: quantitative morphology of electrophysiologically characterized and biocytin labeled cells. Cereb Cortex. 2004 Jun;14(6):690-701

Steriade M, Nuñez A, Amzica F. A novel slow (< 1 Hz) oscillation of neocortical neurons in vivo: depolarizing and hyperpolarizing components. J Neurosci. 1993 Aug;13(8):3252-65

Stosiek C, Garaschuk O, Holthoff K, Konnerth A. In vivo two-photon calcium imaging of neuronal networks. Proc Natl Acad Sci U S A. 2003 Jun 10;100(12):7319-24

Stuart GJ, Sakmann B. Active propagation of somatic action potentials into neocortical pyramidal cell dendrites. Nature. 1994 Jan 6;367(6458):69-72

Svoboda K, Tank DW, Denk W. Direct measurement of coupling between dendritic spines and shafts. Science. 1996 May 3;272(5262):716-9

Svoboda K, Denk W, Kleinfeld D, Tank DW. In vivo dendritic calcium dynamics in neocortical pyramidal neurons. Nature. 1997 Jan 9;385(6612):161-5

Svoboda K, Helmchen F, Denk W, Tank DW. Spread of dendritic excitation in layer 2/3 pyramidal neurons in rat barrel cortex in vivo. Nat Neurosci. 1999 Jan;2(1):65-73

Svoboda K, Yasuda R. Principles of two-photon excitation microscopy and its applications to neuroscience. Neuron. 2006 Jun 15;50(6):823-39

Takahashi T, Svoboda K, Malinow R. Experience strengthening transmission by driving AMPA receptors into synapses. Science. 2003 Mar 7;299(5612):1585-8

Takumi Y, Ramírez-León V, Laake P, Rinvik E, Ottersen OP. Different modes of expression of AMPA and NMDA receptors in hippocampal synapses. Nat Neurosci. 1999 Jul;2(7):618-24

Tanaka YR, Tanaka YH, Konno M, Fujiyama F, Sonomura T, Okamoto-Furuta K, Kameda H, Hioki H, Furuta T, Nakamura KC, Kaneko T. Local connections of excitatory neurons to corticothalamic neurons in the rat barrel cortex. J Neurosci. 2011 Dec 14;31(50):18223-36

Thomson AM, Bannister AP. Interlaminar connections in the neocortex. Cereb Cortex. 2003 Jan;13(1):5-14

Thomson AM, Lamy C. Functional maps of neocortical local circuitry. Front Neurosci. 2007 Nov;1(1):19-42

Trommald M, Hulleberg G. Dimensions and density of dendritic spines from rat dentate granule cells based on reconstructions from serial electron micrographs. J Comp Neurol. 1997 Jan 6;377(1):15-28

Van Der Loos H. Barreloids in mouse somatosensory thalamus. Neurosci Lett. 1976 Mar;2(1):1-6

Varga Z, Jia H, Sakmann B, Konnerth A. Dendritic coding of multiple sensory inputs in single cortical neurons in vivo. Proc Natl Acad Sci U S A. 2011 Sep 13;108(37):15420-5

Veinante P, Deschênes M. Single- and multi-whisker channels in the ascending projections from the principal trigeminal nucleus in the rat. J Neurosci. 1999 Jun 15;19(12):5085-95

Veinante P, Lavallée P, Deschênes M. Corticothalamic projections from layer 5 of the vibrissal barrel cortex in the rat. J Comp Neurol. 2000 Aug 21;424(2):197-204

Vercelli A, Assal F, Innocenti GM. Emergence of callosally projecting neurons with stellate morphology in the visual cortex of the kitten. Exp Brain Res. 1992;90(2):346-58

Viaene AN, Petrof I, Sherman SM. Properties of the thalamic projection from the posterior medial nucleus to primary and secondary somatosensory cortices in the mouse. Proc Natl Acad Sci U S A. 2011 Nov 1;108(44):18156-61

Volgraf M, Gorostiza P, Szobota S, Helix MR, Isacoff EY, Trauner D. Reversibly caged glutamate: a photochromic agonist of ionotropic glutamate receptors. J Am Chem Soc. 2007 Jan 17;129(2):260-1

Wang H, Peca J, Matsuzaki M, Matsuzaki K, Noguchi J, Qiu L, Wang D, Zhang F, Boyden E, Deisseroth K, Kasai H, Hall WC, Feng G, Augustine GJ. High-speed mapping of synaptic connectivity using photostimulation in Channelrhodopsin-2 transgenic mice. Proc Natl Acad Sci U S A. 2007 May 8;104(19):8143-8

Waters J, Larkum M, Sakmann B, Helmchen F. Supralinear Ca2+ influx into dendritic tufts of layer 2/3 neocortical pyramidal neurons in vitro and in vivo. J Neurosci. 2003 Sep 17;23(24):8558-67

Welker C. Microelectrode delineation of fine grain somatotopic organization of (SmI) cerebral neocortex in albino rat. Brain Res. 1971 Mar 5;26(2):259-75

Welker C. Receptive fields of barrels in the somatosensory neocortex of the rat. J Comp Neurol. 1976 Mar 15;166(2):173-89

Welker E, Hoogland PV, Van der Loos H. Organization of feedback and feedforward projections of the barrel cortex: a PHA-L study in the mouse. Exp Brain Res. 1988;73(2):411-35

Welker E, Armstrong-James M, Bronchti G, Ourednik W, Gheorghita-Baechler F, Dubois R, Guernsey DL, Van der Loos H, Neumann PE. Altered sensory processing in the somatosensory cortex of the mouse mutant barrelless. Science. 1996 Mar 29;271(5257):1864-7

White EL, DeAmicis RA. Afferent and efferent projections of the region in mouse SmL cortex which contains the posteromedial barrel subfield. J Comp Neurol. 1977 Oct 15;175(4):455-82

Wilcox M, Viola RW, Johnson KW, Billington AP, Carpenter BK, McCray JA, Guzikowski PA, Hess GP. Synthesis of photolabile precursors of amino acid neurotransmitters. J. Org. Chem. 1990 55(5):1585–89

Wilent WB, Contreras D. Dynamics of excitation and inhibition underlying stimulus selectivity in rat somatosensory cortex. Nat Neurosci. 2005 Oct;8(10):1364-70

Williams SR, Stuart GJ. Role of dendritic synapse location in the control of action potential output. Trends Neurosci. 2003 Mar;26(3):147-54

Williams MN, Zahm DS, Jacquin MF. Differential foci and synaptic organization of the principal and spinal trigeminal projections to the thalamus in the rat. Eur J Neurosci. 1994 Mar 1;6(3):429-53

Wimmer VC, Bruno RM, de Kock CP, Kuner T, Sakmann B. Dimensions of a projection column and architecture of VPM and POm axons in rat vibrissal cortex. Cereb Cortex. 2010 Oct;20(10):2265-76

Wong-Riley M. Changes in the visual system of monocularly sutured or enucleated cats demonstrable with cytochrome oxidase histochemistry. Brain Res. 1979 Jul 27;171(1):11-28

Woolsey TA, Van der Loos H. The structural organization of layer IV in the somatosensory region (S1) of mouse cerebral cortex. The description of a cortical field composed of discrete cytoarchitectonic units. Brain Res. 1970 Jan 20;17(2)205-42

Woolsey TA, Dierker ML, Wann DF. Mouse SmI cortex: qualitative and quantitative classification of golgi-impregnated barrel neurons. Proc Natl Acad Sci U S A. 1975 Jun;72(6):2165-9

Wright AK, Norrie L, Arbuthnott GW. Corticofugal axons from adjacent 'barrel' columns of rat somatosensory cortex: cortical and thalamic terminal patterns. J Anat. 2000 Apr;196 (Pt 3):379-90

Yamada Y, Michikawa T, Hashimoto M, Horikawa K, Nagai T, Miyawaki A, Häusser M, Mikoshiba K. Quantitative comparison of genetically encoded Ca indicators in cortical pyramidal cells and cerebellar Purkinje cells. Front Cell Neurosci. 2011;5:18

Yasuda R, Nimchinsky EA, Scheuss V, Pologruto TA, Oertner TG, Sabatini BL, Svoboda K. Imaging calcium concentration dynamics in small neuronal compartments. Sci STKE. 2004 Feb 3;2004(219):pl5

Yizhar O, Fenno LE, Davidson TJ, Mogri M, Deisseroth K. Optogenetics in neural systems. Neuron. 2011 Jul 14;71(1):9-34.

Yuste R, Denk W. Dendritic spines as basic functional units of neuronal integration. Nature. 1995 Jun 22;375(6533):682-4

Yuste R, Tank DW, Kleinfeld D. Functional study of the rat cortical microcircuitry with voltage-sensitive dye imaging of neocortical slices. Cereb Cortex. 1997 Sep;7(6):546-58

Yuste R. Dendritic spines and distributed circuits. Neuron. 2011 Sep 8;71(5):772-81

Zhu JJ, Connors BW. Intrinsic firing patterns and whisker-evoked synaptic responses of neurons in the rat barrel cortex. J Neurophysiol. 1999 Mar;81(3):1171-83

9. Acknowledgements

I would like to thank Prof. Dr. Arthur Konnerth for providing the opportunity to work in his laboratory, as well as his constant and highly valuable supervision and instructions. I am grateful to Prof. Dr. Bert Sakmann for his enthusiasm and encouraging discussions. I am especially grateful to Dr. Hongbo Jia for his collaboration, his setup constructions, his analysis programs and the excessive amount of help in analysis. I am sincerely grateful for his constant and encouraging support, his optimism and the vivid discussions. I would like to thank Dr. Xiaowei Chen for teaching me the technique of in vivo whole-cell recording and his helpfulness. Finally, I would like to thank all other members of the institute for help in technical and administrative issues.

Without them this study could have not been completed.

10. Publications containing these results

Varga Z, Jia H, Sakmann B, Konnerth A. Dendritic coding of multiple sensory inputs in single cortical neurons in vivo. Proc Natl Acad Sci U S A. 2011 Sep 13;108(37):15420-5